WAVE AND SEDIMENT DYNAMICS AT SHELLY BEACH

Numerical modelling of sediment transport due to waves and tidal currents and an investigation of the efficacy of the Long Mac to maintain beach stability

Prepared for Port Otago Limited

MET OCEAN SOLUTIONS LTD
www.metocean.co.nz

PO Box 441, New Plymouth, New Zealand
T: 64-6-7585035 E: enquiries@metocean.co.nz

MetOcean Solutions Ltd: P0140-01

June 2013

Report status

Version	Date	Status	Approved by
RevA	15/06/2013	Interim draft for internal review	Weppe
RevB	16/06/2013	Interim draft for client review	McComb
Rev0	28/08/2014	Approved for release	McComb

It is the responsibility of the reader to verify the currency of the version number of this report.

PO Box 441, New Plymouth, New Zealand
T: 64-6-7585035 E: enquiries@metocean.co.nz

TABLE OF CONTENTS

LIST OF FIGURES

LIST OF TABLES

1. INTRODUCTION

A requirement of consent for Port Otago's channel deepening consent was research into the function of the "Long Mac" groyne, which is immediately adjacent to this shipping channel, opposite Harington Point.

One of the current dredge spoil disposal grounds is located just offshore of Shelly Beach which is partially bounded to the east by the submerged groyne commonly referred to as "Long Mac". This structure and other groynes and rock structures on the eastern side of the channel were implemented between 1905 and 1910 to help stabilise the beach, prevent direct sediment recirculation back into the channel and hold the alignment of the main shipping channel. However, the state of this structure has degraded over time and the efficacy of its function in stabilising the beach has been called into question.

As a first step in addressing the issue, a study has been commissioned to investigate the wave and sediment transport dynamics in this highly complex area, with particular attention to the functional aspects of the local features and the potential for sediment recirculation into the channel and Harbour. A numerical model of the area has been implemented to characterize the local sediment morphodynamics and the effect of the Long Mac – both in its current form and in an optimised configuration.

The study region necessarily incudes the wider Otago Harbour entrance region (Figure 1.1). This captures the large submerged ebb delta bar east of the shipping channel, Shelly Beach, enclosed by the Mole to the west and the Long Mac to the east, and the bend of the channel south of Shelly Beach known as "Harrington Bend". In the following text the harbour "entrance" refers to this area.

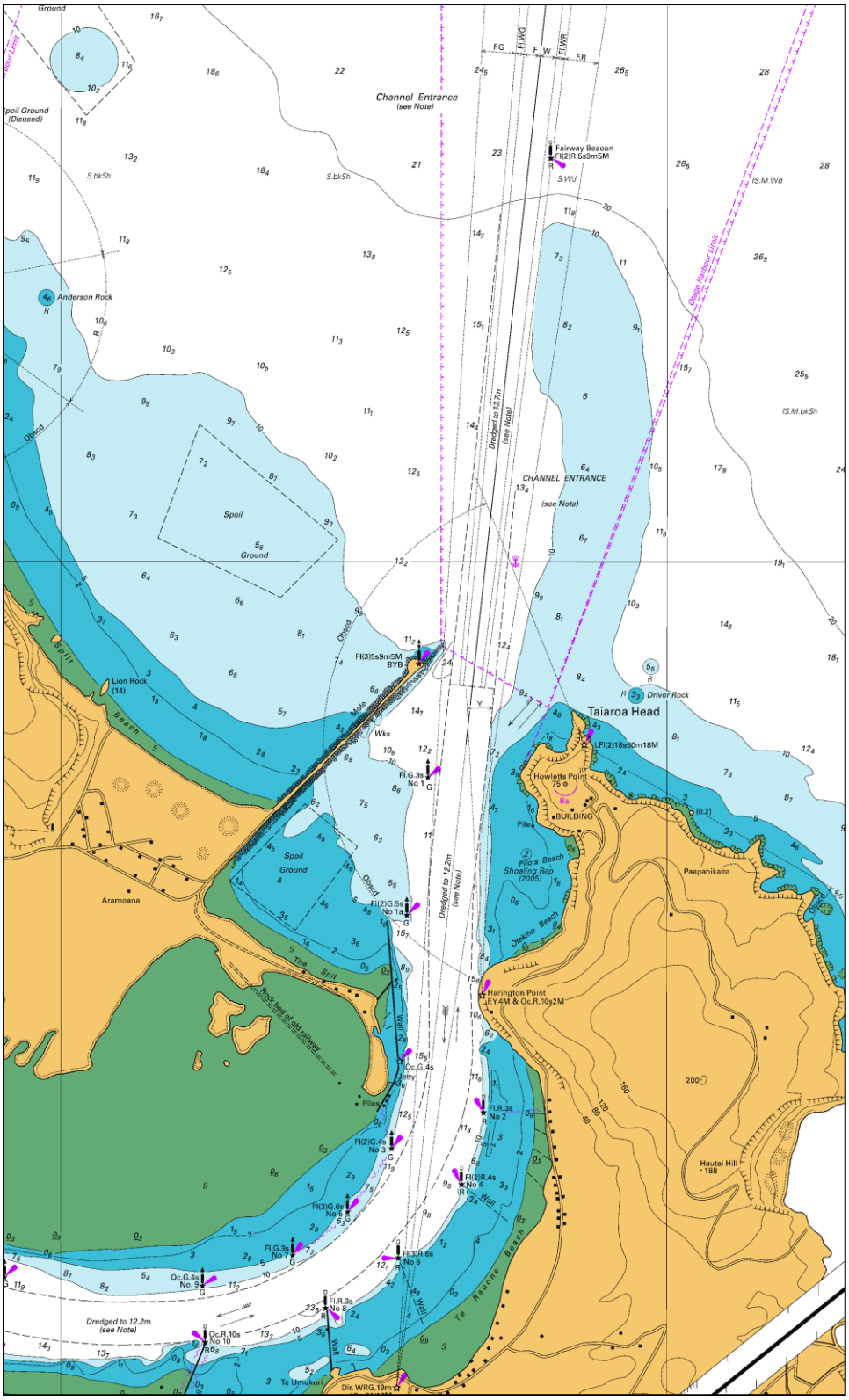

Figure 1.1 Nautical chart of the study area including the submerged ebb delta bar, Shelly Beach, the Mole and Long Mac.

2. NUMERICAL MODELLING METHODOLOGY

The numerical modelling approach included the use of a regional hydrodynamic model covering the whole Otago Harbour and Peninsula eastern and northern coasts, and a local high-resolution morphodynamic model focusing on the entrance region and coupling flow, wave and sediment transport models. The regional hydrodynamic model was required to ensure correct representation of the complex tidal dynamics developing in the entrance region due to the coupling of the Harbour with the larger scale regional tidal regime, and allowed nesting of the high resolution domain.

2.1. Regional tidal hydrodynamic modelling (SELFE)

SELFE is a prognostic finite-element unstructured-grid model designed to simulate 3D baroclinic, 3D barotropic or 2D barotropic circulation. The barotropic mode equations employ a semi-implicit finite-element Eulerian-Lagrangian algorithm to solve the shallow-water equations, forced by relevant physical processes (atmospheric, oceanic and fluvial forcing). SELFE uses either pure terrain-following sigma, or S-layer coordinates in the vertical, or a hybrid system using both S and Z-layers as required and uses sophisticated vertical turbulent closure models. A detailed description of the SELFE model formulation, governing equations and numerics can be found in Zhang and Baptista (2008). For the purposes of this study, SELFE was run in full 3D barotropic mode, with tidal velocity fields at each sigma level.

2.1.1. Model domain

The model domain is shown on Figure 2.1. It includes the entire Otago Harbour and a wide stretch of the Otago coast, from Wickliffe Bay to the east to Karitane to the north, and extends ~ 10km offshore to depths of about 80 meters. The finite element mesh was refined in shallow regions and around complex features. The vertical discretization used 10 sigma levels with 30, 0.7 and 10 as the hc, θb and θf constants in the Song and Haidvogel's (1994) S-coordinate system.

2.1.2. Subgrid parameterisations

Vertical mixing was modelled using a k-kl model with a Kantha & Clayson (1994) stability function. A minimum and maximum diffusivity is applied, set to 1x10e-5 and 1x10e-1 m^2/s respectively. A constant surface mixing length of 0.1 m was used throughout. Frictional stress at the seabed was approximated with a quadratic drag law, with the drag coefficient (CD) determined using a bottom roughness of 0.001 m and an upper limit of CD set to 0.01.

2.1.3. Boundary and initial conditions

The SELFE grid was nested within the MetOcean Solutions Ltd. New Zealand tidal model which was run using an implementation of POM (Princeton Ocean Model). Both tidal surface elevation and current velocity were prescribed along the hemispheric (open) boundary. No residual currents were considered.

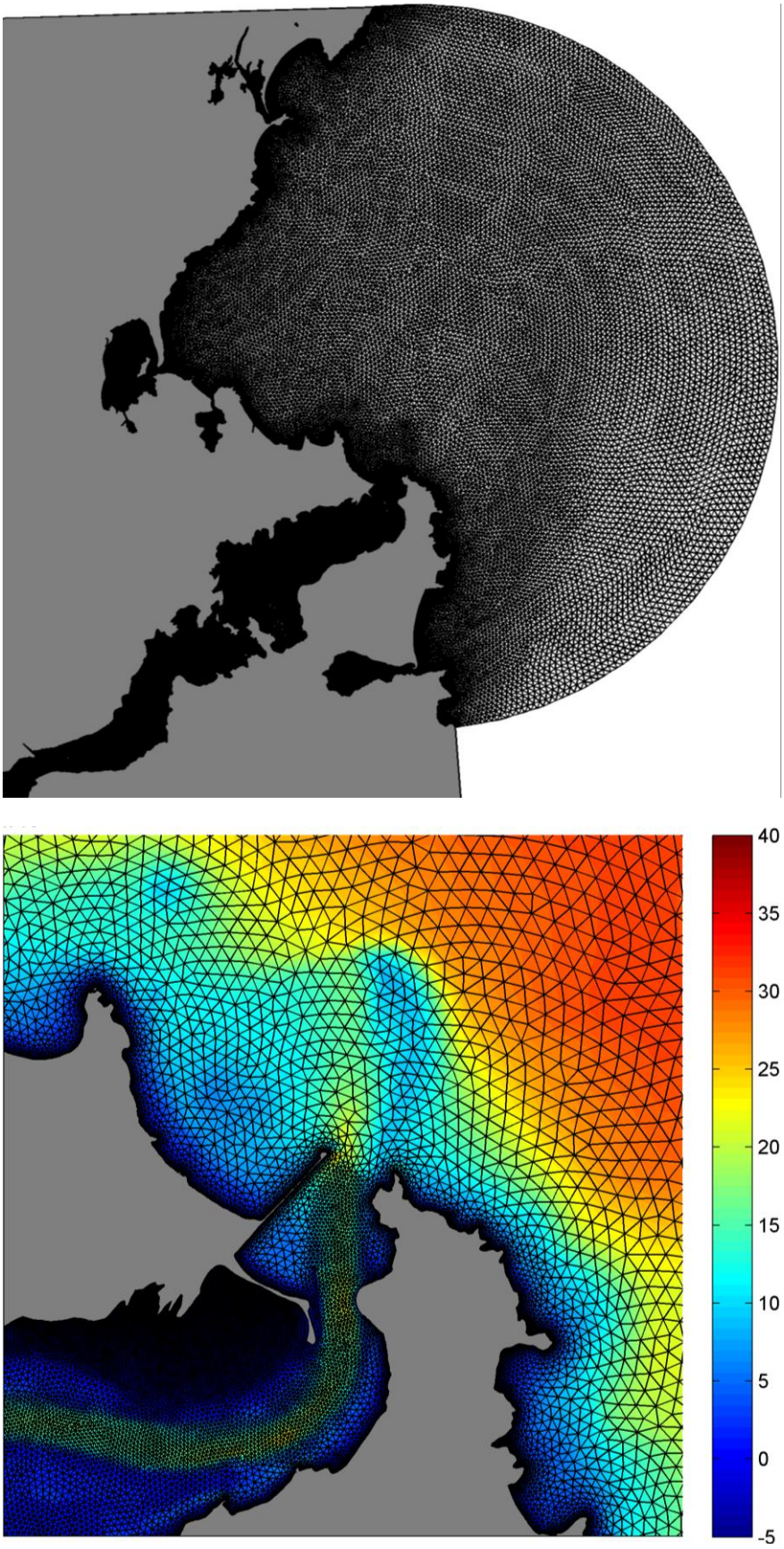

Figure 2.1 The hemispheric SELFE model domain (upper) and a zoomed in view of the entrance region with bathymetry (lower).

2.2. Local hydrodynamics, waves and sediment transport modelling (DELFT3D)

The Delft3D numerical model system (Lesser et al., 2004) was used to carry out the numerical simulations of coupled wave, current and sediment transport. The modelling system consists in three modules:

- Delft3D-WAVE is a nearshore wave propagation model which simulates the evolution of the incoming wave field.
- Delft3D-FLOW is a multi-dimensional (2D or 3D) hydrodynamic model which calculates non-steady flows and transport phenomena that result from tidal, meteorological and wave forcing.
- Delft3D-MOR computes the sediment transport fluxes and the resulting morphodynamic evolution based on the combined action of currents and waves.

The three modules are fully coupled to simulate the morphodynamic feedbacks. Every coupling time step, a new flow field (depth-averaged currents and water levels) is supplied from the hydrodynamic module to the wave module. The wave module propagates waves within the domain, accounting for the ambient hydrodynamics, and in turn provides radiation stress fields and basic wave parameters that will be used as forcing by the hydrodynamic module. Delft3D-MOR computes sediment transport based on the combined wave and current action, and updates the seabed morphology, thus affecting subsequent wave and flow computations.

Note that the updating of the seabed morphology can be switched off. In that case, the sediment transport fluxes are computed, but the model bathymetry is left unchanged. This is a useful option for studying general sediment transport pathways, without the unrealistic divergence that can occur due to uncorrected non-linear feedbacks between waves, currents and morphology. At this stage of the study, the model was run in non-updating mode to investigate the main sediment transport patterns in the entrance region and in the vicinity of the Long Mac.

2.2.1. Delft3D-WAVE

The third-generation SWAN model (Simulating WAves Nearshore) is used as the wave module (Holthuijsen et al., 2007). SWAN computes the evolution of random, short-crested waves in coastal regions with deep, intermediate and shallow water depths. The SWAN model accounts for (refractive) propagation due to depth and current and can represent the processes of wave generation by wind, dissipation due to white-capping, bottom friction and depth-induced wave breaking, and non-linear wave-wave interactions explicitly with state-of-the-art formulations (Deltares, 2013a).

For the present work, the local wave model boundary conditions are nested 2D spectral boundaries obtained from a regional scale grid forced by idealized wave events. This allows retaining the spatial variability of the incident wave field due to large scale regional refraction and sheltering effects. Bottom friction was modelled using the formulation of Collins (1972) and the default coefficient value of 0.015. Wave breaking was

modelled using a constant critical wave height to water depth ratio of 0.73 with a proportionality coefficient for the rate of dissipation of 1. No meteorological forcing was applied, so friction and wave breaking are the only dissipative mechanisms considered.

Since no updating of the seabed was considered, wave conditions were updated every 3 hours using the hydrodynamic field provided by the hydrodynamic module. This allowed saving some computational time while still representing variation of wave energy penetration due to tidal effects.

2.2.2. Delft3D-FLOW

The hydrodynamic module Delft3D-FLOW solves the Navier-Stokes equations for an uncompressible fluid under the shallow water and Boussinesq assumptions. The system of equations consists of the horizontal equations of motion, the continuity equation, the transport equations for conservative constituents, and a turbulence closure model. The details of equations and associated sub-models are fully described in Lesser et al.(2004) and the Delft3D-FLOW user manual (Deltares, 2013b)

The model was run in 2D mode, thus providing water levels and depth-averaged flows at each computational time step. Bed shear stresses are computed using a standard quadratic friction law using the bed roughness predictor of Van Rijn (2007) for the friction coefficients. The Van Rijn model allows prediction of time and spatially varying bed roughness based on basic hydrodynamic parameters and sediment characteristics. The non-linear enhancement of the bed shear stress in presence of waves was taken into account by means of the wave-current interaction model of Van Rijn et al. (2004). Turbulence effects are modelled using constant background horizontal and vertical eddy viscosity and eddy diffusivity coefficients. Horizontal background eddy viscosity and diffusivity are set equal to 5 m^2/s. A value of 10e-6 is used for the vertical background viscosity and diffusivity.

Water levels were prescribed at the northern (offshore side) and southern (harbour side) boundaries of the model domain, and so called “Neumann boundary conditions” were used on the cross-shore domain boundaries. Specifying cross-shore boundary condition can be problematic since a combination of processes will act throughout the model domain and may result in a water level and/or velocity distribution differing from that prescribed. Neumann boundaries let the model determine the correct solution at the boundaries imposing an alongshore water level gradient instead of a fixed water level or velocity (Roelvink and Walstra, 2006). Given the limited extents of the model domain, a uniform zero gradient was assumed along the domain lateral boundaries. The water levels prescribed at the model boundaries were generated from the regional scale (SELFE) tidal model, at half hourly interval. A time period covering several spring tidal cycles (16/04/2011 - 20/04/2011) was simulated to capture some of the most critical flows expected in the entrance region.

A time step of 3 seconds was used for the Delft3D-FLOW simulations, equivalent to maximum Courant numbers of approximately 8. The Courant number is a numerical stability criterion that needs to be less than 10 in Delft3D-FLOW (Deltares, 2013b).

2.2.3. Delft3D-MOR

The module Delft3D-MOR combines the information provided by the flow and wave modules to compute the sediment transport fluxes. The seabed level can then be updated as a result of the sediment sink and sources terms and computed transport gradients.

The updated expressions of Van Rijn, known as TRANSPOR2004 (Van Rijn, et al., 2004; Van Rijn, 2007a; Van Rijn, 2007b) were used to calculate the total sediment transport, including the bed load transport q_b and the suspended load transport q_s.

The bed load transport component consists of a current-related contribution (in the current direction), and a wave-related contribution (in the wave direction, following or opposing, depending on conditions). The suspended load transport includes a current-related contribution, due to advective processes (in the current direction) and the wave-related contribution, (in the wave direction, always onshore). Both wave contributions account for the wave asymmetry effects that develop as waves propagate in shallow waters due to non-linear processes.

The computation of the bed-load transport is based on the concept of the instantaneous bed-shear stress. The instantaneous bed-load transport rate $q_{b,t}$ is related to the instantaneous bed-shear stress, which is based on the instantaneous velocity vector (including both wave-related and current-related components; numerical intrawave approach) defined at the top of the bed load layer (i.e. small height above seabed) (Van Rijn, 2007 a). The oscillating wave-induced near bed orbital velocity due to asymmetry effects is modelled using the method of Isobe–Horikawa (1982) modified by Grasmeijer (2002).

The instantaneous bed load transport is computed as follows:

$$q_{b,t} = 0.5\,.\,\rho_s\,.\,d50\,.\,D_*^{-0.3}\,.\left(\frac{\tau_{b,cw,t}}{\rho}\right)^{0.5}\left(\frac{\max(0,\tau_{b,cw,t}-\tau_{b,cr})}{\tau_{b,cr}}\right) \qquad (2.1)$$

in which ρ_s is the sediment volumic mass, d50 is median grain size, D* is the dimensionless particle size, ρ is water volumic mass, $\tau_{b,cw,t}$ is the instantaneous bed shear stress due to combined wave and current action and $\tau_{b,cr}$ the critical bed shear stress according to Shields.

The net bedload transport vector is obtained by time-averaging of the instantaneous bed-load transport vector over a wave period T.

$$q_b = \frac{1}{T}\int q_{b,t}\;.dt \qquad (2.2)$$

Furthermore, the magnitude and direction of the bed load transport vector can be adjusted for bed slope effects.

The current-related suspended load transport consists in the transport of sediment particles by the time-averaged current velocities. It is calculated as the product of the velocity profile and the concentration profile, obtained by solving the advection-diffusion equation (Van Rijn, 2007 b) :

$$q_{s,c} = \int_a^h u\,.\,c\,.\,dz \qquad (2.3)$$

in which is the c is concentration profile, u the velocity profile; a is the reference height (top of bed-load layer), and h is total water depth.

The wave-related suspended transport is modelled following Van Rijn (2007b):

$$q_{s,w} = \gamma . \left(\frac{U_{on}^4 - U_{off}^4}{U_{on}^3 + U_{off}^3} \right) \int_a^\delta c . dz \qquad (2.4)$$

where U_{on} and U_{off} are near-bed peak orbital velocities in onshore and offshore (wave) direction, c is the time-averaged concentration, δ the thickness of suspension layer near the bed and γ a phase lag function (0.1).

Sediment transport computations are undertaken at each computational time step of the hydrodynamic module (3 seconds).

Each contribution to the total sediment transport can be separately calibrated using the coefficients f_{BED}, f_{SUS},f_{BEDW},f_{SUSW}, for the bed load transport due to currents, suspended transport due to currents, bed load transport due to waves and suspended load due to waves. In this study these coefficient were set to [1.0 1.0 1.0 0.3] respectively. A reduced value for f_{susw} was used according to suggestions in Van Rijn et al. (2004). Briere and Walstra (2006) also noted potentially unrealistic morphological evolution with a coefficient of 1 (particularly in barred beached) and used 0.3 as default value (see also Walstra et al., 2004, and Walstra et al., 2004 2008).

The sediment within the model domain was assumed to be sandy, with constant median grain size d50 of 0.3 mm. A map of sediment availability was used in simulation to reproduce non erodible areas and structures such as the Long Mac and nearshore rocky features. Sediment density was set equal to 2650 kg/m^3 and the dry bed density was set equal to 1600 kg/m^3.

2.2.4. Model Domain

The curvilinear model grids used are shown in Figure 2.2. The high resolution grid is centred on the Harbour entrance area including the Mole, Shelly Beach, and Harrington bend. The large ebb delta feature off Tairoa Heads and adjacent coastlines are also included to ensure correct representation of the complex tidal hydrodynamics (e.g. tidal jet) and properly represent the relevant the nearshore wave processes, including shoaling over the delta and wave penetration in the harbour. The wave grid used was slightly larger than the hydrodynamic grid to avoid any disturbance due to boundary effects. The hydrodynamic grid was also further refined throughout the area of interest. Grid cell sizes range from 50 m offshore to about 10-15 m near Shelly's Beach and the Long Mac.

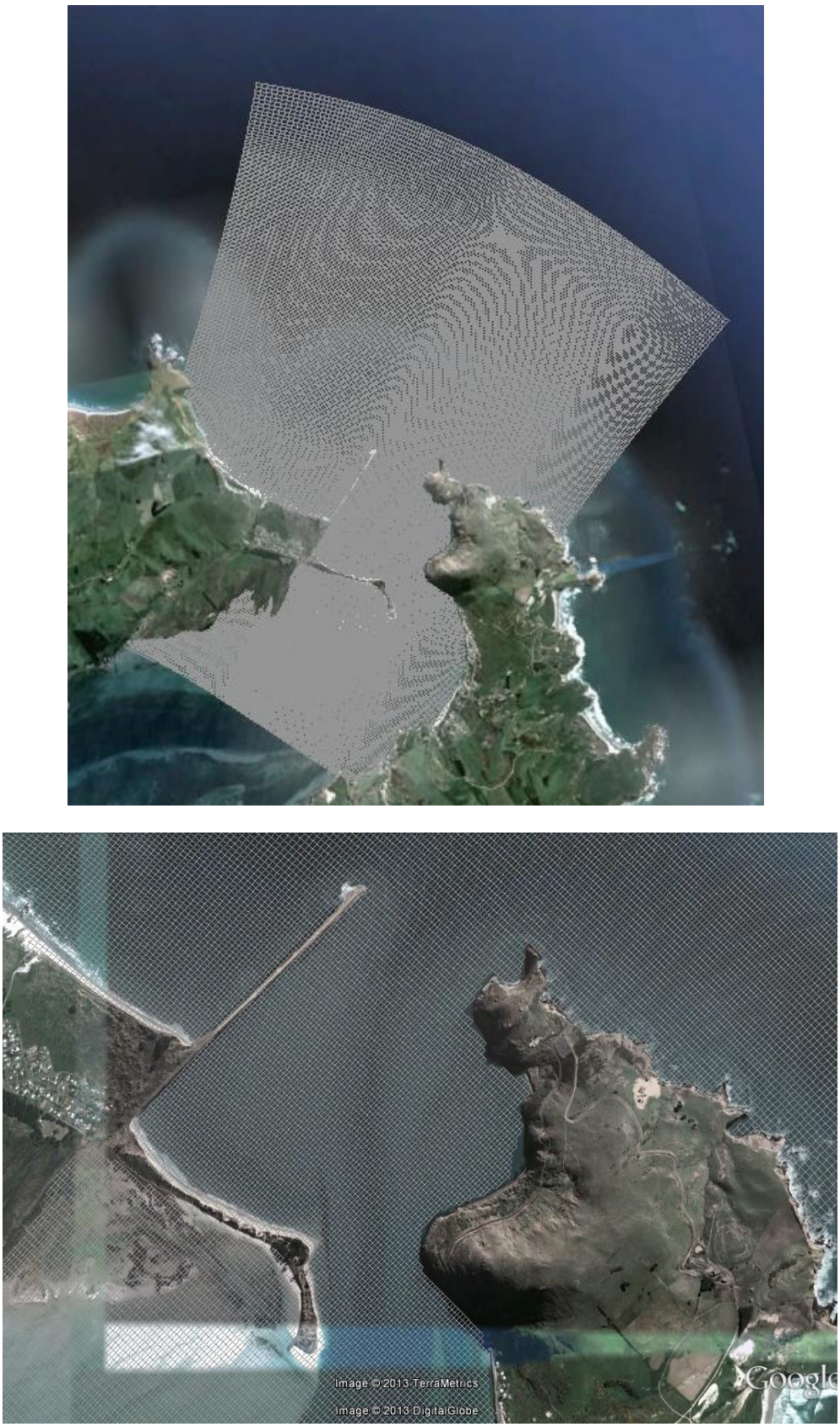

Figure 2.2 Delft3D model domain (top) and zoomed-in view near the Harbour entrance.

2.2.5. Model Setup

The key parameters used for the present study are listed in Table 2.1.

Table 2.1 Delft3D Model parameters.

Parameter	Description	Value
Wave		
BedFriction	Seabed friction formulation	collins Collins (1972)
BedFricCoef	Collins's frictions coefficient	0.015
Breaking	Depth induced breaking model	TRUE (Battjes and Janssen,1978)
BreakAlpha	Rate of dissipation	1
BreakGamma	Breaker parameter Hmax/h	0.73
WaveSetup	Wave-induced setup model	TRUE
Hydrodynamics		
Dt	Computational time step	3 s.
DryFlc	Minimum depth for drying/flooding	0.1
Vicouv	Horizontal background eddy viscosity	5
Dicouv	Horizontal background eddy diffusivity	5
Vicoww	Vertical background eddy viscosity	1.00E-06
Dicoww	Vertical background eddy diffusivity	1.00E-06
Rouwav	Model for bottom stress formulation due to combined wave and current action	#VR04# (Van Rijn et al., 2004)
BdfRou	Bedform roughness height predictor	#vanrijn07# (Van Rijn, 2007)
Sediment transport		
TraFrm	Sediment transport formulation	IFORM=-2 (Van Rijn et al.,2004)
RhoSol	Sediment density [kg/m3]	2650
SedDia	Median sediment diameter (D50) [m]	3.00E-06
CDryB	Dry bed density	1600
IniSedThick	Initial sediment layer thickness at bed [m]	space varying (5 to 0 m.)
SedThr	Minimum water depth for sediment computations [m]	0.1
Islope	Formulation of bed slope effect on bed load transport	2 (Bagnold, 1966)
AlfaBs	Streamwise bed gradient factor for bed load transport	1
AlfaBn	Transverse bed gradient factor for bed load transport	1.5
Sus	Current-related suspended sediment transport factor	1
Bed	Current-related bed-load sediment transport factor	1
SusW	Wave-related suspended sediment transport factor	0.3
BedW	Wave-related bed-load sediment transport factor	1
FWFac	Wave streaming calibration factor	0

2.3. Bathymetry data

The bathymetric dataset used for the development of the regional and local model domain bathymetries combined data from several sources including soundings and digitized nautical chart contours. In particular, a recent high resolution bathymetric survey covering the area of the Harbour entrance including the navigation channel, Shelly Beach, the Mole, the Long Mac and Harrington bend was provided by Pot Otago. Priority was given to survey data and charts contours were used in region were soundings were scarce or inexistent. Careful editing assisted with aerial photographs was employed to fill regions where no data was available, including some of the intertidal areas, and some discrete structures (e.g. subaerial section of the Long Mac). The bathymetric dataset is shown in Figure 2.3. Bathymetries of SELFE and Delft3D model domains are shown in Figure 2.4 and 2.5.

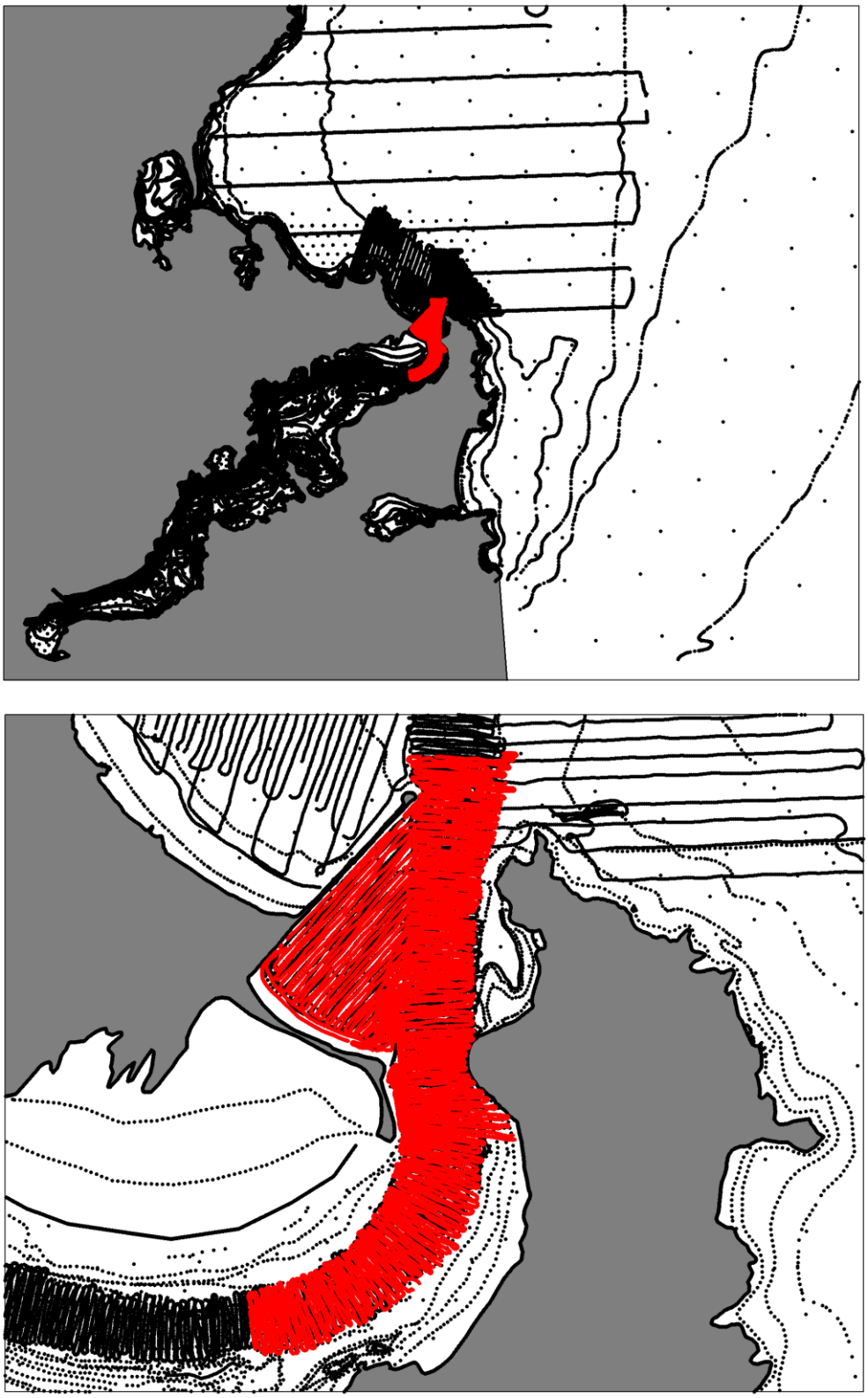

Figure 2.3 Bathymetric dataset used for model domain bathymetries. The recent survey covering the Harbour entrance is shown in red.

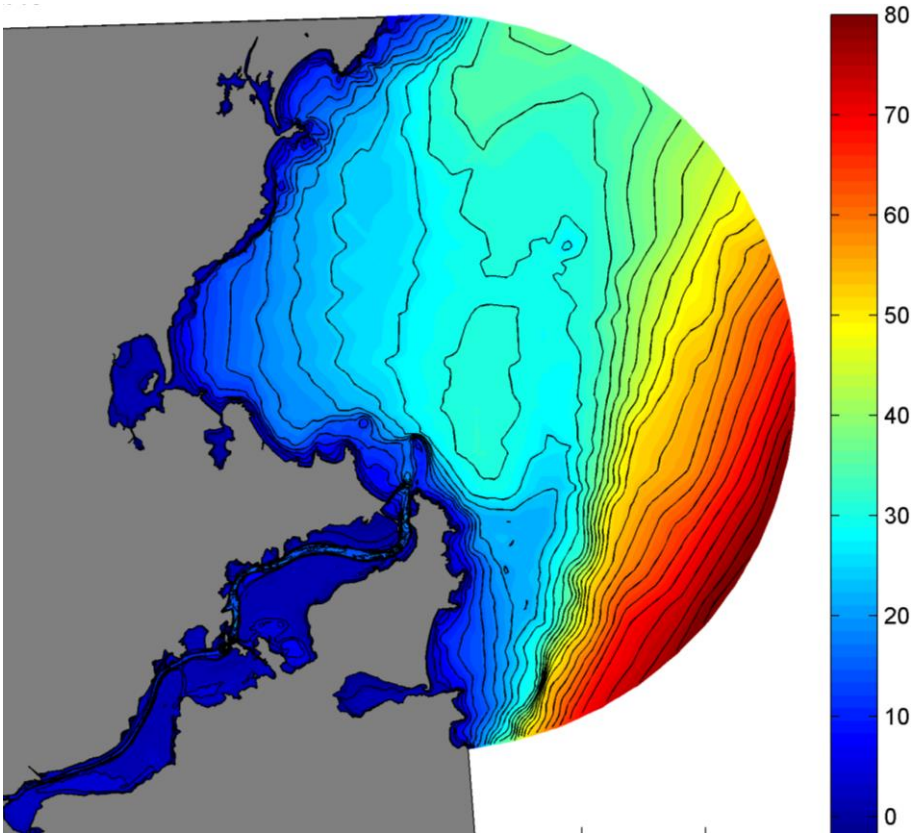

Figure 2.4 SELFE domain bathymetry.

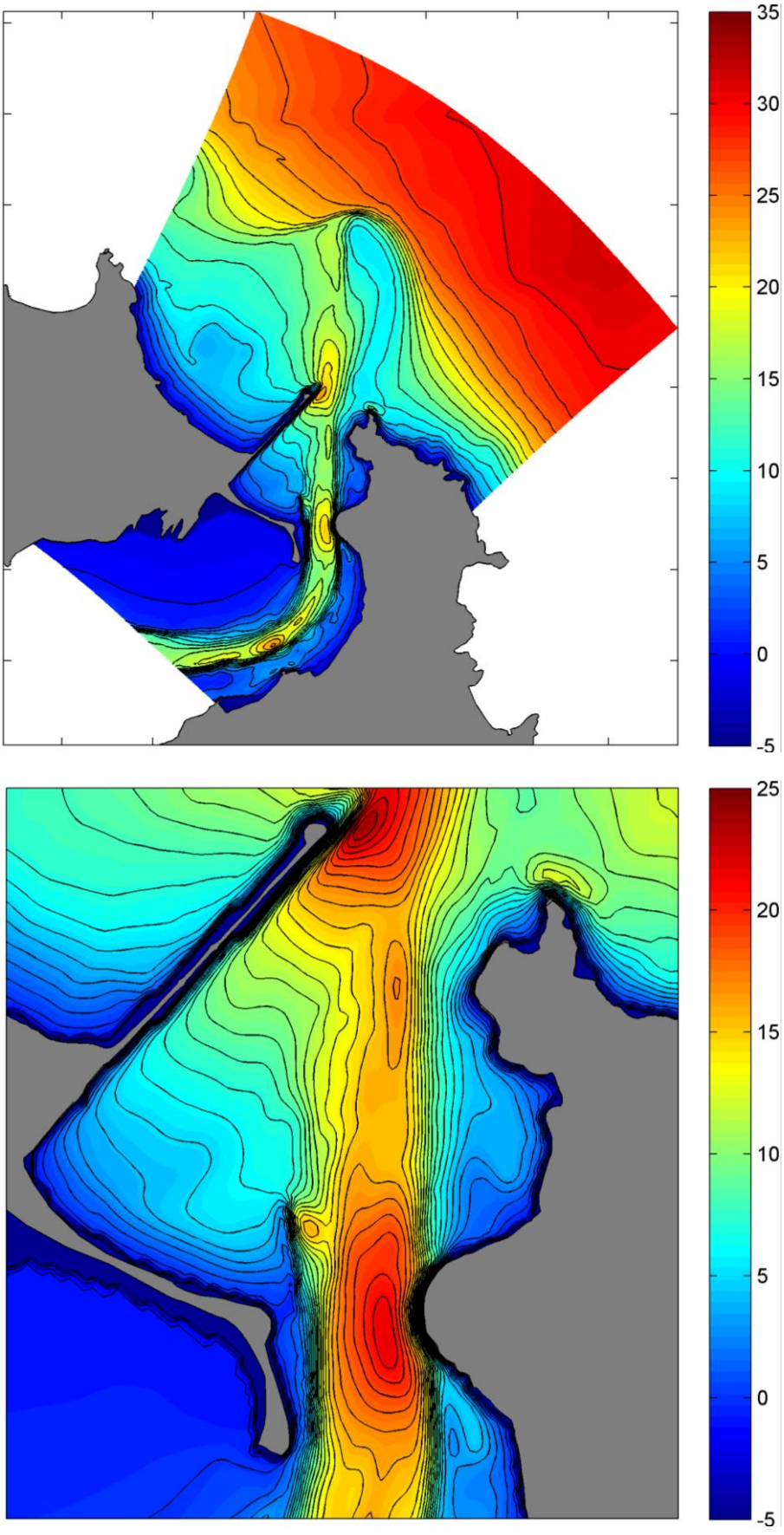

Figure 2.5 Delft3D domain bathymetry (top) and zoomed-in view of the Harbour entrance (bottom).

3. RESULTS FOR EXISTING CONDITIONS

3.1. Sensitivity analysis

To ensure robustness of the model, a qualitative sensitivity analysis was undertaken. Since we are concerned with the underlying sediment dynamics of the area rather than quantitative estimates at this stage, particular attention was given to processes that could significantly change the main flow and transport patterns developing within the Otago Harbour entrance. Based on the model setup provided in 2.2.5, without waves (i.e. tide only), some parameters were varied keeping all others the same.

3.1.1. Computational time step

As a first test, the time step of the simulation was reduced to ensure that the model was numerically stable and results were consistent for time steps within the appropriate range. The time step was reduced from 3 seconds to 1.5 seconds, thus resulting in maximum Courant numbers of ~4, which is about half of what is suggested as a limit in Deltares (2013b). No notable differences were noted and a time step of 3 seconds was retained for time efficiency reasons.

3.1.2. Friction

In Delft3D-FLOW, bottom friction can be specified following formulations of Chezy, Mannings or White-Colebrook. All these formulations require a user-input coefficient that will have direct effect on the bed shear stress estimation.

In the default setup, the bed roughness height predictor of Van Rijn (2007) is used to provide estimates of the instantaneous roughness height field (based on wave, flow and sediment parameters) in turn providing space and time-varying Chezy coefficients. This predictor provides the most sophisticated way of treating the bottom friction in Delft3D to date since instantaneous friction coefficient fields are estimated for each computational time step, which is potentially more realistic. To ensure overall consistency in results, simulations using a simpler constant Chezy or Manning coefficient, as commonly applied for coastal simulations, were undertaken for comparison with the model results with the default setup. It is noted that specifying a constant Mannings coefficient will result in friction coefficients dependent on the water depth, while a constant Chezy coefficient result in a truly constant friction coefficient throughout the model domain. Chezy coefficient of 50 and 65 and Mannings coefficient of 0.02 and 0.026 were used. They are within a range commonly used in coastal applications (e.g Deltares, 2013b Briere and Walstra, 2006) and also in the range obtained using the bed roughness predictor.

The different schemes and coefficients tested did modulate the magnitude of flows and sediment transport fluxes but main patterns were conserved with only slight variations in directions. Only the case with a constant chezy coefficient of 50 resulted in some unrealistic sediment transport fluxes on the steepest slopes of the channel. (Note that a smaller Chezy coefficient is equivalent to a larger friction). Given the overall consistency in results, the predictor of Van Rijn (2007) was conserved as default friction scheme.

3.1.3. Eddy viscosity

In coastal applications, model grids are generally too coarse and time step used too long to resolve all the turbulent scales of motions. Turbulent processes at sub-grid scale and associated energy dissipation is modelled using an eddy viscosity model. In the present study a model with constant eddy viscosity coefficient is used. The coefficient will also affect the behaviour of the flow including formation of larger eddies developing at grid scale. More simply, it can be seen as a measure of how viscous or "thick" the seawater mass will be as it propagates over the bathymetry. The value of the horizontal eddy viscosity coefficient depends on the flow and the grid size used in the simulation. The grid used here is relatively detailed and will resolve much of the details of the flow and a typical range for the coefficient value is 1 to 10 m^2/s. (Deltares, 2013b). Coefficients of 1,5, and 10 were tested.

Snapshots of circulations within the Harbour entrance with different eddy viscosity coefficients are shown in Figures 3.1 and 3.2 for outgoing and incoming tides. During an outgoing tide, the ebb flow spreads and slightly weakens past the Long Mac seaward tip and the flow portion that veering westwards tend to drive a return easterly flow along Shelly beach. The eddy viscosity coefficient has an effect on the flow "spreading" and in turn modulates the magnitude of the return flow along Shelly Beach. A smaller coefficient results in more water veering westwards and a stronger return flow along Shelly Beach. A distinct eddy is visible just west of the Long Mac for the simulation with an eddy viscosity of 1 m^2/s. As the tide comes in, a water level gradient is expected to develop along Shelly Beach, relative to the channel level. This drives a longshore easterly flow along the beach that accelerates over the Long Mac. Consistent patterns are reproduced for the different eddy viscosities with slight variations in flow direction and magnitudes. The main difference is a return flow that develops along the Mole for a coefficient of 1 m^2/s that is not reproduced in the other cases.

The difference in circulation and eddy formation is clearly relevant with respect to the morphodynamic response of the area. However, these processes are hard to verify without field information. The central range value of 5 m^2/s was conserved.

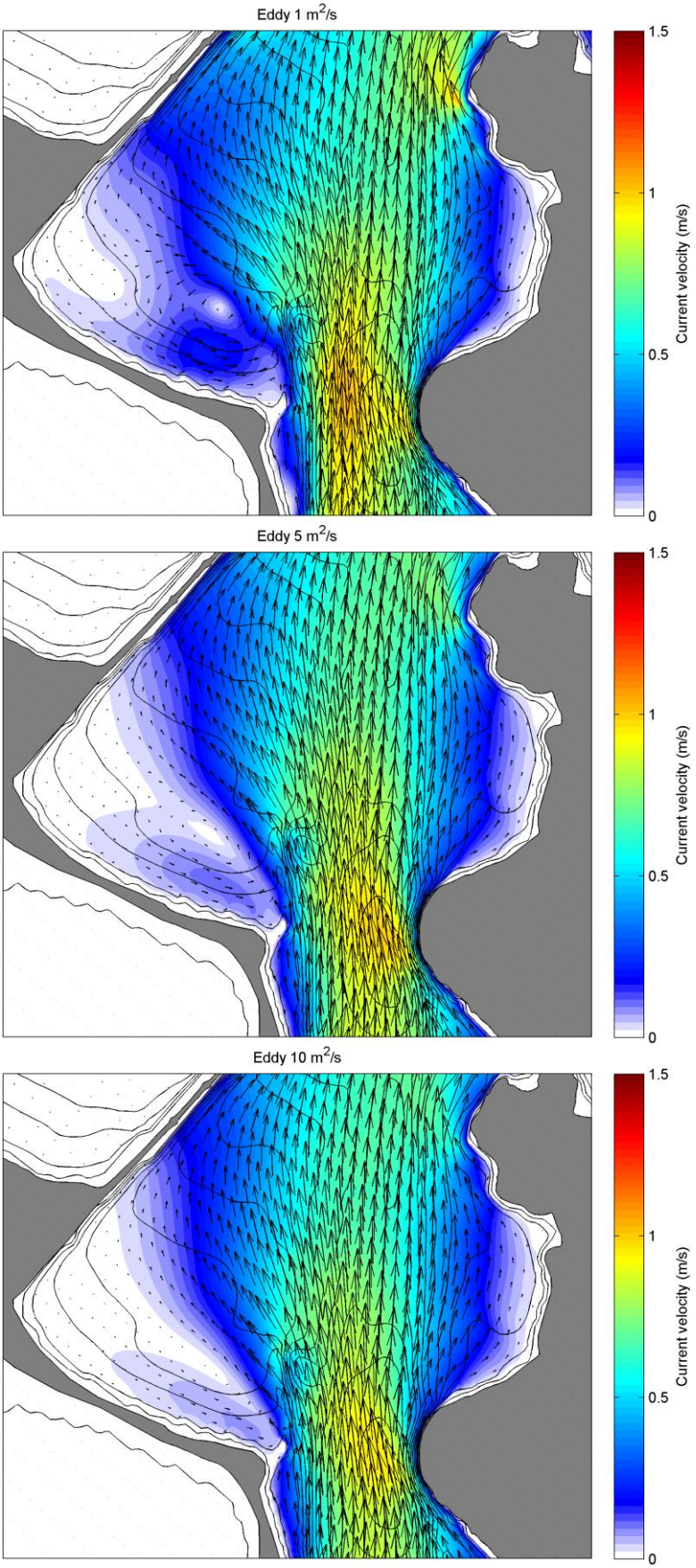

Figure 3.1 Snapshot of modelled flow fields with different eddy viscosity coefficients at an outgoing tide.

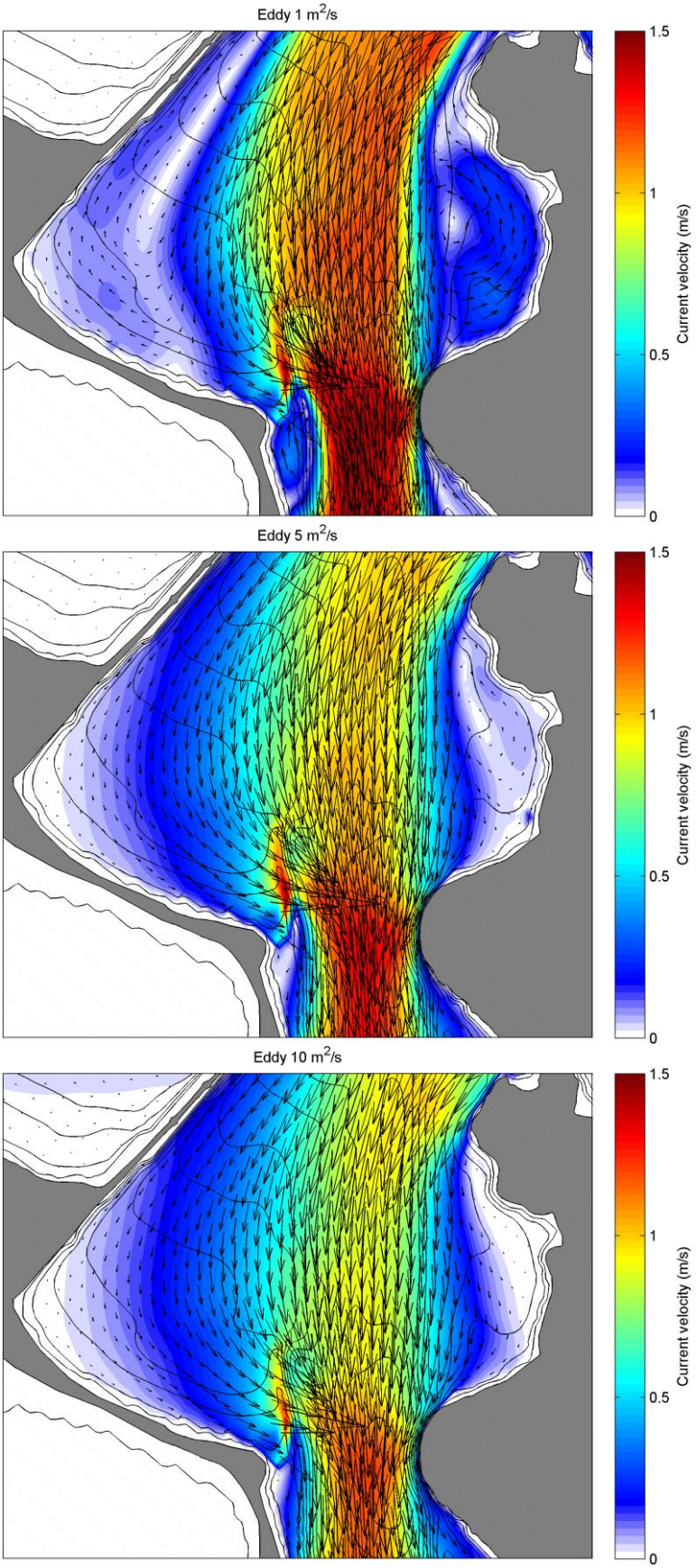

Figure 3.2 Snapshot of modelled flow fields with different eddy viscosity coefficients at an incoming tide.

3.1.4. Grain size

The specified median grain *d50* is a key parameter in the computations of the bed roughness field and sediment transport fluxes, particularly the bed-load fraction. The default value of 300 microns used in the basic setup was supplemented by simulations using *d50* of 200 and 400 microns.

The roughness predictor appears to be relatively stable with respect to the user-input *d50* and derived friction coefficients are relatively consistent. An example at a given time step is given in Figure 3.3. This will modulate flow magnitudes but is not expected to induce any significant variations in flow patterns. Predicted transport fluxes for the different grain sizes are compared in Figure 3.4 and 3.5. Difference in magnitude are clearly visible however underlying patterns are quasi identical. Given the absence of field information these flux magnitudes can hardly be calibrated. This is not critical at this stage since we are more concerned with general sediment patterns rather than quantitative estimates.

3.1.5. Conclusion

Based on the brief sensitivity analysis, it is identified that the eddy coefficient will potentially have the most effects in the predicted flows and transport patterns. However, results are still relatively consistent and it is expected that the default model setup will allow identifying the key processes of the area. Variations related to friction and grain size are not significant at this stage but are identified as important parameters for future applications when a more quantitative approach is required.

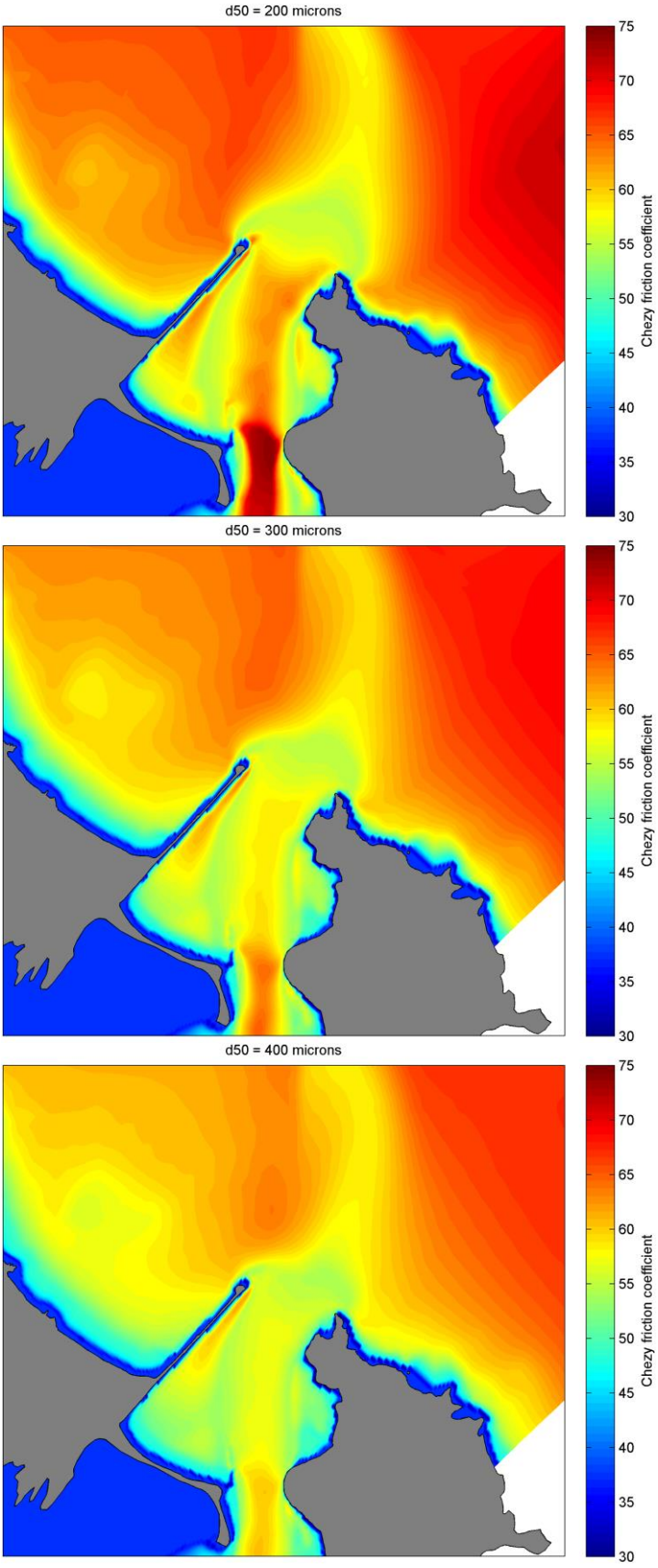

Figure 3.3 Predicted Chezy friction coefficients using the bed roughness predictor of Van Rijn (2007) for different median grain sizes, at same time step.

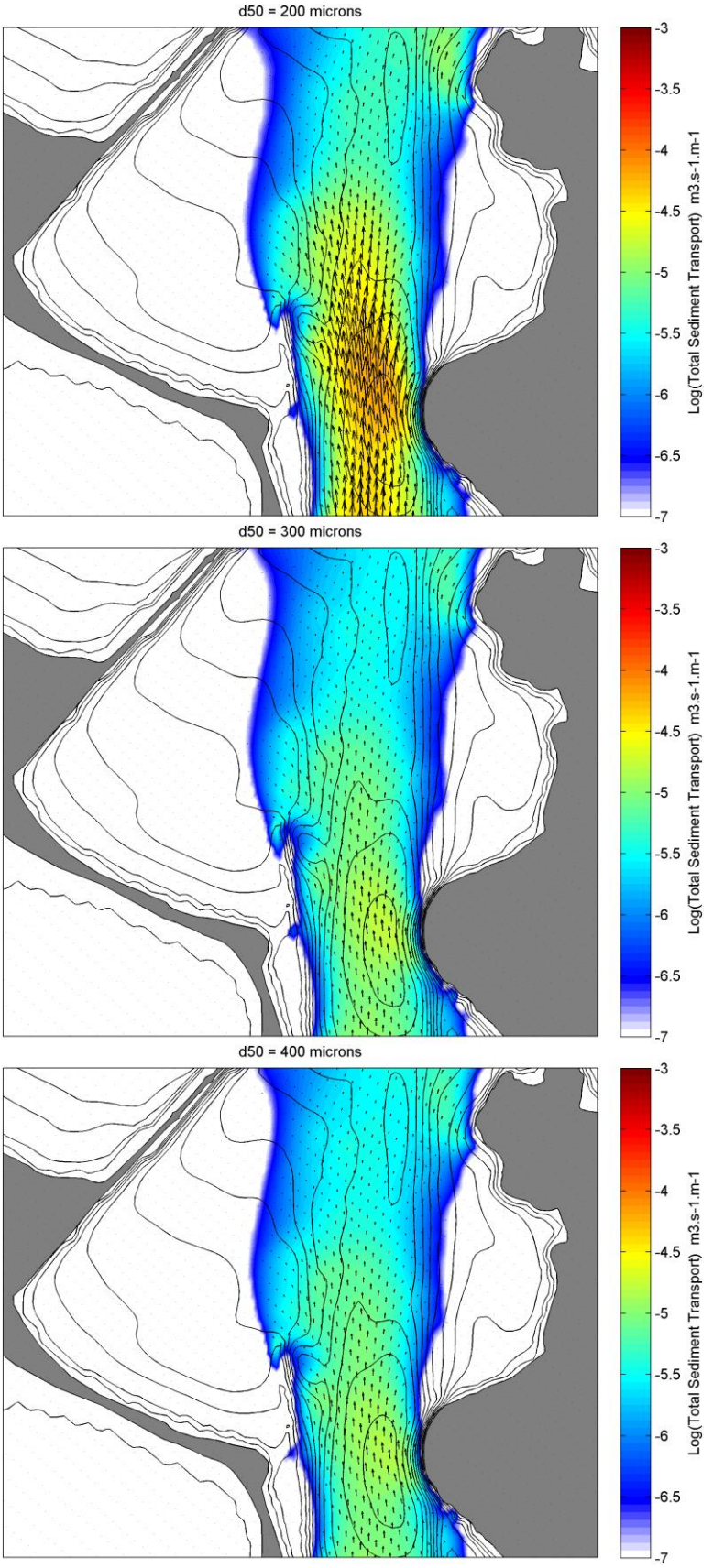

Figure 3.4 Snapshot of modelled total sediment transport fluxes with different median grain sizes at an outgoing tide.

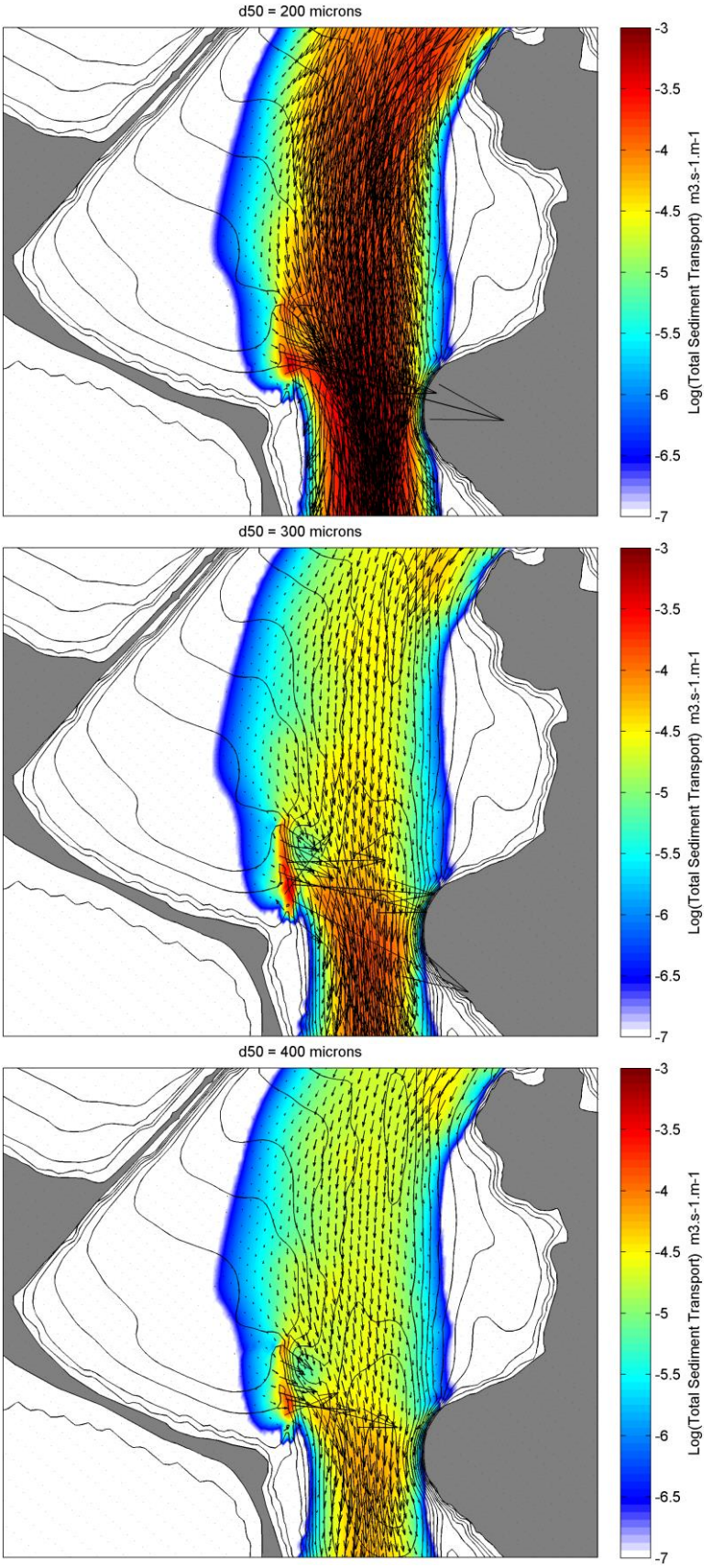

Figure 3.5 Snapshot of modelled total sediment transport fluxes with different median grain sizes at an incoming tide.

3.2. Scenario results

3.2.1. Events simulated

For all events, the simulation period covered several spring tidal cycles (16/04/2011 - 20/04/2011) to capture some of the most critical ambient tidal flows expected to occur in the entrance region. The model was run without wave action to get a picture of the underlying hydrodynamics, and for different idealized wave events. The idealized events aimed at covering the range of wave conditions expected at the site, with a particular interest on cases when wave energy penetration within the entrance area and potential for sediment transport is important. Wave events were selected based on joint probabilities available from a previous study (MetOcean Solutions Ltd., 2011). Events are summarized in Table 3.2. They include large swells from the southeast and northeast, and both high energy swell and low energy sea waves from the north.

To identify the key transport pathways within the entrance region, the simulation outputs were averaged over the incoming and outgoing tidal phases, and over the complete tidal cycles. Incoming and outgoing phases were defined based on the water level at the mouth. These averaged outputs are supplemented by particular model snapshot.

Table 3.1 Simulated events

Simulations	Hs (m)	Tp (s)	Dp (deg. true)
SE event	3	14	135
NE event	3	10	45
N event swell	2	14	0
N event sea	1	8	0

3.2.2. Tidal circulation and sediment transport

Snapshots of peak ebb and flood flows are shown in Figures 3.6. During an outgoing tide, strong water level gradients due to the water mass retained within the Harbour drive a clear ebb jet. The flow is constricted by the Harbour mouth and slightly widens past the seaward tip of the Long Mac. The jet extends well offshore, following the channel along the large submerged delta bar. During a flood tide state, opposed water level gradients drive strong southwards flows within the channel as the Harbour fills. It is evident that the entrance region enclosed by the Mole fills in faster than the volume that can enter the Harbour and as a result a water level gradient develops along Shelly Beach. This drives an easterly-directed flow along the beach that accelerates over the Long Mac as it meets the constricted channel flows.

To serve as a reference point for future comparison with cases with wave action, incoming, outgoing and full-cycle averaged flows and transport fields were processed for the tide-only simulation (Figs. 3.7 to 3.9). For incoming tides, the mean flow pattern appears as a smoothed version of the peak flood flow shown in Figure 3.6. There is a distinct alonghsore current along the eastern half of Shelly Beach, which accelerates over the

Long Mac before meeting with the channel flood flows constricted by the mouth.

This process is very significant with respect to potential sediment recirculation in the Harbour. Sediment transport vectors over the Long Mac are clearly directed eastwards and to the channel and tend to direct sediment towards the area of increased ambient southwards transport developing throughout the mouth due stronger constricted flow velocities. However it is noted that the transport further west from the structure rapidly reduces. This means that the tide-driven alongshore flow is not of sufficient strength to mobilize sediments from Shelly Beach.

Outgoing tidal flows and transport are shown in Figure 3.8. The ebb jet clearly dominates the flow and transport regime at outgoing tide phases. The Long Mac tends to slightly constrain the local jet, and a slight spreading of the flow is visible past its seaward tip. The full cycle mean maps (Fig. 3.9) reproduce the 2 main features discussed above with a net northwards flow within the channel and a net east-southeast component along Shelly Beach and over the Long Mac.

3.2.3. Wave-driven circulation and sediment transport

The tidal processes identified in 3.2.2 will be modulated by the wave-driven currents and water level setups when wave energy penetrates the entrance region.

Mean significant wave heights for the different wave events simulated are shown in Figures 3.10 and 3.11. For the southeast and northeast events, the wave energy tends to predominantly reach the western half of Shelly Beach (Fig. 3.10). A secondary region of larger height is noted in the bay east of the channel that receives wave energy refracted by the channel margin. Larger heights are experienced for the northeast event with significant wave heights of 1.5-1.8 m along the beach. The northerly events result in a more homogeneous height distribution along the beach. A distinct band of larger height reaching the centre of the beach develops for the long period swell event. Note that the local bathymetry showing remnant of the dump mounds will further focus incident wave energy. The Long Mac structure is seen to provide some limited sheltering from incident waves during the high energy northeast and north events along the eastern end of Shelly Beach. Some mild focusing of wave heights can be identified on the seaward tip of the structure.

Mean incoming flows are shown in Figure 3.12 for the southeast and northeast events. The underlying tidal flow patterns are mostly conserved but some wave-driven flows develop along the beach. Flow velocities in the Long Mac vicinity are slightly stronger for the northeast case, which is due to the larger transmitted wave energy and a relative increase in the local water level gradients. More significant differences relative to the tide-only case are visible in the mean incoming sediment transport maps (Figure 3.13). The wave action results in an onshore transport flux at Shelly Beach and mobilization of the sediment along the beach. This is the most distinct for the northeast event for which ambient wave energy is larger. Easterly transport fluxes are predicted in the vicinity of the Long Mac, with stronger magnitude for the northeast event.

The mean incoming flows and transport for the northerly events are compared in Figures 3.14 and 3.15. For the swell event, the wave energy forces an alongshore westerly flow along the western half of Shelly Beach, eventually being redirected (clockwise) along the Mole. Easterly sediment transport fluxes are reproduced in the vicinity of the Long Mac however it is noted that the transport magnitude for the northerly swell event is visibly less than that for the northeast event (Fig. 3.13). This is likely due to a different water level gradient distribution along the beach during the northerly swell event, for which the more central position of transmitted wave energy and associated water level setup will force some of the incoming water mass west and along the Mole rather than east towards the Long Mac and channel. As expected, the wave-driven sediment transport is much less for the low energy sea wave event.

Results for the outgoing tide phases are shown in Figures 3.16 to 3.19. The mean outgoing flow field for the southeast and northeast events (Fig. 3.16) indicates that the circulation is still dominated by the ebb jet. For the northeast event, a wave-driven return flow develops along the western half of Shelly Beach and corresponds in the sediment transport map (Fig. 3.17) to a distinct westerly longshore transport vector. This feature was not present in at incoming tide phases. This is likely due to the ambient tidal water levels gradients working against such flow at during incoming tides (see water levels during peak flood flows Fig. 3.6). Comparison of mean wave heights during incoming and outgoing tide phases (Fig. 3.24) suggest that this may also be related to slight shift of location of the band of highest wave energy along the beach. Refraction of the incident wave filed will be modified by the different water level and ambient flow fields which will result in slightly different patterns within the entrance. It is noted that the incident wave filed is subject to intense refraction processes off the entrance due to the submerged ebb delta bar (see Metocean Solution Ltd., 2013). In that case the band of higher wave energy is slightly shifted east thus forcing a return flow along the Mole. This alonghsore feature tends to dominate the sediment transport regime along the beach for the northeast event. Some wave-induced transport develops along the eastern half of Shelly Beach and in the vicinity of the Long Mac, which was not observed for the tide-only case or even the south east case. It is however an order of magnitude weaker than west of the beach. Patterns are relatively consistent but one to two orders of magnitude weaker for the southeast case, due to the less energetic ambient wave forcing.

Mean summary maps for the northerly events for outgoing tide phases are provided in Figures 3.18 and 3.19. The main wave-driven flow and transport patterns along Shelly Beach are mostly conserved relative to the incoming tide phases (Figs. 3.12 and 3.13). However, the magnitude of the longshore westerly transport along the western half of the beach is clearly enhanced for the swell event (left). This is again likely due to more favourable ambient water level gradients. A slight shift of the transmitted wave energy band towards the centre of the beach is again evident for the outgoing phases (Fig. 3.25), which seems to force the flow more to the west. A small area of wave-induced transport is visible over the tip of the Long Mac due to local wave focusing by the structure. The lower energy sea wave event results in less intense transport, limited to the intertidal region of the beach and predominantly directed offshore.

It is noted that for both northerly events and the northeast event, for both incoming and outgoing phases, some sediment is mobilized on the small bay east of the channel mouth, although generally with an order of magnitude less than along Shelly Beach.

The flow and sediment transport fields averaged over the complete tidal cycles are provided in Figures 3.20 to 3.23. Generally they reproduce and combine processes identified at incoming and outgoing phases thus providing summary maps. Features reproduced for all cases include the wave-driven onshore transport seaward of Shelly Beach, with variations in direction in magnitudes, and a net northwards (outgoing) flow and sediment transport component within the channel. The onshore transport at Shelly Beach and over the disposal ground clearly coincides with the region of transmitted wave energy. This indicates that the wave-driven transport due to wave asymmetry effects as wave propagates shoreward possibly further shoaling over the remnant mound is an important process for the area. This will result in a progressive shoreward migration of the dumped sediments, providing direct sediment supply to the Shelly Beach system. A comparison of bathymetric contours from the older data available, and that from the latest survey shows a clear onshore translation of the depth contours over an area coinciding with the general position of the wave energy band (Fig. 3.26).

More locally, some contrasting net flow patterns are obtained for the southeast and northeast events (Fig. 3.20). For the northeast event, the more significant wave energy penetration and associated wave-driven setup and flows strengthen the easterly tidal currents flowing towards the Long Mac and channel along the eastern half of Shelly Beach and drive a return flow towards the Mole, along the western part of the beach. This results in net sediment transport vectors pointing to the channel in the vicinity of the Long Mac, and longhsore sediment transport fluxes towards Shelly Beach western corner further to the west. In contrast, mean flows for the southeast case are overall very similar to the tide-only mean flow field (Fig. 3.9). With respect to sediment transport in the Long Mac vicinity, the easterly vectors are reproduced but magnitudes are smaller than for the northeast case and wave-induced transport along the beach is not significant.

The energetic northerly swell forcing (Fig. 3.22, left) disturbs the underlying net tidal flows developing seaward and along Shelly Beach, i.e. first southwards then veering eastwards and towards the channel. Wave-driven flow and water level setup result in a longshore flow towards Shelly Beach western corner and along the Mole. This “evacuation” of water through a different path reduces the flow magnitude along the Shelly Beach eastern half and over the Long Mac (relative to the tide-only case and northeast event). Interestingly, the flow component along the Mole appears to merge with incoming south-southeastwards flows further off Shelly Beach, eventually meeting with the easterly flows in the vicinity of the Long Mac. The wave-induced flow towards the Mole mobilizes sediment with distinct net northwesterly longshore fluxes. Although not obvious in the total transport maps it is expected that some of that sediment be eventually redirected in the channel vicinity through the return flow pattern off Shelly beach identified above. This return pattern is visible in net suspended transport fluxes for the north swell event (Fig. 3.27), although an order of magnitude less than the total transport fluxes shown. This signal is masked

by the bed load transport that obviously dominates the sediment transport regime. Easterly-directed sediment transport vectors due to flow acceleration over the Long Mac are again reproduced for both cases over the Long Mac. However, magnitudes are visibly smaller than for the northeast event, even for the high energy event. This is likely due to the development of a stronger return along the Mole providing a degree of "relaxation" to the flow forcing in the vicinity of Long Mac.

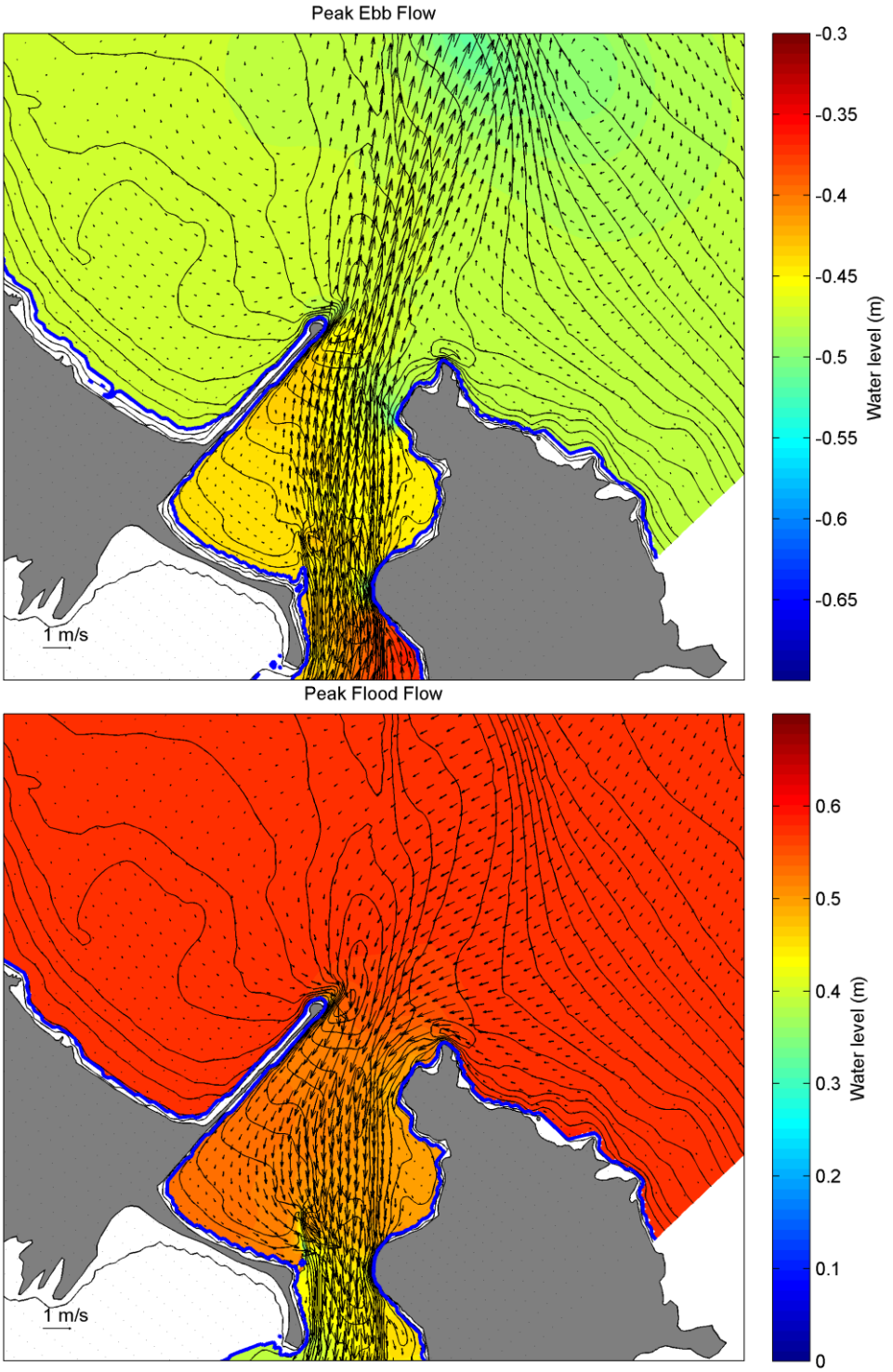

Figure 3.6 Snapshot of peak ebb (top) and flood (bottom) water levels and flow fields for the case without wave action.

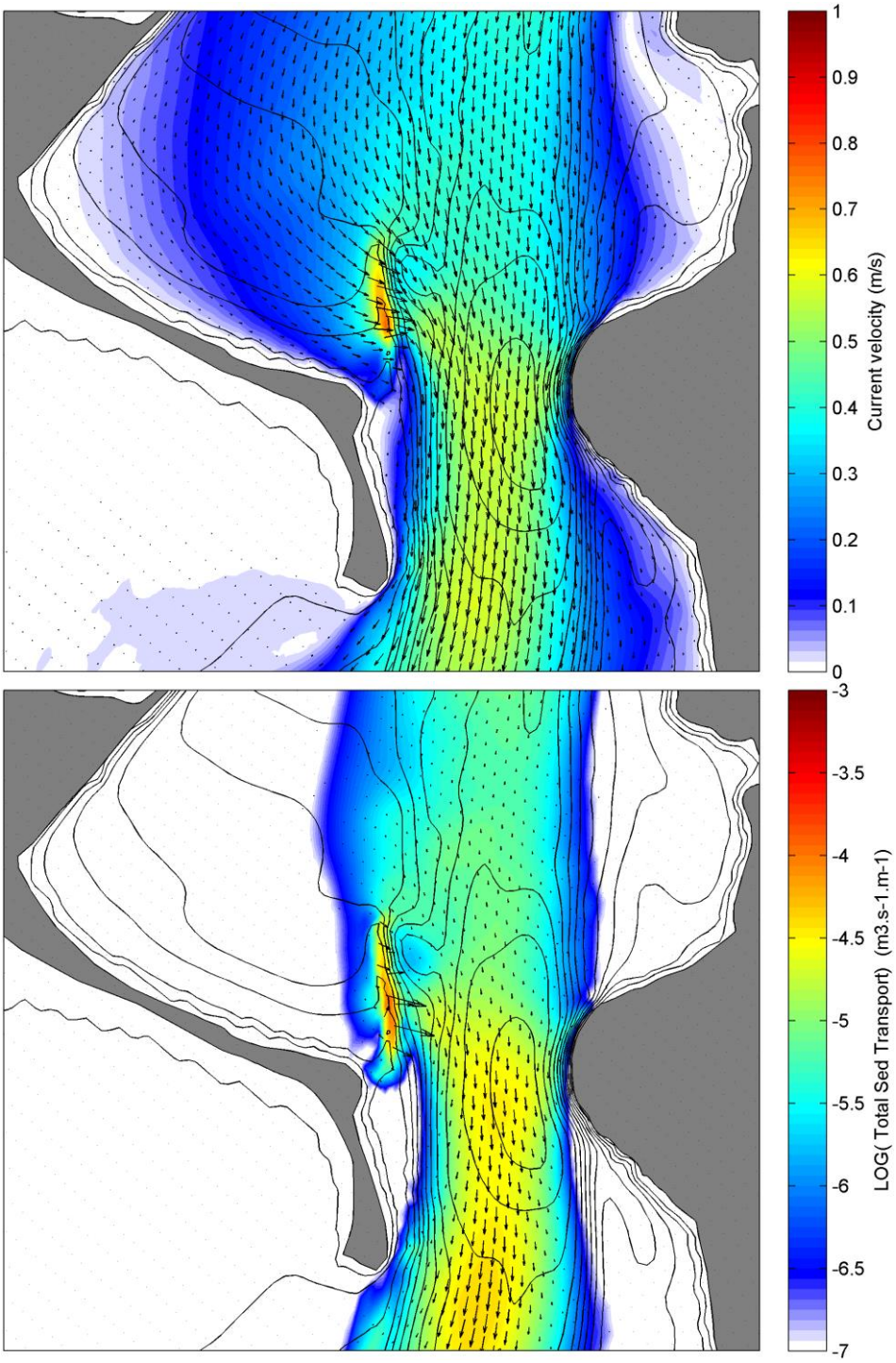

Figure 3.7 Mean flow field (top) and total sediment transport fluxes (bottom) for incoming tide phases, for the case without wave action.

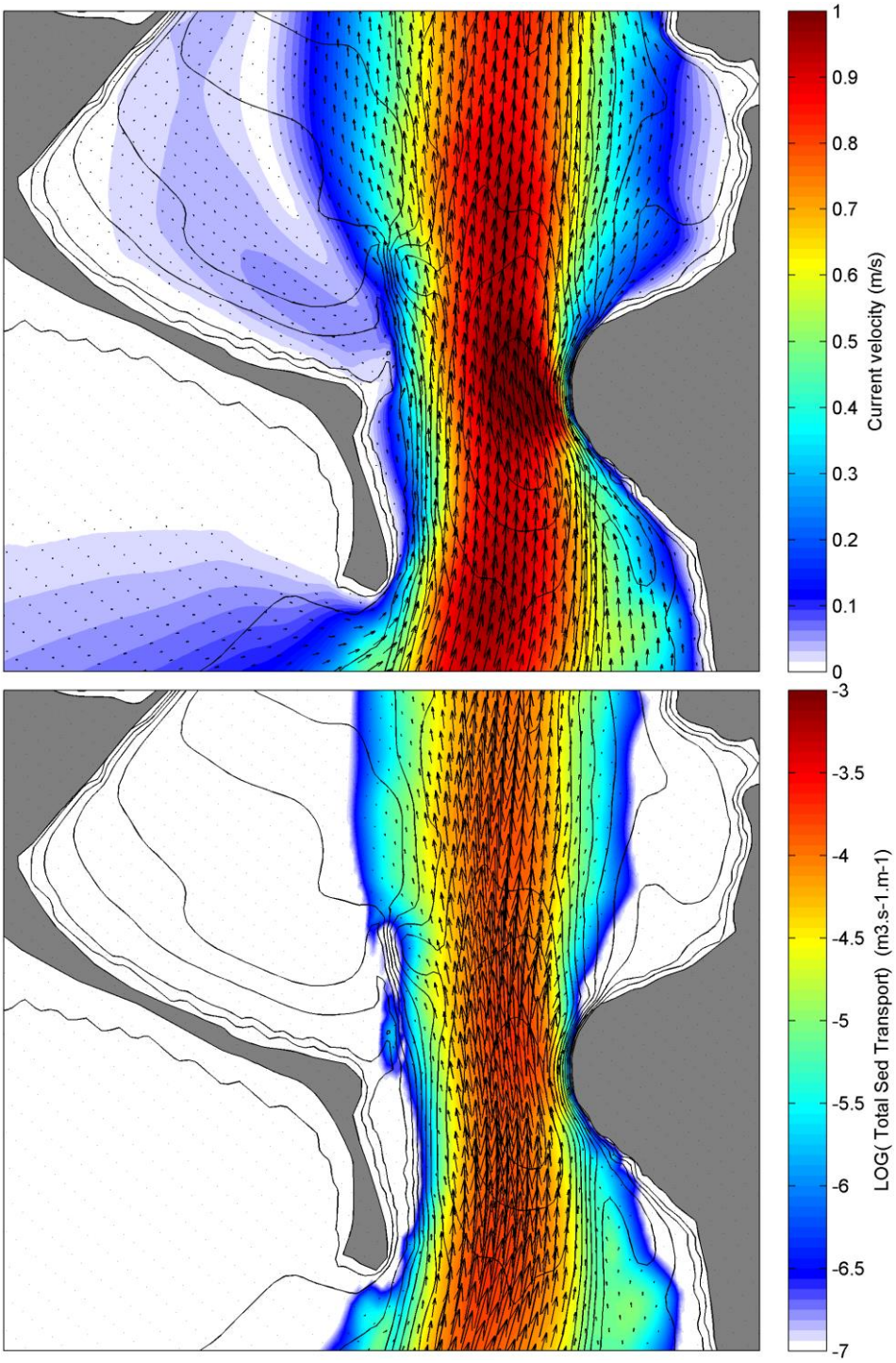

Figure 3.8 Mean flow field (top) and total sediment transport fluxes (bottom) for outgoing tide phases, for the case without wave action.

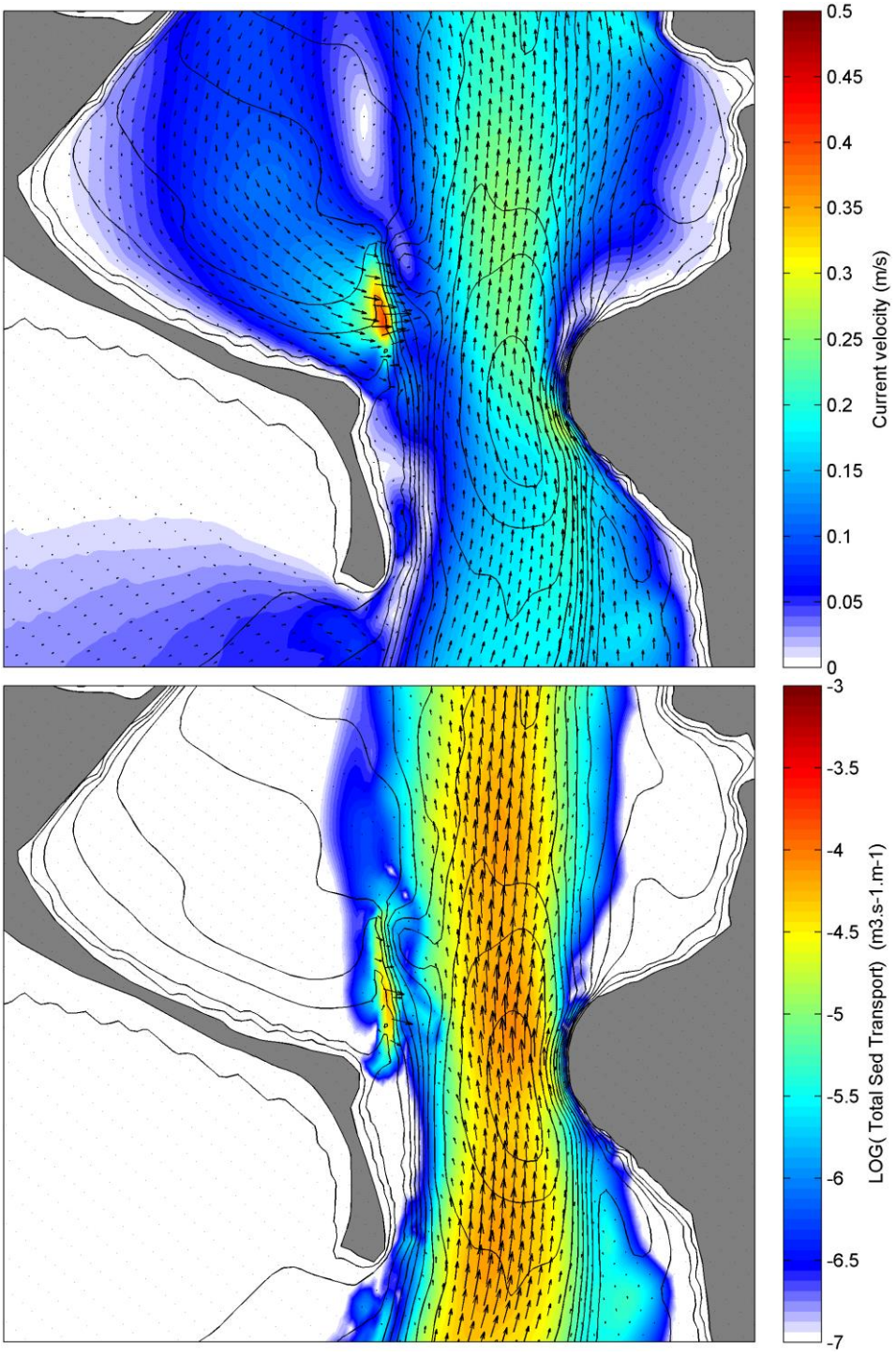

Figure 3.9 Mean flow field (top) and total sediment transport fluxes (bottom) for the full tidal cycles, for the case without wave action.

Hs=3m, Dir=135 deg., Tp=14 s.

Hs=3m, Dir=45 deg., Tp=10 s.

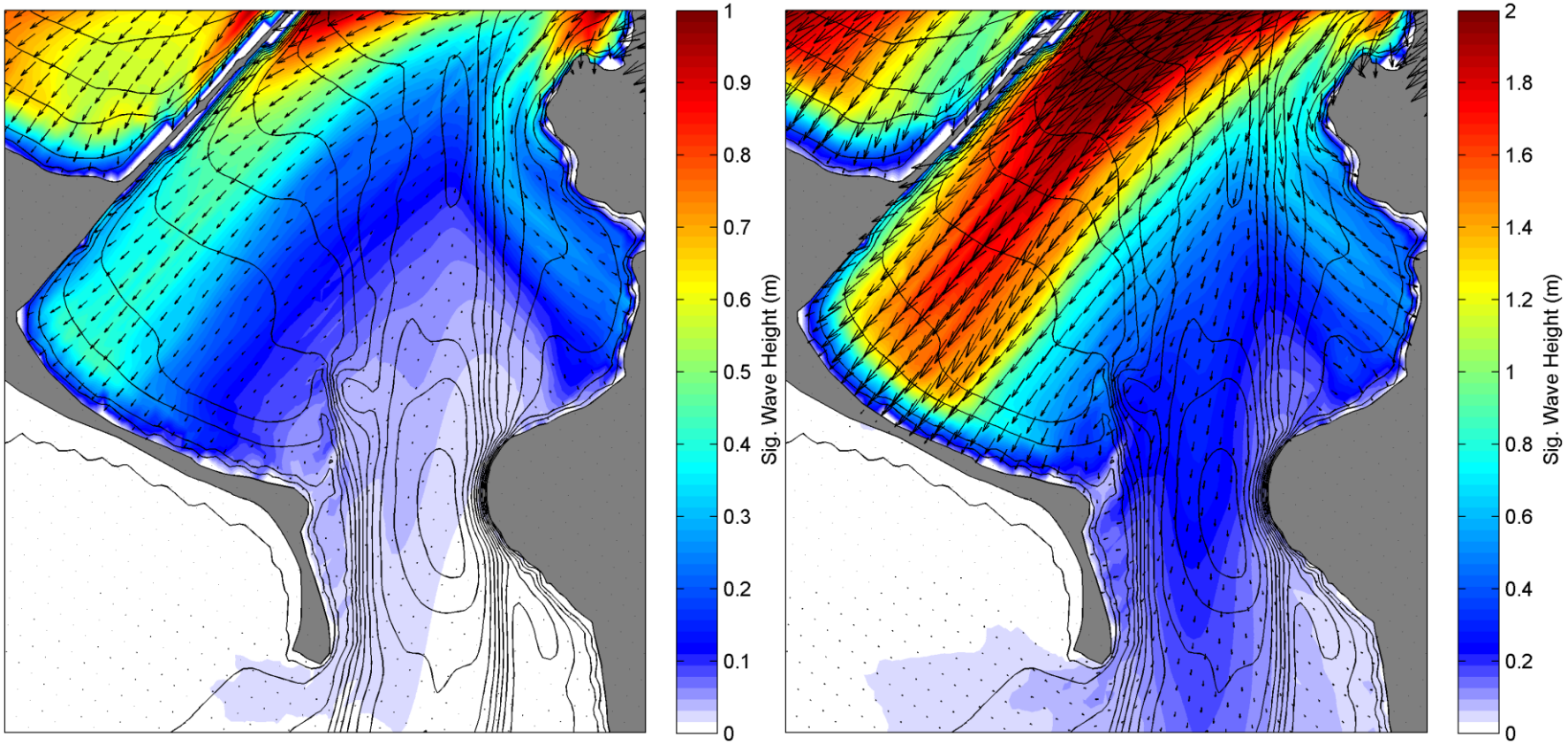

Figure 3.10 Mean significant wave heights within the entrance region for high energy southeast (left) and northeast (right) wave events (southeast event: Hs=3m, Dir=135 deg., Tp=14 s.; northeast event: Hs=3m, Dir=45 deg., Tp=10 s.). Note the different color scales for the 2 events

Hs=2m, Dir=0 deg., Tp=14 s.

Hs=1m, Dir=0 deg., Tp=8 s.

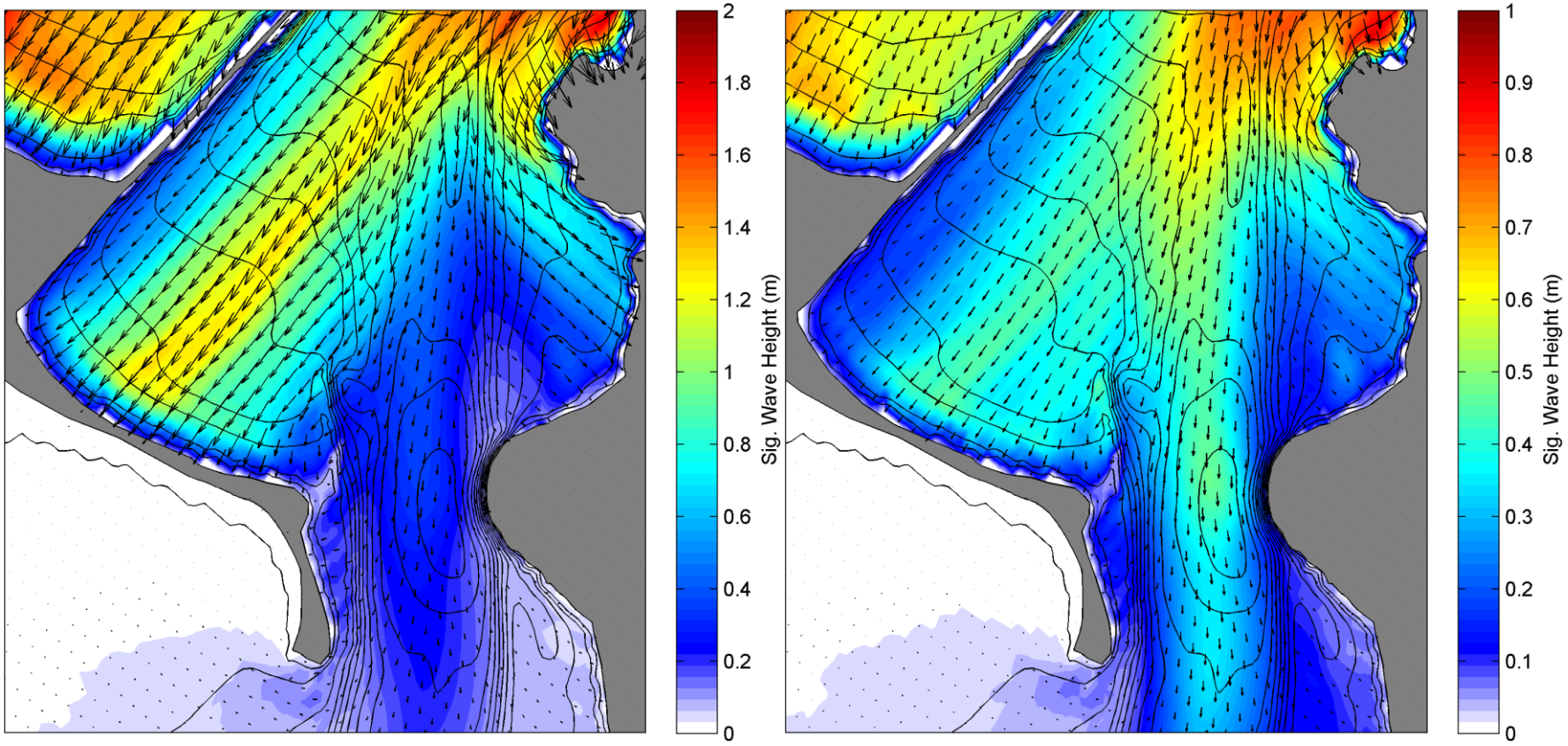

Figure 3.11 Mean significant wave heights within the entrance region for high energy north swell waves (left) and low energy sea waves (north swell event: Hs=2m, Dir=0 deg., Tp=14 s.; north sea event: Hs=1m, Dir=0 deg., Tp=8 s.). Note the different color scales for the 2 events.

Hs=3m, Dir=135 deg., Tp=14 s. **Hs=3m, Dir=45 deg., Tp=10 s.**

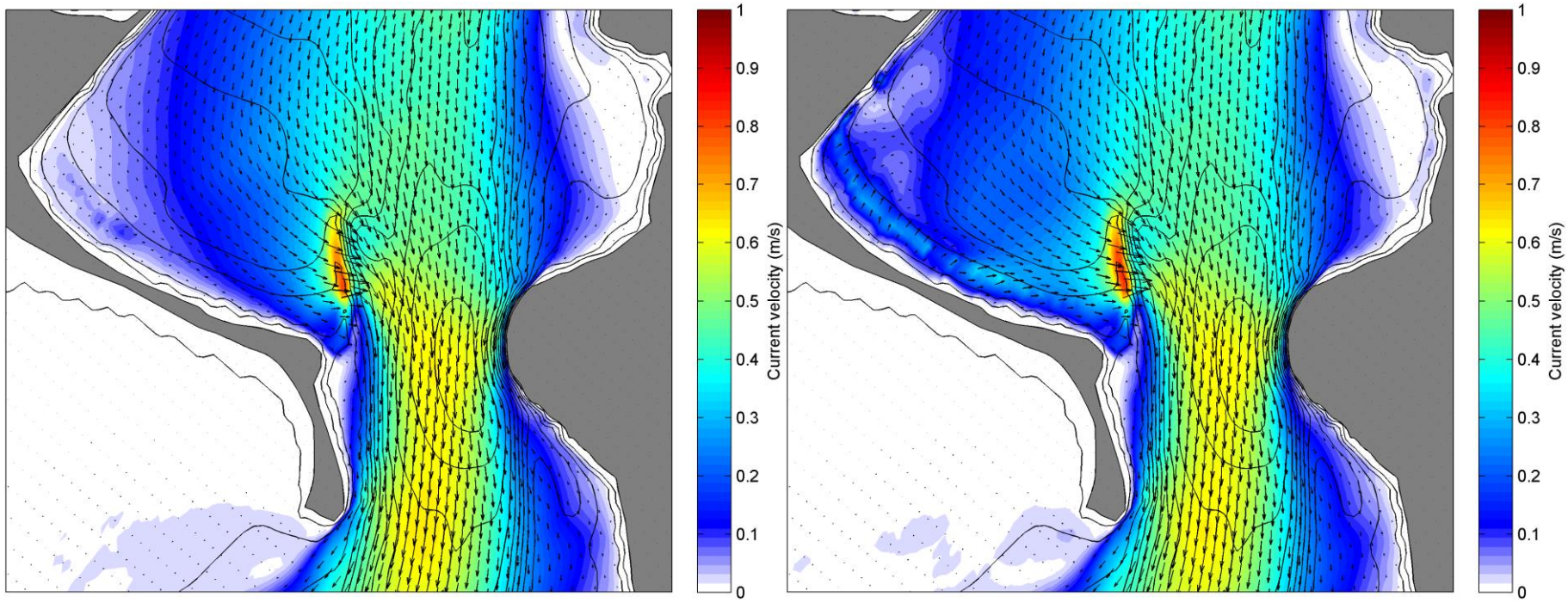

Figure 3.12 Mean flow fields within the entrance region for incoming tide phases, for high energy southeast (left) and northeast (right) wave events (southeast event: Hs=3m, Dir=135 deg., Tp=14 s.; northeast event: Hs=3m, Dir=45 deg., Tp=10 s.)

Hs=3m, Dir=135 deg., Tp=14 s. **Hs=3m, Dir=45 deg., Tp=10 s.**

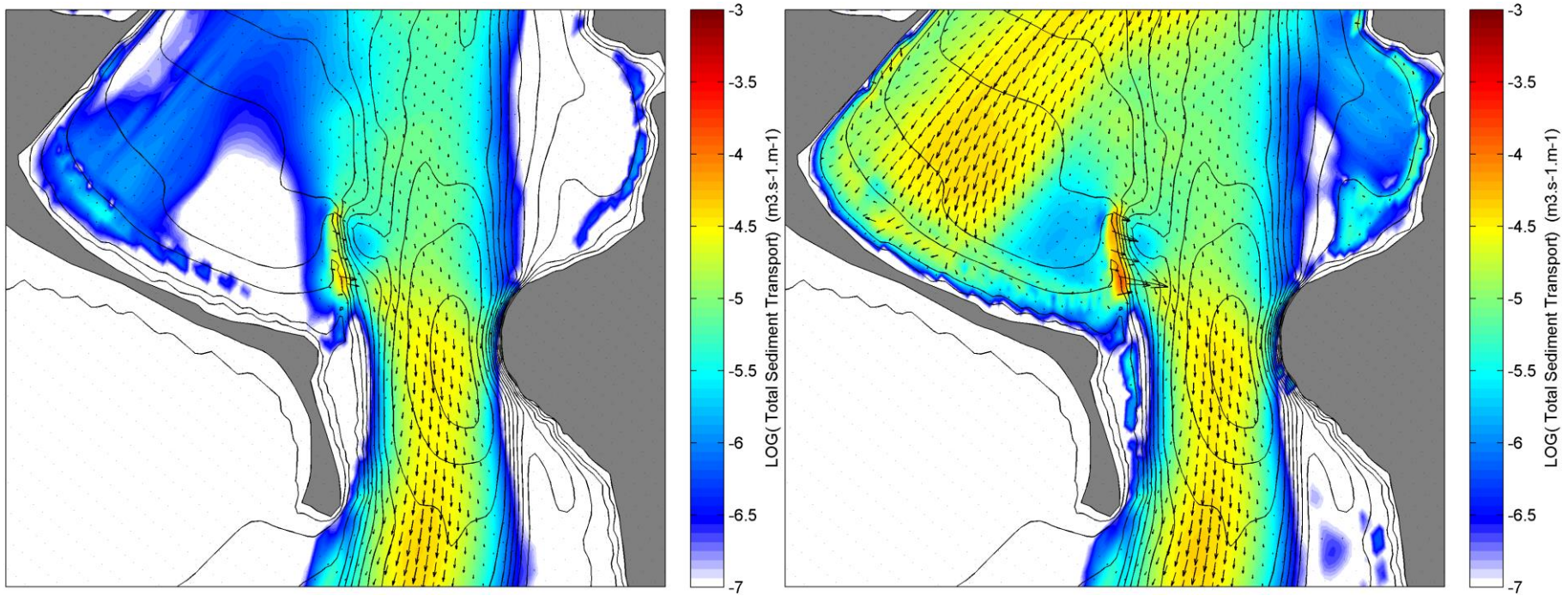

Figure 3.13 Mean total sediment transport fluxes within the entrance region for incoming tide phases, for high energy southeast (left) and northeast (right) wave events (southeast event: Hs=3m, Dir=135 deg., Tp=14 s.; northeast event: Hs=3m, Dir=45 deg., Tp=10 s.)

Hs=2m, Dir=0 deg., Tp=14 s. **Hs=1m, Dir=0 deg., Tp=8 s.**

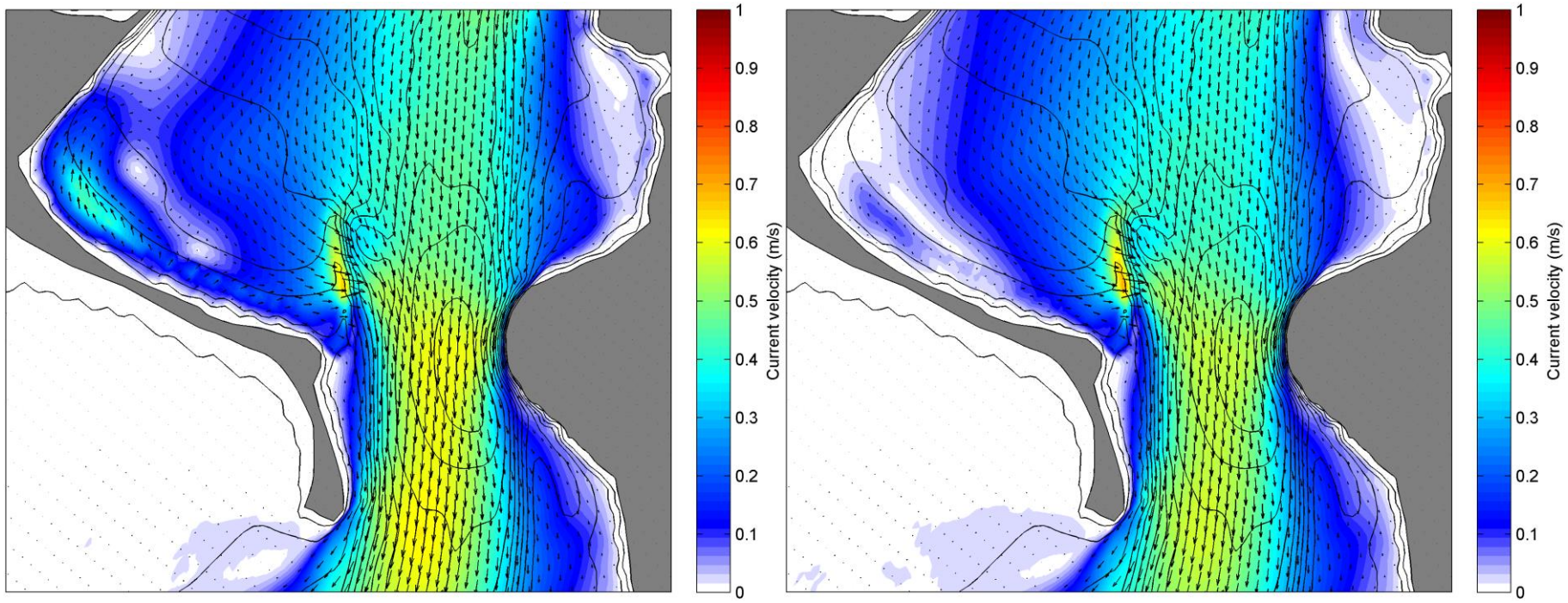

Figure 3.14 Mean flow fields within the entrance region for incoming tide phases, for high energy north swell waves (left) and low energy sea waves (north swell event: Hs=2m, Dir=0 deg., Tp=14 s.; north sea event: Hs=1m, Dir=0 deg., Tp=8 s.)

Hs=2m, Dir=0 deg., Tp=14 s.

Hs=1m, Dir=0 deg., Tp=8 s.

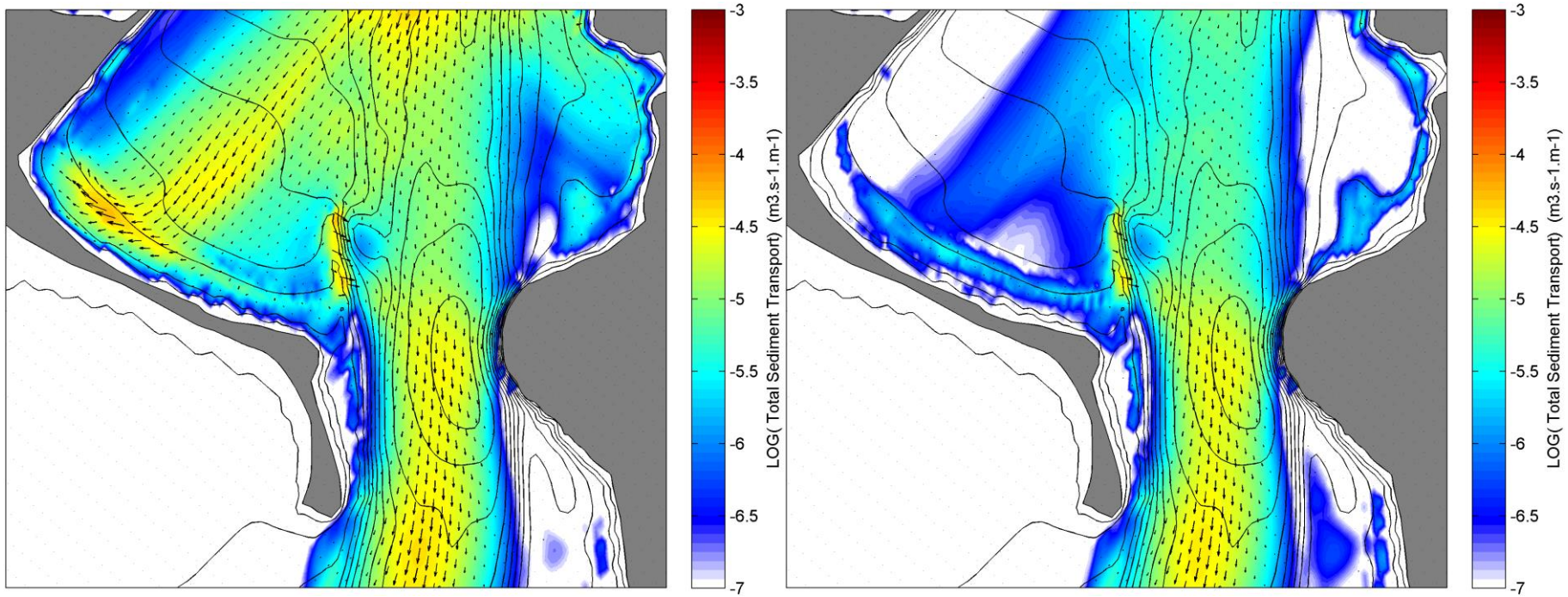

Figure 3.15 Mean total sediment transport fluxes within the entrance region for incoming tide phases, for high energy north swell waves (left) and low energy sea waves. (north swell event: Hs=2m, Dir=0 deg., Tp=14 s.; north sea event: Hs=1m, Dir=0 deg., Tp=8 s.)

Hs=3m, Dir=135 deg., Tp=14 s. **Hs=3m, Dir=45 deg., Tp=10 s.**

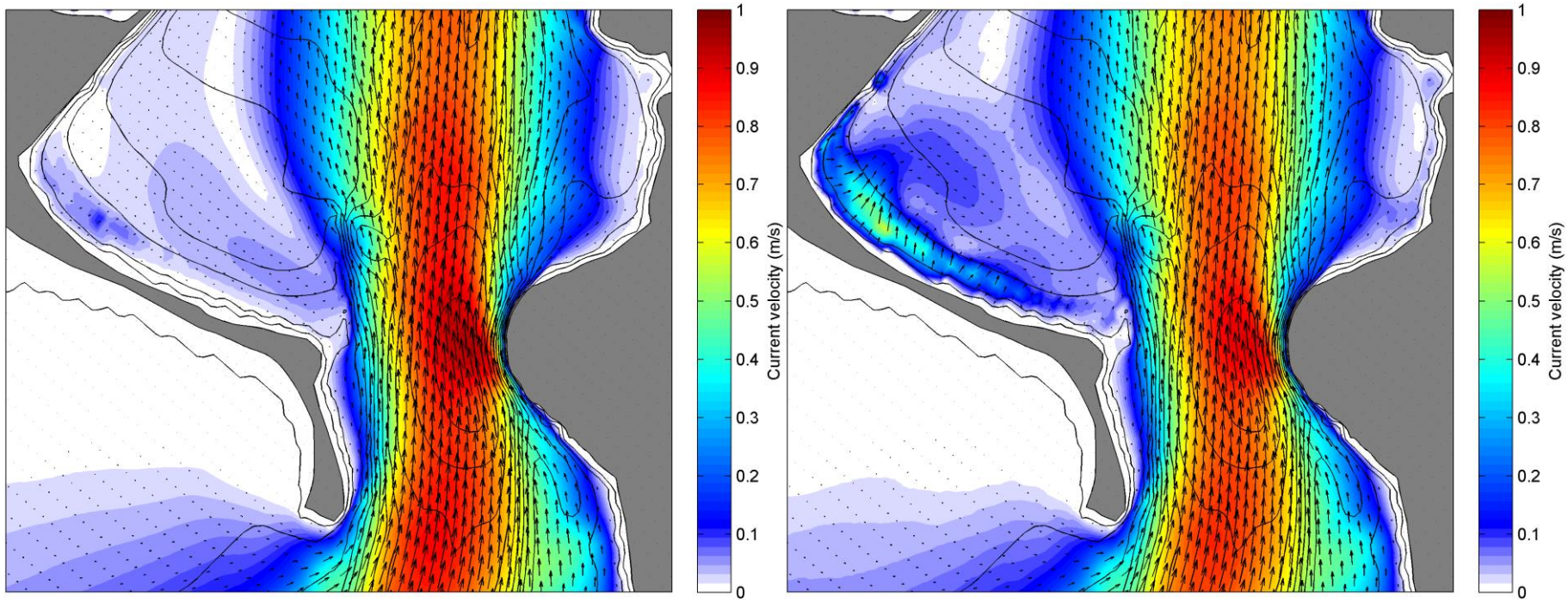

Figure 3.16 Mean flow fields within the entrance region for outgoing tide phases, for high energy southeast (left) and northeast (right) wave events (southeast event: Hs=3m, Dir=135 deg., Tp=14 s.; northeast event: Hs=3m, Dir=45 deg., Tp=10 s.)

Hs=3m, Dir=135 deg., Tp=14 s. **Hs=3m, Dir=45 deg., Tp=10 s.**

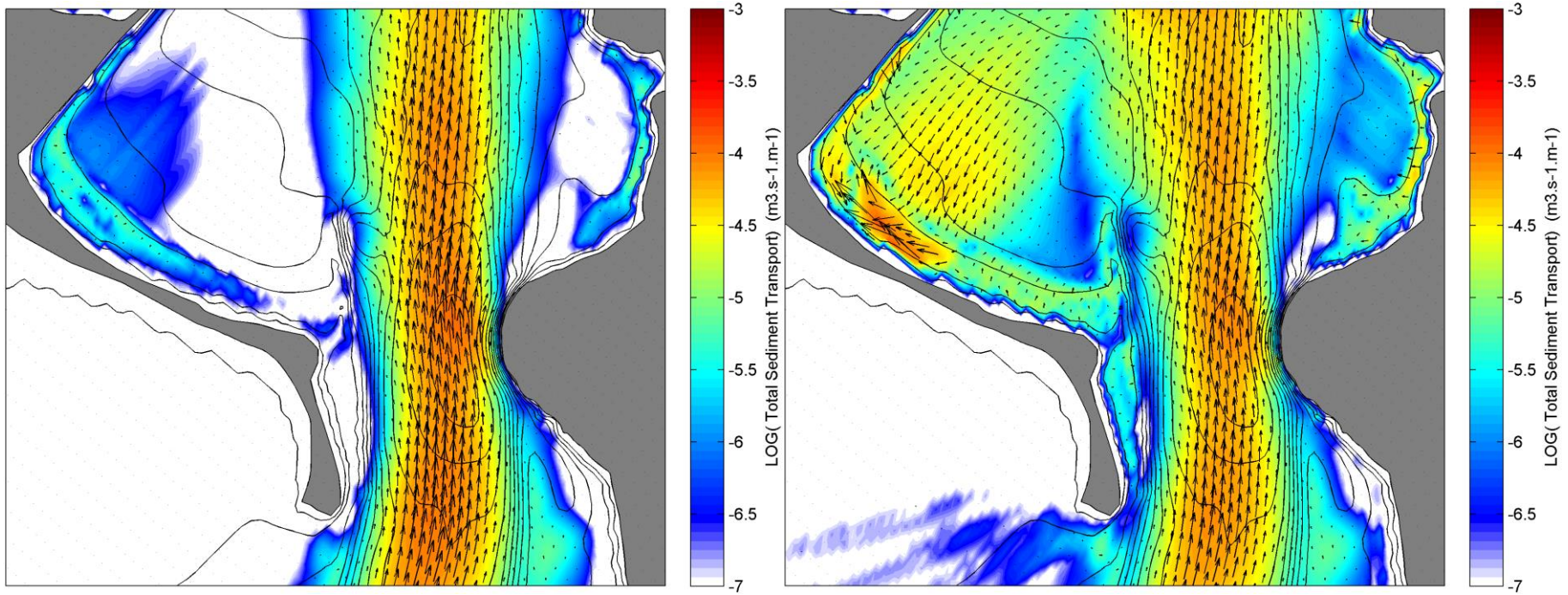

Figure 3.17 Mean total sediment transport fluxes within the entrance region for outgoing tide phases, for high energy southeast (left) and northeast (right) wave events (southeast event: Hs=3m, Dir=135 deg., Tp=14 s.; northeast event: Hs=3m, Dir=45 deg., Tp=10 s.)

Hs=2m, Dir=0 deg., Tp=14 s.

Hs=1m, Dir=0 deg., Tp=8 s.

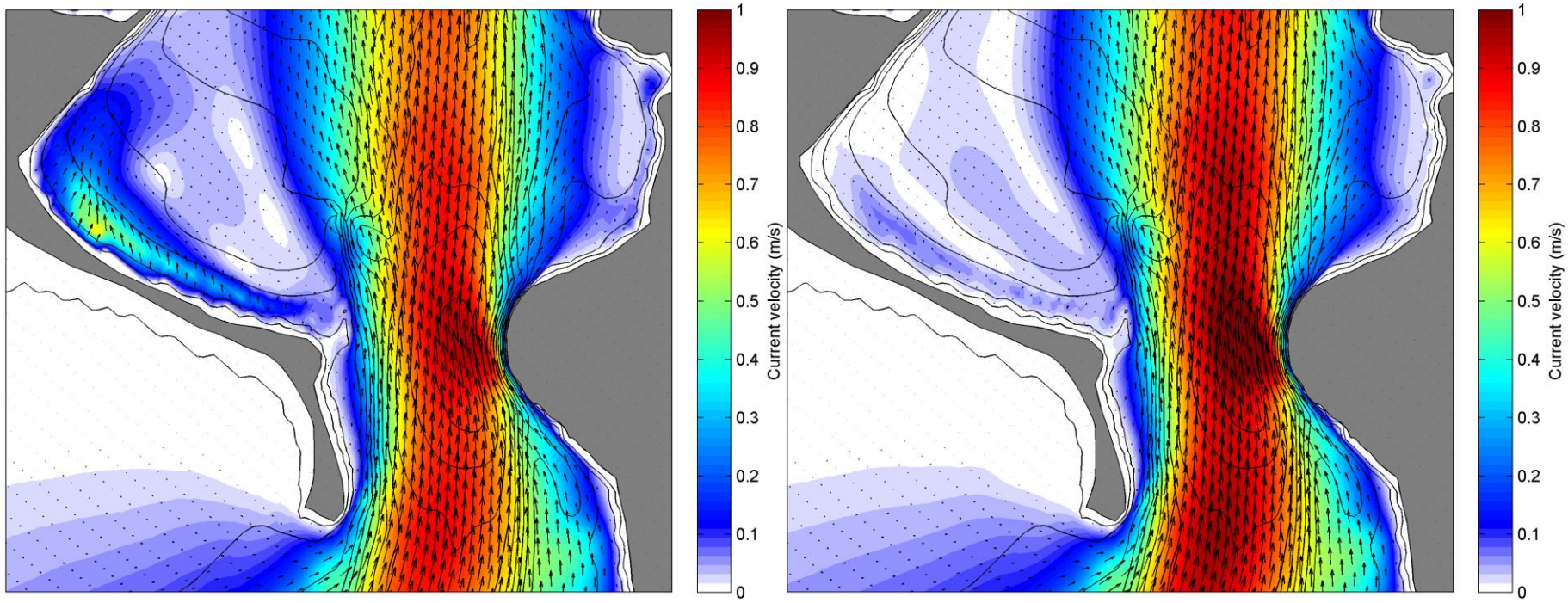

Figure 3.18 Mean flow fields within the entrance region for outgoing tide phases, for high energy north swell waves (left) and low energy sea waves (north swell event: Hs=2m, Dir=0 deg., Tp=14 s.; north sea event: Hs=1m, Dir=0 deg., Tp=8 s.)

Hs=2m, Dir=0 deg., Tp=14 s.

Hs=1m, Dir=0 deg., Tp=8 s.

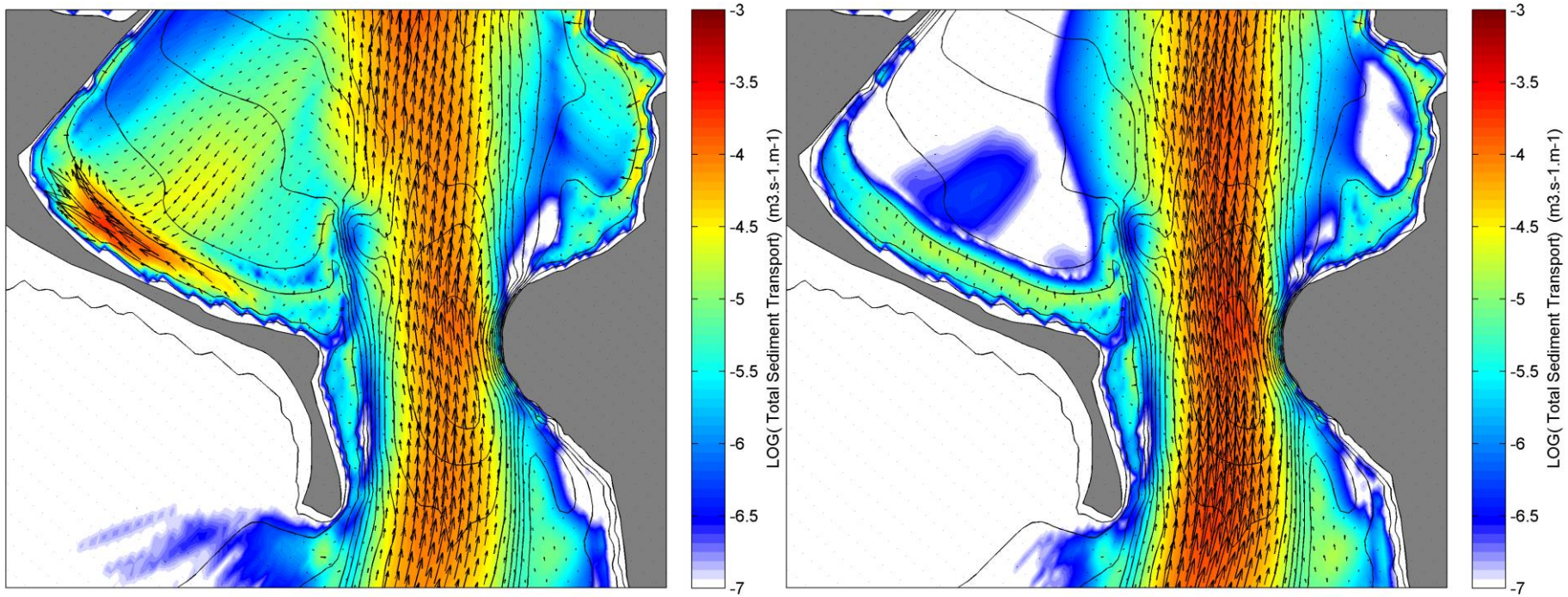

Figure 3.19 Mean total sediment transport fluxes within the entrance region for outgoing tide phases, for high energy north swell waves (left) and low energy sea waves. (north swell event: Hs=2m, Dir=0 deg., Tp=14 s.; north sea event: Hs=1m, Dir=0 deg., Tp=8 s.)

Hs=3m, Dir=135 deg., Tp=14 s. **Hs=3m, Dir=45 deg., Tp=10 s.**

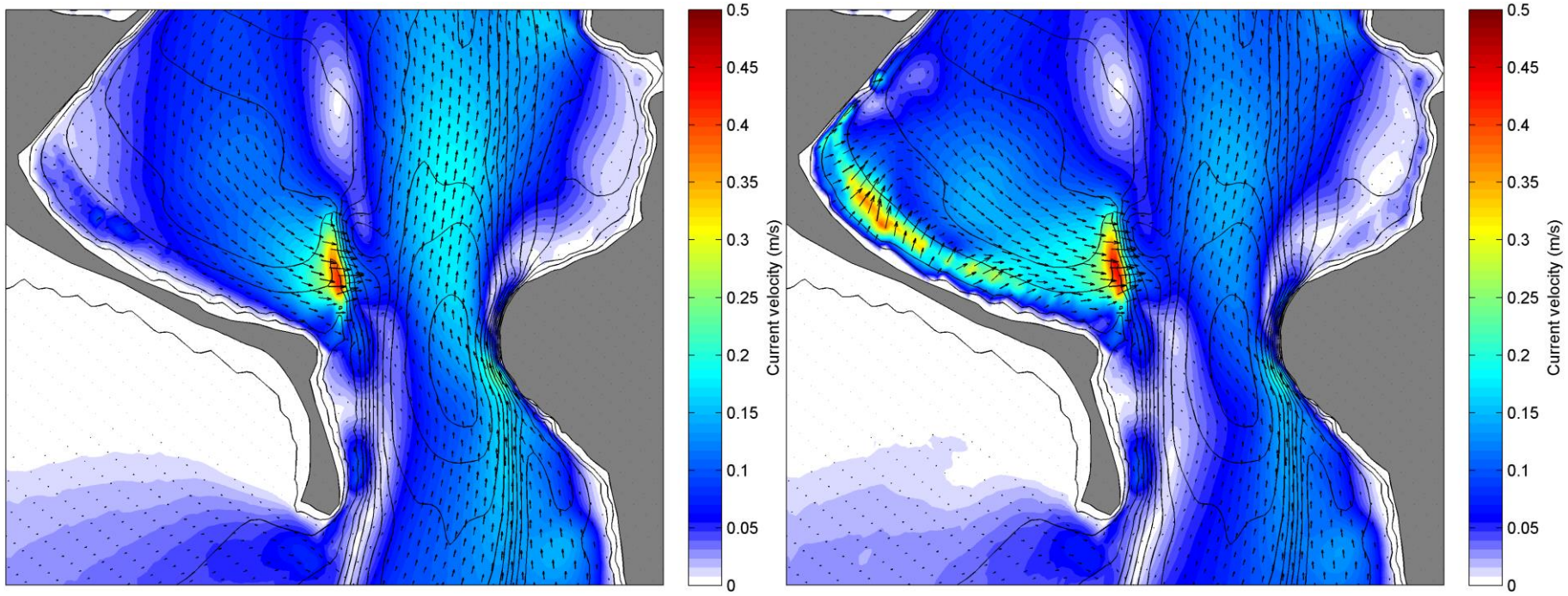

Figure 3.20 Mean flow fields within the entrance region for the full tidal cycles, for high energy southeast (left) and northeast (right) wave events (southeast event: Hs=3m, Dir=135 deg., Tp=14 s.; northeast event: Hs=3m, Dir=45 deg., Tp=10 s.)

Hs=3m, Dir=135 deg., Tp=14 s.

Hs=3m, Dir=45 deg., Tp=10 s.

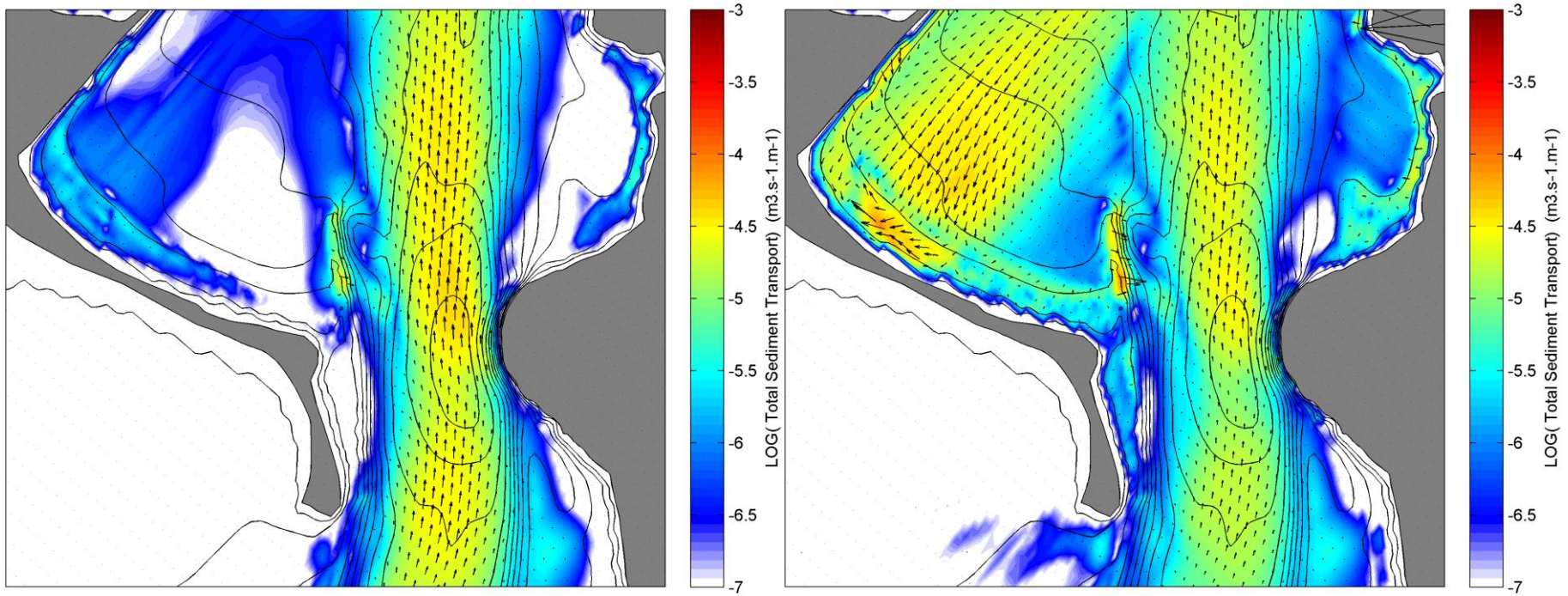

Figure 3.21 Mean total sediment transport fluxes within the entrance region for the full tidal cycles, for high energy southeast (left) and northeast (right) wave events (southeast event: Hs=3m, Dir=135 deg., Tp=14 s.; northeast event: Hs=3m, Dir=45 deg., Tp=10 s.)

Hs=2m, Dir=0 deg., Tp=14 s.

Hs=1m, Dir=0 deg., Tp=8 s.

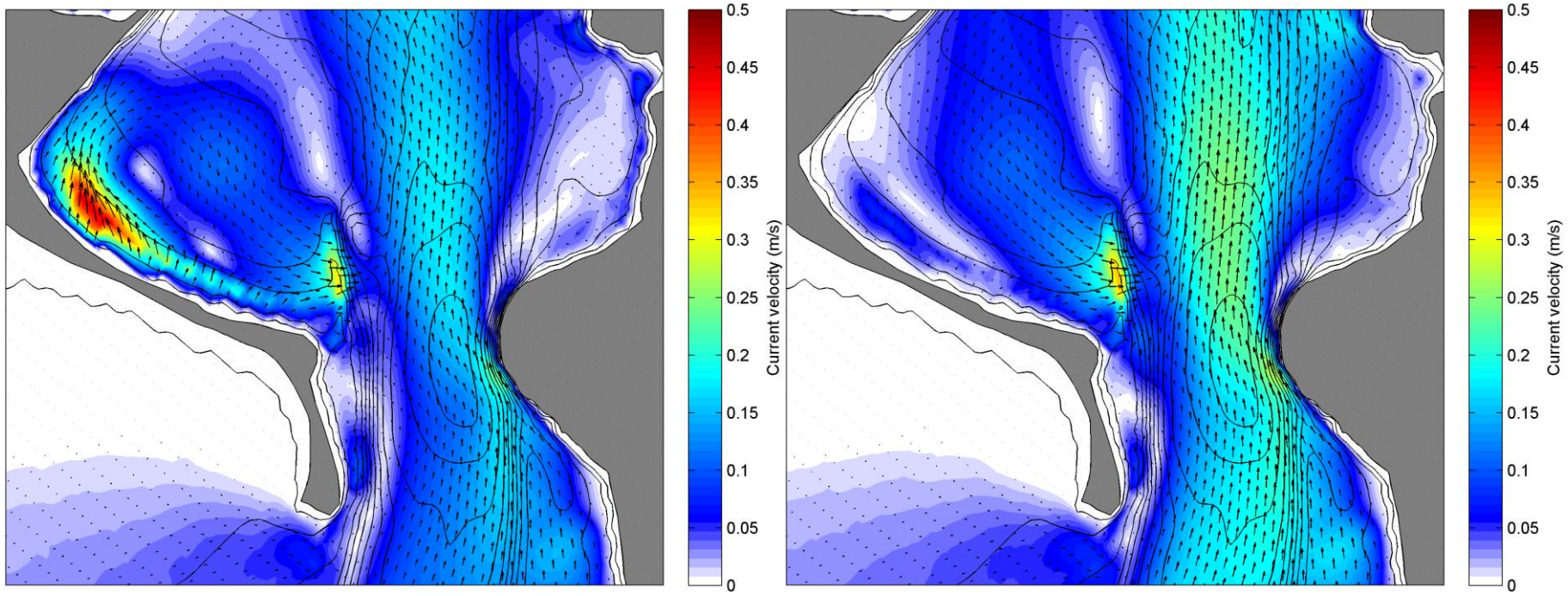

Figure 3.22 Mean flow fields within the entrance region for the full tidal cycles, for high energy north swell waves (left) and low energy sea waves (north swell event: Hs=2m, Dir=0 deg., Tp=14 s.; north sea event: Hs=1m, Dir=0 deg., Tp=8 s.)

Hs=2m, Dir=0 deg., Tp=14 s.

Hs=1m, Dir=0 deg., Tp=8 s.

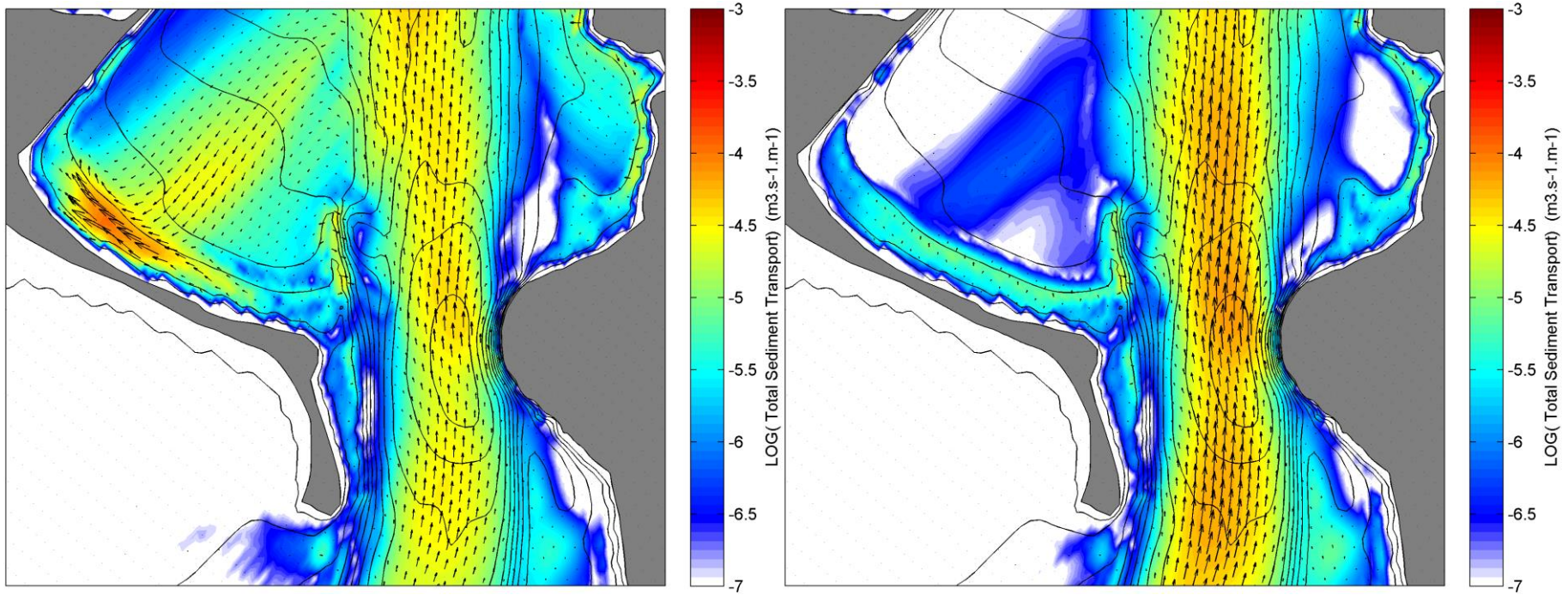

Figure 3.23 Mean total sediment transport fluxes within the entrance region for the full tidal cycles, for high energy north swell waves (left) and low energy sea waves. (north swell event: Hs=2m, Dir=0 deg., Tp=14 s.; north sea event: Hs=1m, Dir=0 deg., Tp=8 s.)

Incoming tides **Outgoing tides**

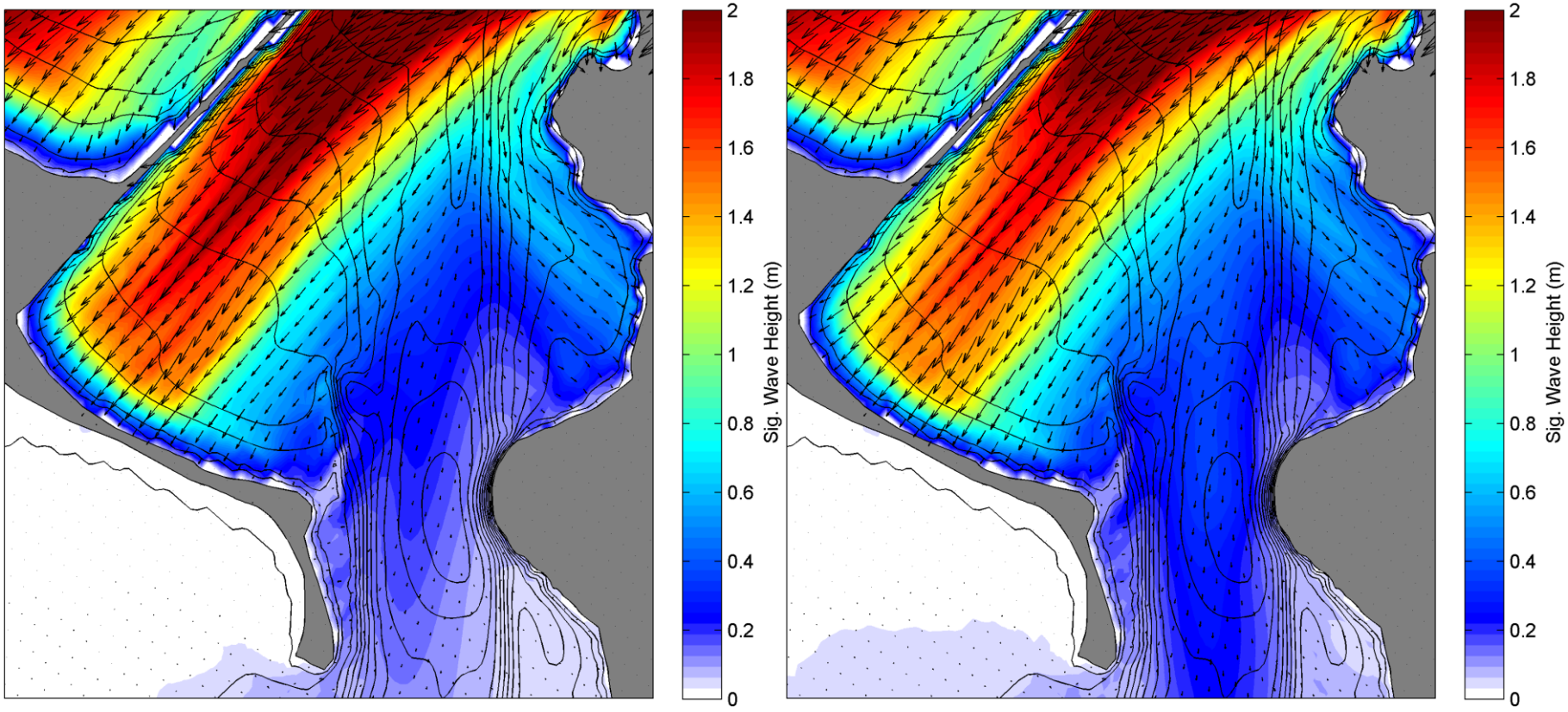

Figure 3.24 Mean significant wave heights at incoming and outgoing tide phases for the high energy northeast event (Hs=3m, Dir=45 deg., Tp=10 s.)

Incoming tides **Outgoing tides**

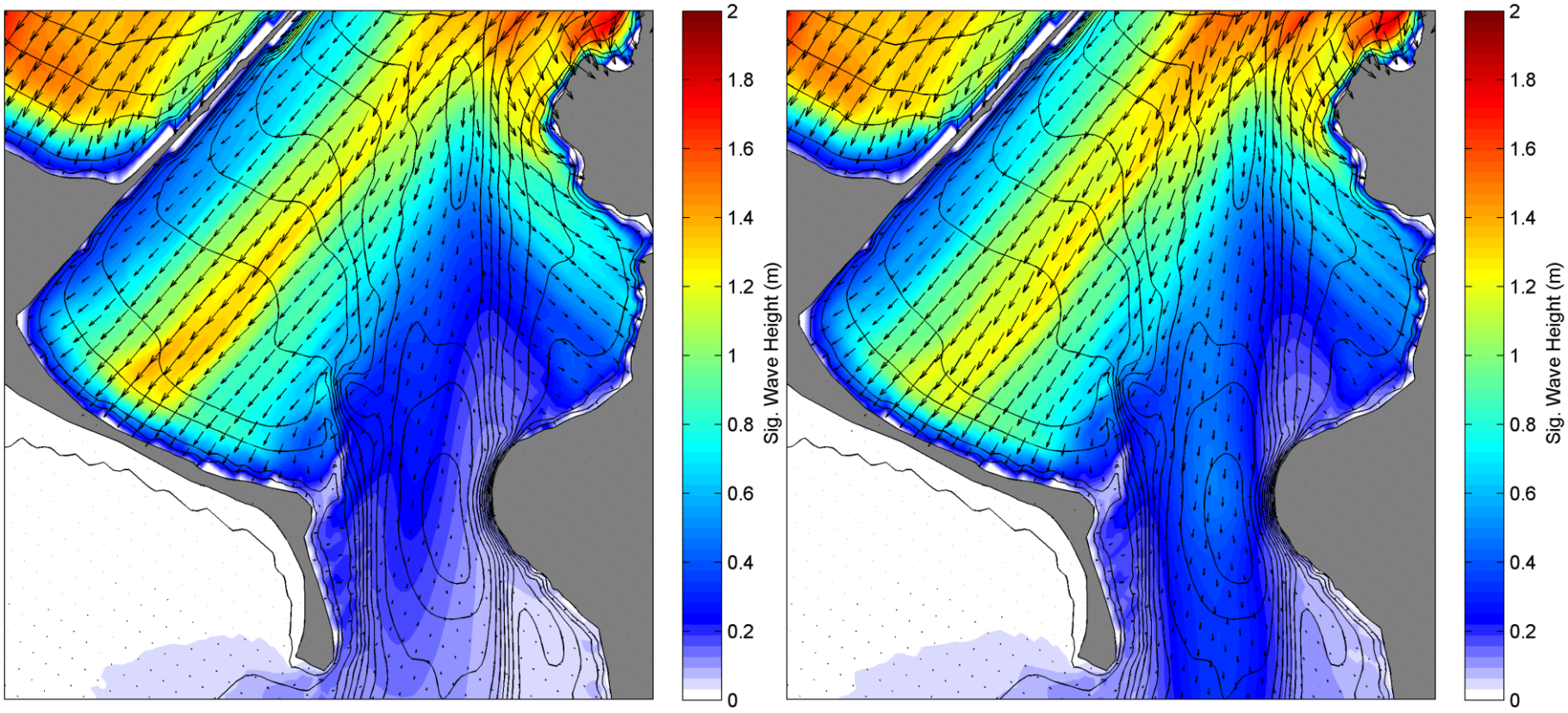

Figure 3.25 Mean significant wave heights at incoming and outgoing tide phases for the high energy north swell event (Hs=2m, Dir=0 deg., Tp=14 s).

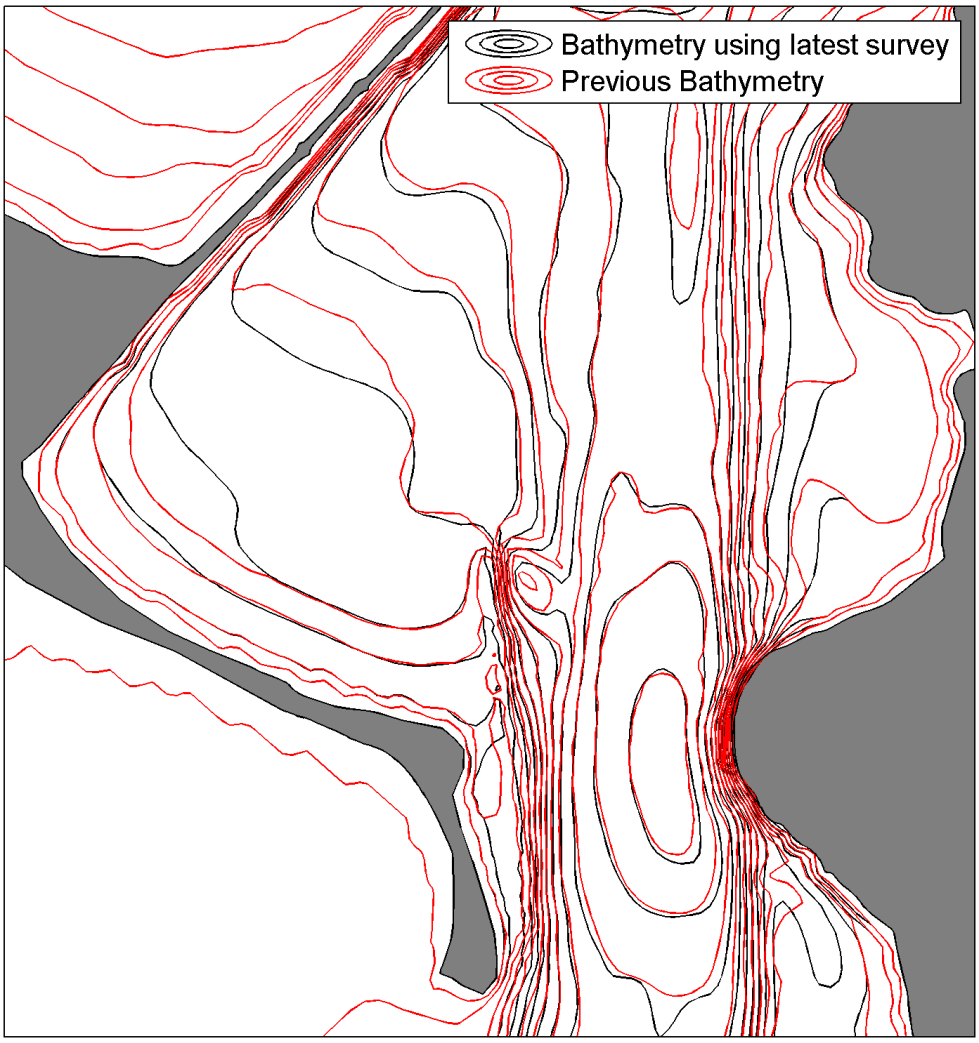

Figure 3.26 Depth contours of previous bathymetry (red) and bathymetry including the latest survey from the entrance region (black). Note the onshore translation of contours coinciding with the wave penetration zones in Figures 3.10 and 3.11.

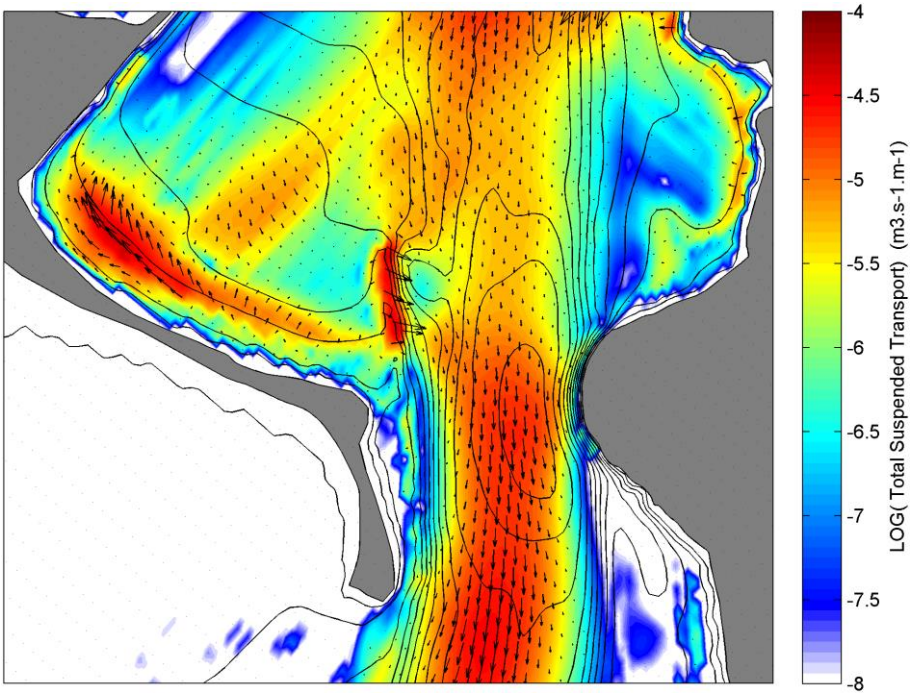

Figure 3.27 Mean suspended sediment transport fluxes within the entrance region for the full tidal cycles, for the high energy north swell event (Hs=2m, Dir=0 deg, T=14 s.). Note the different color scale relative to total transport maps.

4. LONG MAC OPTIMISATION RESULTS

4.1. Bathymetry modifications

The implemented numerical model provides a tool to test the efficacy of different structure configurations to reduce sediment recirculation into the Harbour. Based on the previous findings, incoming tides are of particular interest since the ambient tidal dynamics and wave-driven forces will work in combination to drive strong longshore flows and transport fluxes over the existing structure and into the channel. In that sense an option could be to try to physically block this longhsore transport feature by keeping the existing structure position but raising its crest.

Net flow and transport patterns during incoming tides clearly indicate that the central part of the existing structure, just west of the existing beach/spit bend is a critical spot with respect to sediment transport (see Figures 3.9 and 3.11 to 3.14). The existing structure was split into three segments of similar lengths. Two scenarios were considered, one in which only the central part is raised, and another in which the central and north sections are raised, thus providing a more significant blocking of the flow. In both cases, the structure level in the model was raised to +1.1 m relative to mean sea level which is the predicted highest astronomical tide (HAT) so that the structure is emergent at all tidal stages. Note that in addition to raising the structure in its longitudinal axis (i.e. approximately North-South), the junction to the existing beach (i.e. in the vicinity of the existing groin) is raised to a similar level so that the Shelly Beach cell is enclosed. A definition sketch of the segments considered is shown in Figure 4.1 and the existing bathymetry and configurations with emerged segments are shown in Figure 4.2. Bed level differences between the modified and existing bathymetries are shown in Figure 4.3 for both configurations.

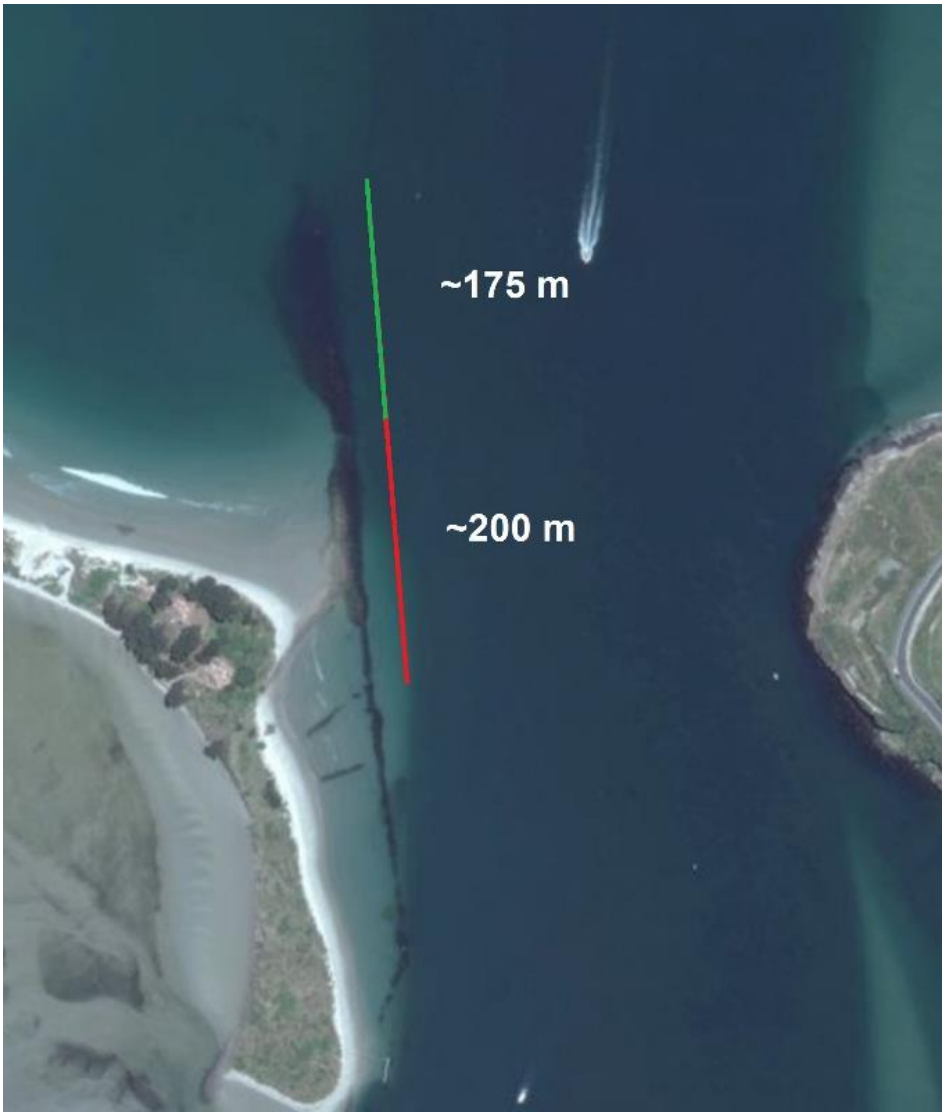

Figure 4.1 Aerial view of the Long Mac structure with definition of segments raised to +1.1 m MSL (highest astronomical tide).

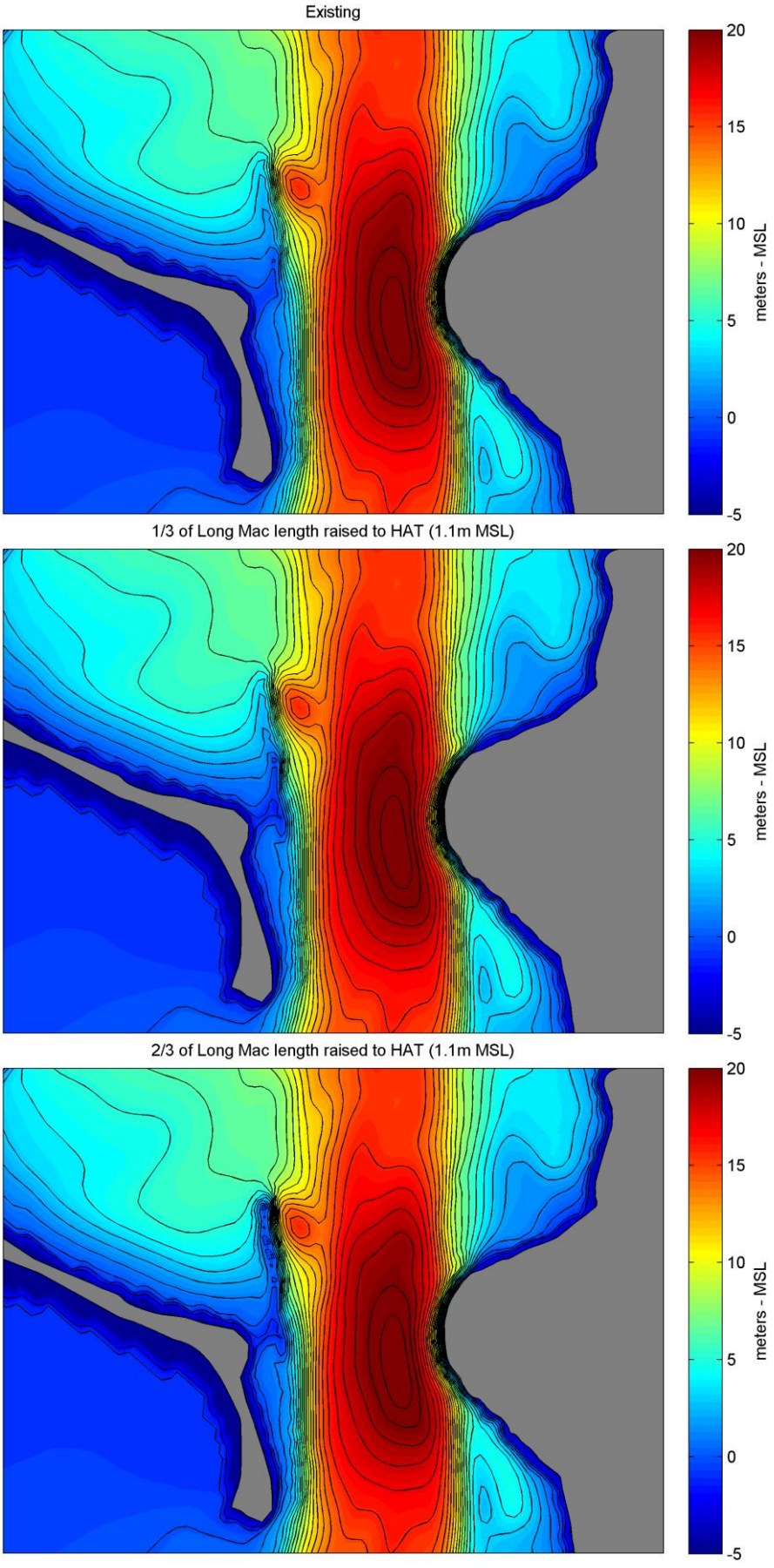

Figure 4.2. Existing and modified model bathymetries.

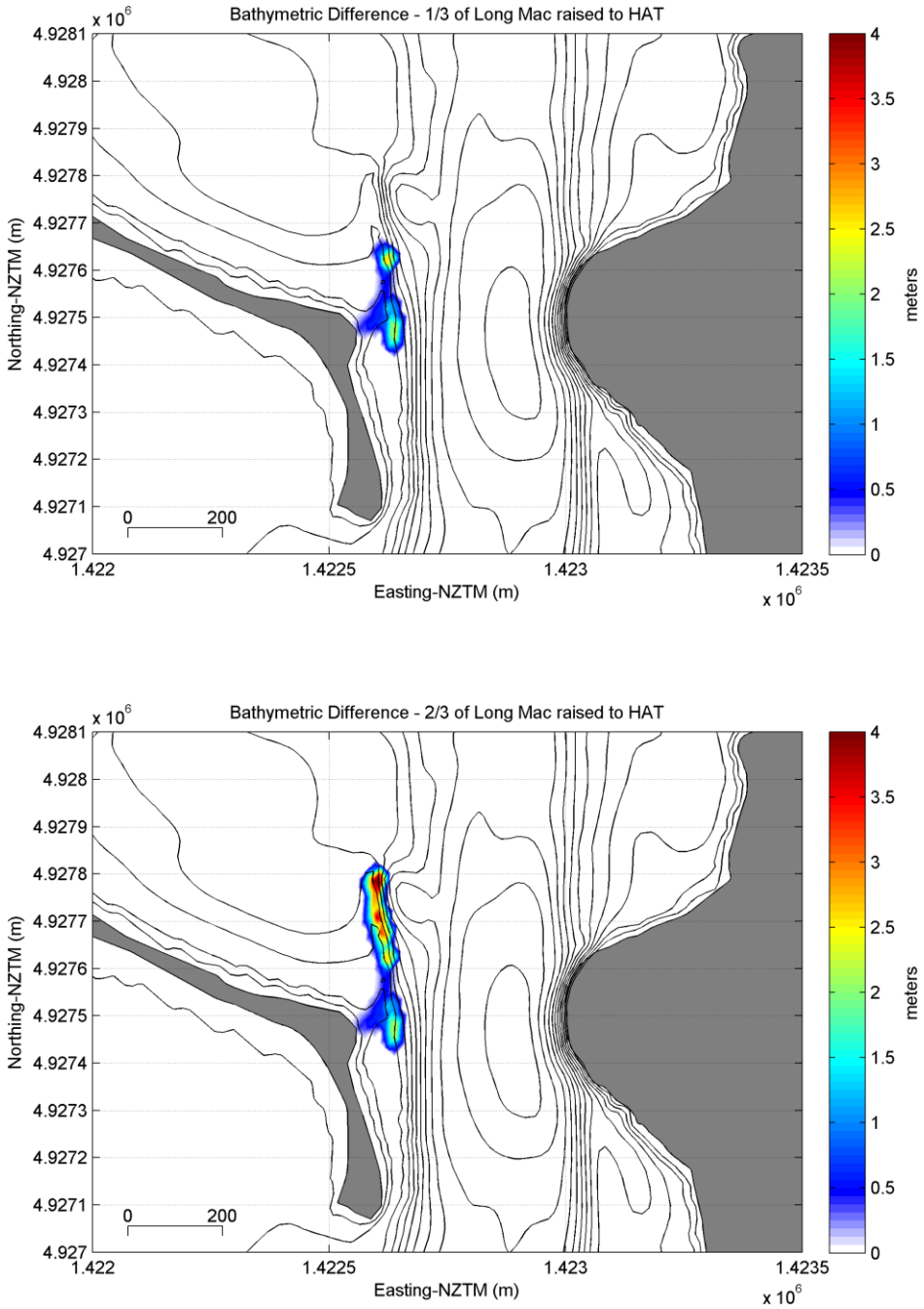

Figure 4.3 Bed level difference between existing and modified model bathymetries (central segment raised to HAT, top, central and north segments raised to HAT, bottom). Note that the bed level at the junction from the eastern tip of Shelly Beach (spit bend) to the structure was also raised so that the beach cell enclosed.

4.2. Scenario results

A complete spring tide cycle was run using the modified bathymetries. The cases with no waves and idealized wave events (see Table 3.1) were simulated to identify modifications of the underlying tidal dynamics and wave-driven processes.

As in section 3.2, simulation outputs were averaged over the incoming, outgoing and total periods of that one spring tide, using the water level at the mouth as reference. Here the focus is mainly on the incoming phase that causes the most sediment transport into the Harbour.

4.2.1. Effects on tidal dynamics

Snapshots of peak flood water levels and currents are shown in Figure 4.4 for the existing and modified configurations (no waves).The main effect of the emergent segments is to enclose the Shelly Beach cell. During incoming tides, this modifies significantly the water level distribution along the beach, as the strong alongshore gradient that is currently developing (Figure 4.4, top) is compensated by the water mass being blocked by the emergent structure at the eastern end of the beach (Figure 4.4, middle and bottom). The balancing of water level significantly reduces the longshore currents along the eastern half of the beach and the emergent segments prevent the flow acceleration that is presently predicted over the Long Mac. The longer emergent structure (i.e. central and north segments emerged) provides a more significant retention of the incoming water mass, and is clearly more efficient in reducing the longhsore flow and transport along the eastern beach and in the vicinity of the existing structure.

The water mass compartmented by the emergent structure will have to eventually flow back into the channel. The relatively higher water levels along the eastern beach allowed by the enclosing result in a new surface gradient developing in the structure vicinity in a north/south axis, which is seen to force a northwards flow component along the structure. These flows are however opposite to the ambient incoming flows and their intensities appear relatively limited. It is noted that emerged longitudinal structure segments without a junction to the eastern beach tip would compress and guide the existing easterly flow and transport southwards along the lower spit shores, with likely adverse impacts on its stability.

A more problematic area is near the seaward end of the emerged segments. More intense water level gradients force currents bending around the tip, and the process is further enhanced as the flow merge with strong incoming channel flows. It is noted that the presence of emergent segments also changes the position where the flows originating from and off Shelly Beach branch to the channel flow. Snapshots of the predicted total tidal sediment transport (Figure 4.5) clearly show the differences in position of the strongest sediment transport zones, over and north of the channel trough. This will have likely consequences with respect to the equilibrium channel morphology, which may include a relative deepening of the trough northern slopes with associated infilling of its deepest part.

Peak ebb flows are provided in Figure 4.6 for completeness. The emergent sections of the Long Mac tend to slightly focus the ebb jet in its near vicinity, but overall changes are very limited.

4.2.2. Effects on wave-driven circulation and sediment transport

The sediment transport fluxes averaged over the incoming tide are presented in Figures 4.7 to 4.10 for the idealized wave events listed in Table 3.1. The raising of the central or central and north segments to emergent levels consistently result in a reduction of the eastwards fluxes predicted along the eastern half of Shelly Beach and over the existing Long Mac structure. The emergent segments act as physical barriers to the longhsore transport feature predicted for the existing configuration and also provide some local sheltering from the wave energy that would otherwise reach that region, thus further reducing the transport magnitude. Furthermore, the relatively higher water levels on the western side of the Long Mac with emergent segments will work against the wave-driven water level gradient that develop in the west-east direction due to gradients in wave energy exposure (e.g. Figure 3.24) and resulting wave setup distribution. In other words, the modified ambient water level distribution will balance the wave-driven gradient, instead of enhancing it as can presently occur (e.g. see net incoming flows in Figure 3.7, top, tide only, and Figure 3.12, right, northeast event).

A feature that is also consistently predicted in Figures 4.7 to 4.10 is the migration of the net sediment transport pathway from the Shelly Beach cell over, or around, the Long Mac and into the channel, during incoming tides. This “net” transport signal is due to a modification of the position where the flows originating from and off Shelly Beach merge with the main incoming channel flow. This was already identified in the snapshots of the tidal peak flood flows and transports shown in Figures 4.4 and 4.5.

These differences in sediment transport patterns are further characterized in Figure 4.11. An emergent structure guides the incoming flows from Shelly Beach around its seaward tip. This results in a locally increased eastwards transport component, which links to a zone of stronger transport magnitude within the channel over the northern slopes of the trough adjacent to Harrington Point. For completeness, the net transport field over the entire tide cycle is shown in Figure 4.12. The enhancement of the eastwards transport feature near the seaward end of the emergent structures is reproduced, particularly for the case with both central and north segments emerged. The channel region remains ebb-dominated however a reduction of the net magnitude is visible north of the channel trough for the cases with emerged segments.

These modifications of the net transport fields are expected to result in morphological adjustments of the channel and Long Mac vicinity. Near the existing Long Mac seaward tip, a small depositional feature is already present just north of the scour hole on the eastern side of the structure. This is likely due to the process identified here, either as a residual signal from times when the structure was shallower and/or progressive formation even with the present submerged level. The enhancement of the eastwards transport component (i.e. normal to channels flows) due to the raising of the structure central and north segments will likely further build this small delta-like depositional feature. A relocation and possible deepening of the scour hole is also likely to occur given the strong flows bending around the structure tip. In contrast, we can expect that the growth of the similar depositional feature south of scour hole, coinciding with the present eastward transport feature, will stop. For the configuration with

only the central segment emerged, the predicted eastwards transport in the vicinity of the present transport feature remains significant so the present depositional feature south of the scour hole will likely continue its growth with only a slight readjustment of its position.

To provide a more quantitative characterization of these processes, predicted total sediment transport were extracted along a transect following the structure axis (Figure 4.13). It is noted that actual transport numbers should be interpreted with care as no calibration of the transport fluxes was undertaken, however, their relative importance is expected to remain relevant. The time series of total sediment volumes (i.e integrated along transect) moving across the transect over the tidal cycle considered is shown in Figure 4.14. The reduction of the eastwards transport for the configurations with emergent segments is clearly visible at incoming tide. The reduction is much more efficient when both the central and north segments are raised. The profile of net volumes transported across each transect point (i.e. integrated over the entire tidal cycle) are shown in Figure 4.15. The northwards shift of maximum transported volumes and overall reduction is again clearly seen for the configurations with emergent segment. It is noted that an intermediate length for the emerged section could be envisaged here, as along as the transport feature presently predicted is blocked. That being, it is likely that the residual sediment volume eventually transported past the seaward tip will generally decrease as the emerged section length is increased, since the driving flows will have more distance to be compensated by ambient adverse gradients. Overall, the significant reduction in transported sediment volumes when both segments are raised suggests that the “new” shifted eastwards transport feature near the structure seaward tip may not be as problematic as what is presently occurring, with respect to sediment recirculation the Harbour.

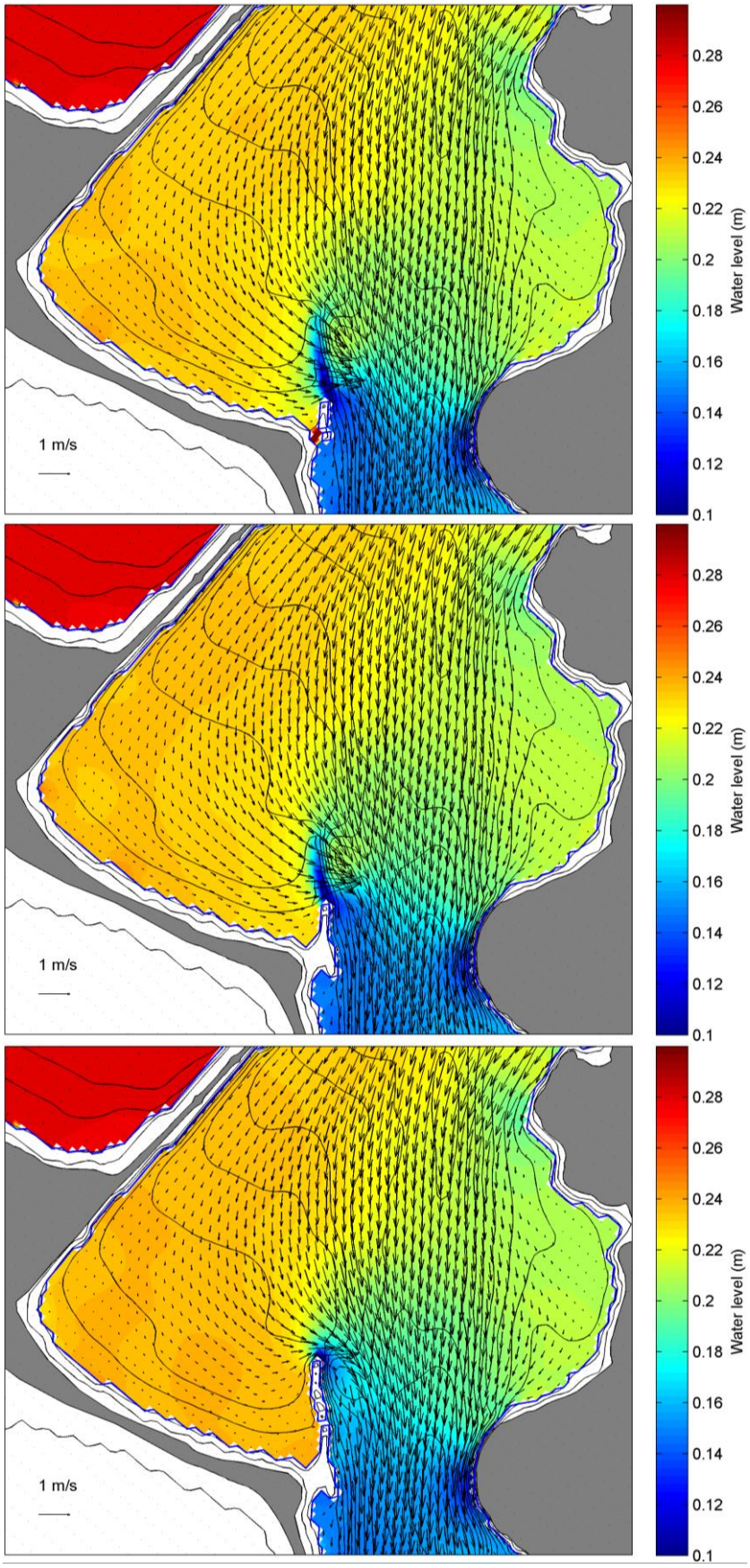

Figure 4.4 Peak flood flows for existing (top) and modified bathymetries (middle: central segment emerged, bottom: central and north segments emerged).

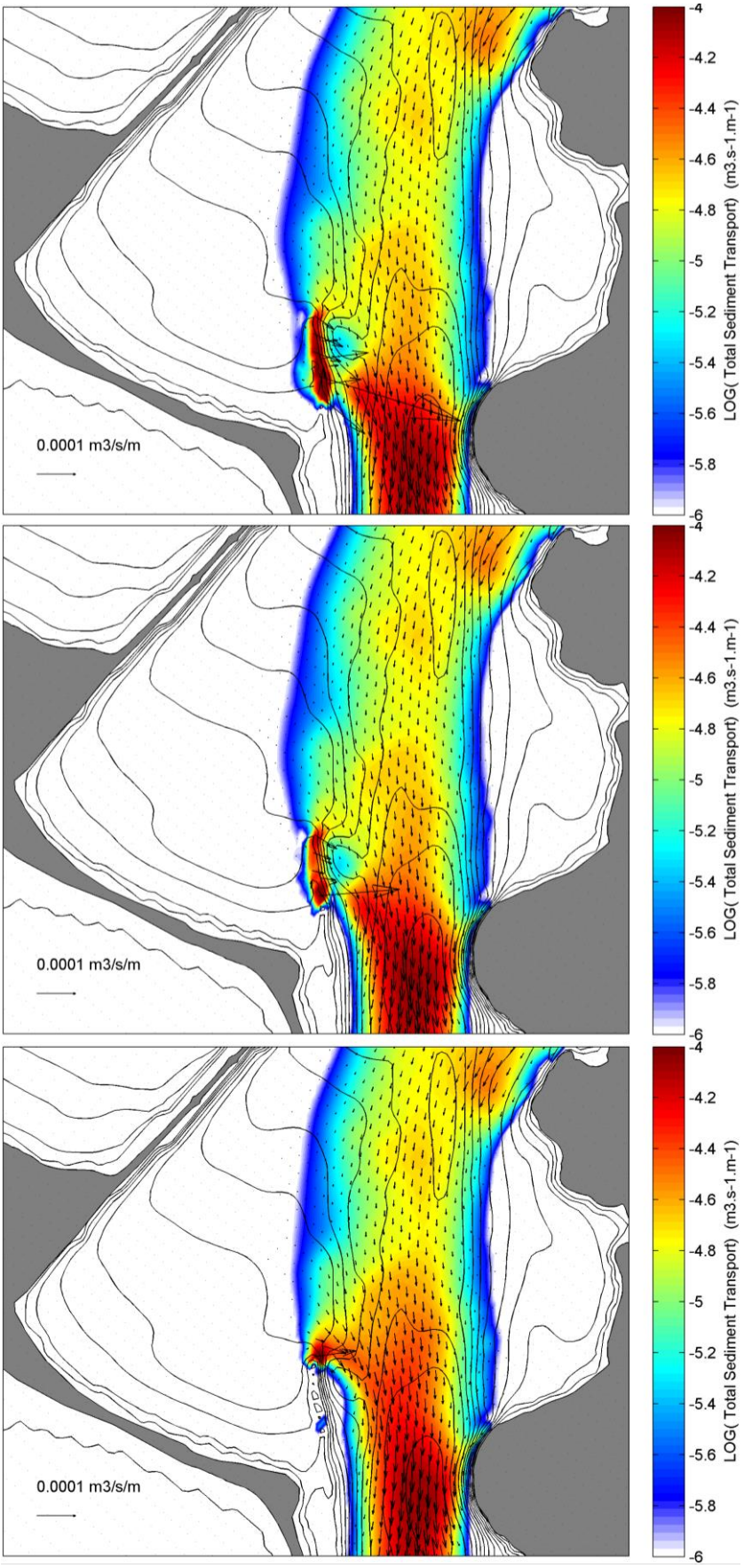

Figure 4.5 Peak flood total transport for existing (top) and modified bathymetries (middle: central segment emerged, bottom: central and north segments emerged).

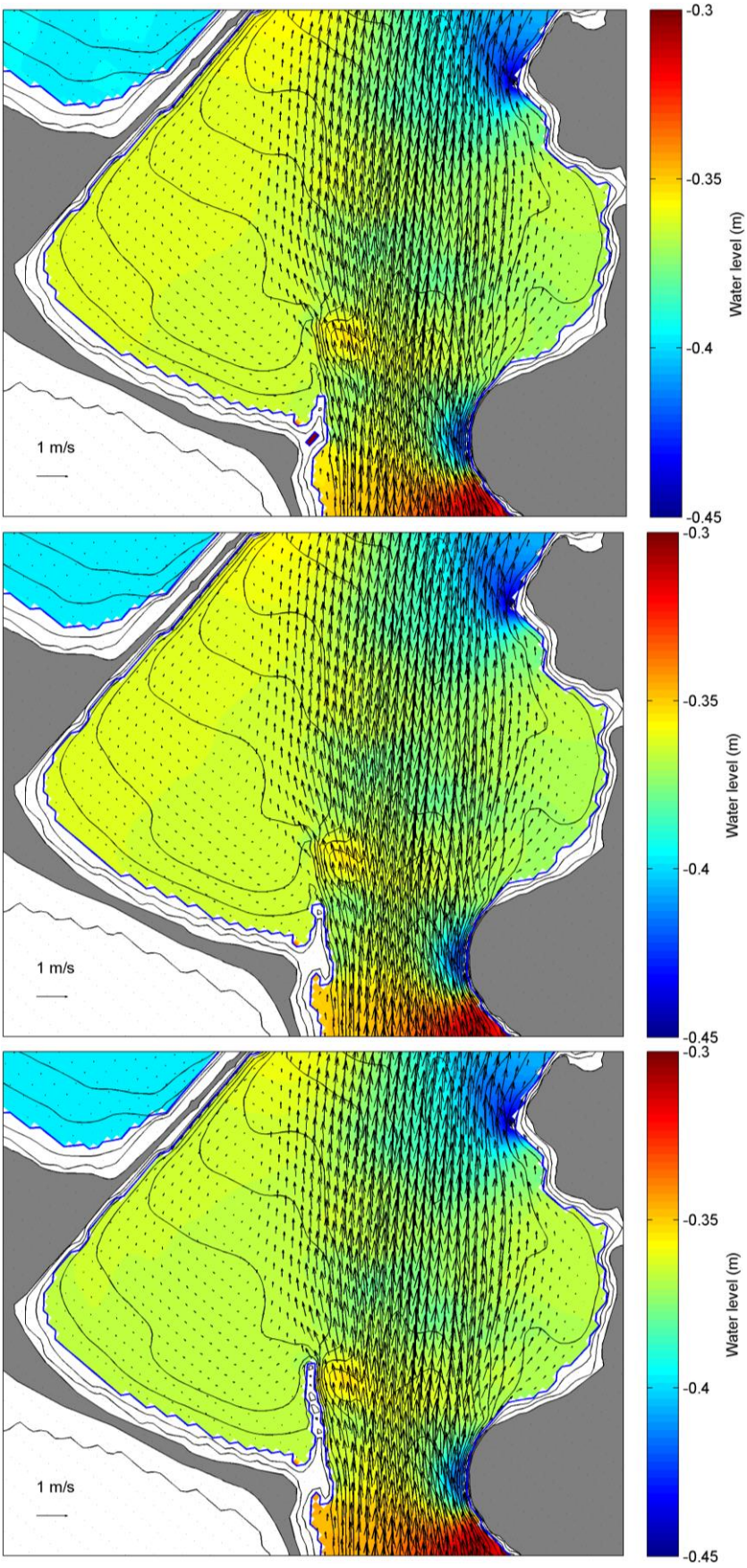

Figure 4.6 Peak ebb flows for existing (top) and modified bathymetries (middle: central segments emerged, bottom: central and north segments emerged).

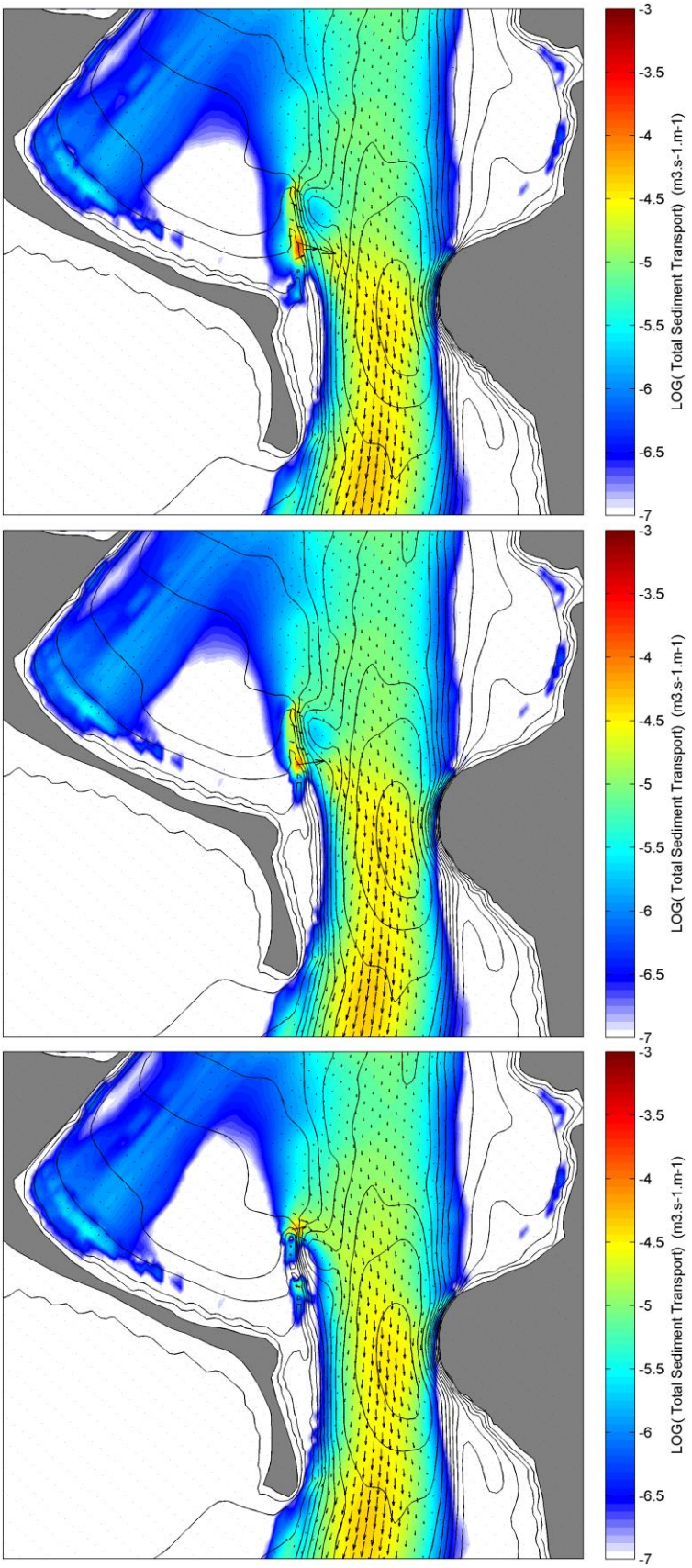

Figure 4.7 Mean total sediment transport fluxes within the entrance region over an incoming tide, for a high energy southeast event (Hs=3m, Dir=135 deg., Tp=14 s), (top:existing, middle: central segment emerged, bottom, central and north segments emerged).

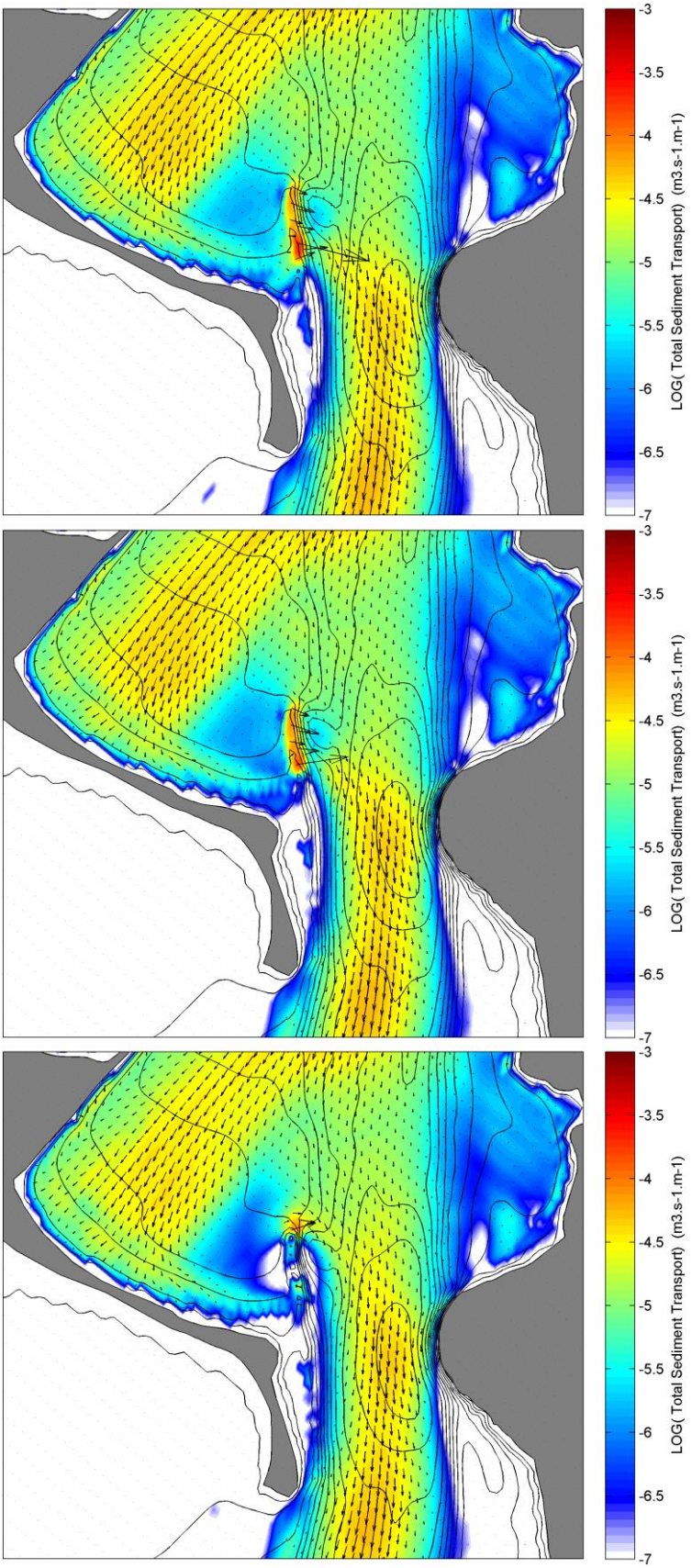

Figure 4.8 Mean total sediment transport fluxes within the entrance region over an incoming tide for a high energy northeast event (Hs=3m, Dir=45 deg., Tp=10 s.) (top:existing, middle: central segment emerged, bottom, central and north segments emerged).

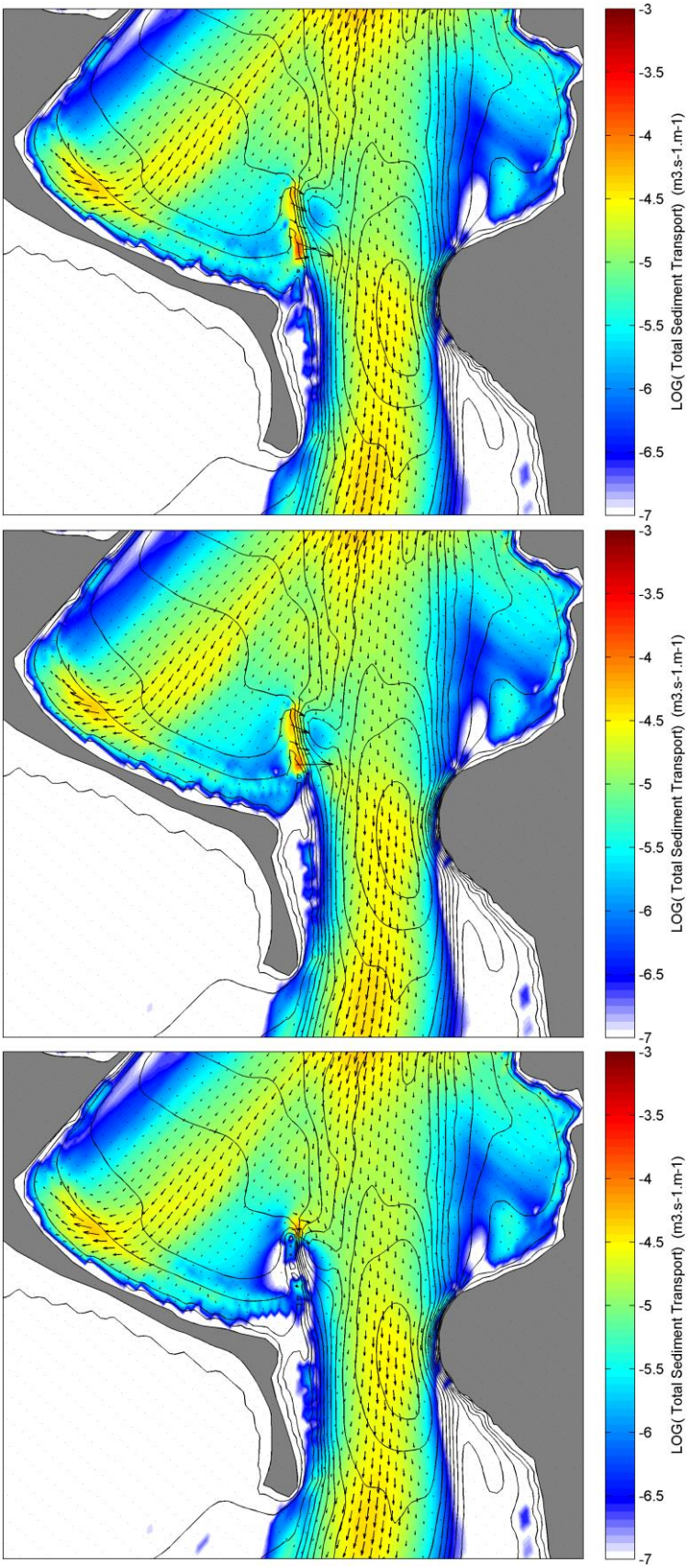

Figure 4.9 Mean total sediment transport fluxes within the entrance region over an incoming tide, for a high energy north swell event (Hs=2m, Dir=0 deg., Tp=14 s) (top:existing, middle: central segment emerged, bottom, central and north segments emerged).

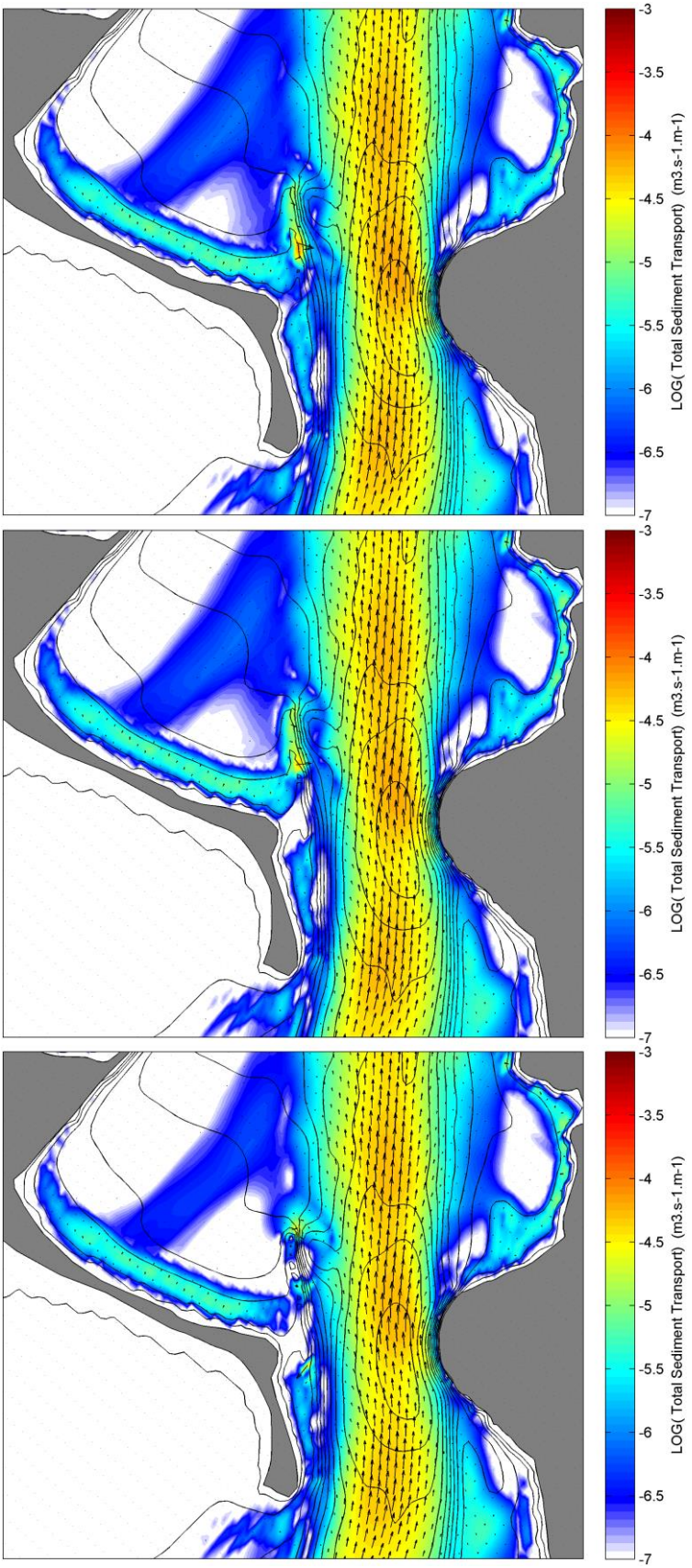

Figure 4.10 Mean total sediment transport fluxes within the entrance region over an incoming tide, for low energy north sea waves (Hs=1m, Dir=0 deg., Tp=8 s.) (top:existing, middle: central segment emerged, bottom, central and north segments emerged).

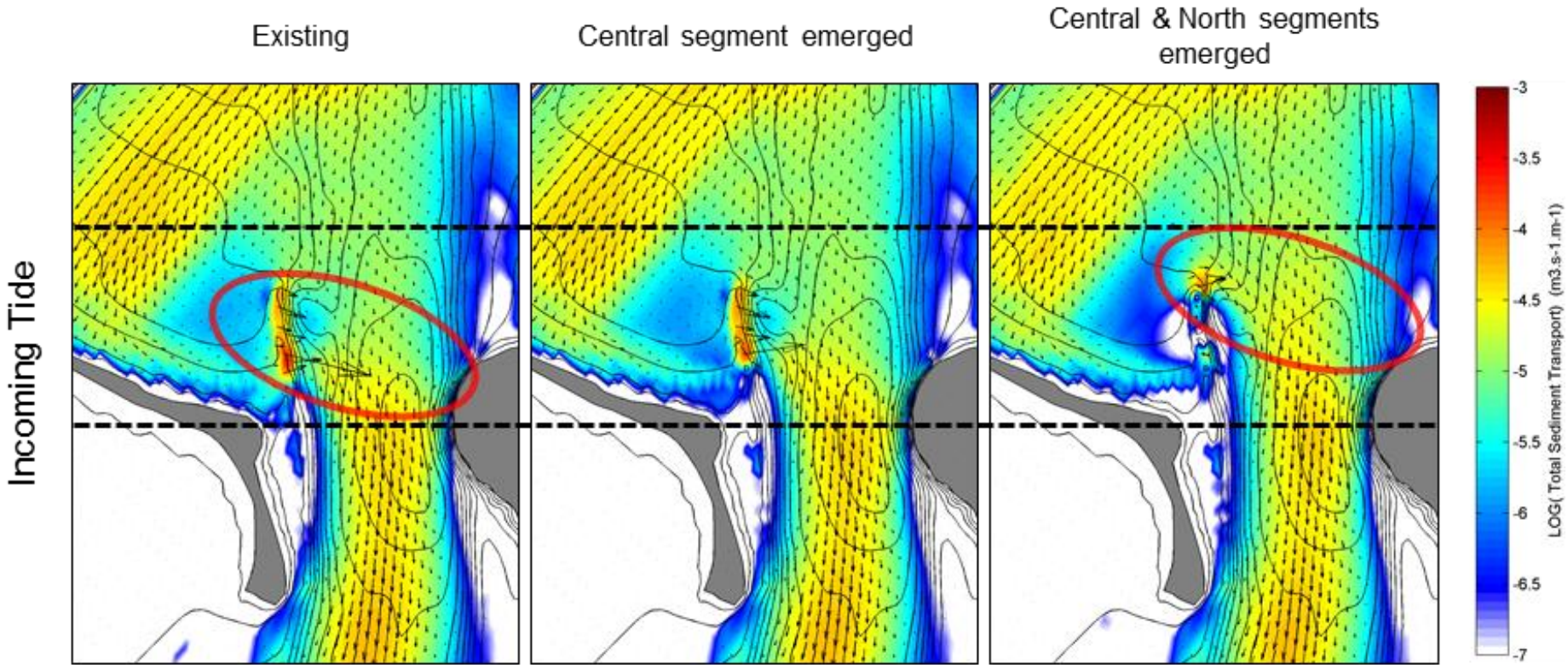

Figure 4.11 Difference in net sediment transport fluxes over the incoming tide for a high energy northeast event (Hs=3m, Dir=45 deg., Tp=10 s.), for the 3 bathymetries considered (left to right, existing, central segment emerged, central and north segments emerged). Note the difference in sediment transport patterns and magnitudes in the vicinity of the Long Mac structure and within the adjacent channel area. Eastwards transport over the existing Long Mac (left) is reduced by an emergent structure (right) but this tends to result in an enhanced transport around its seaward end.

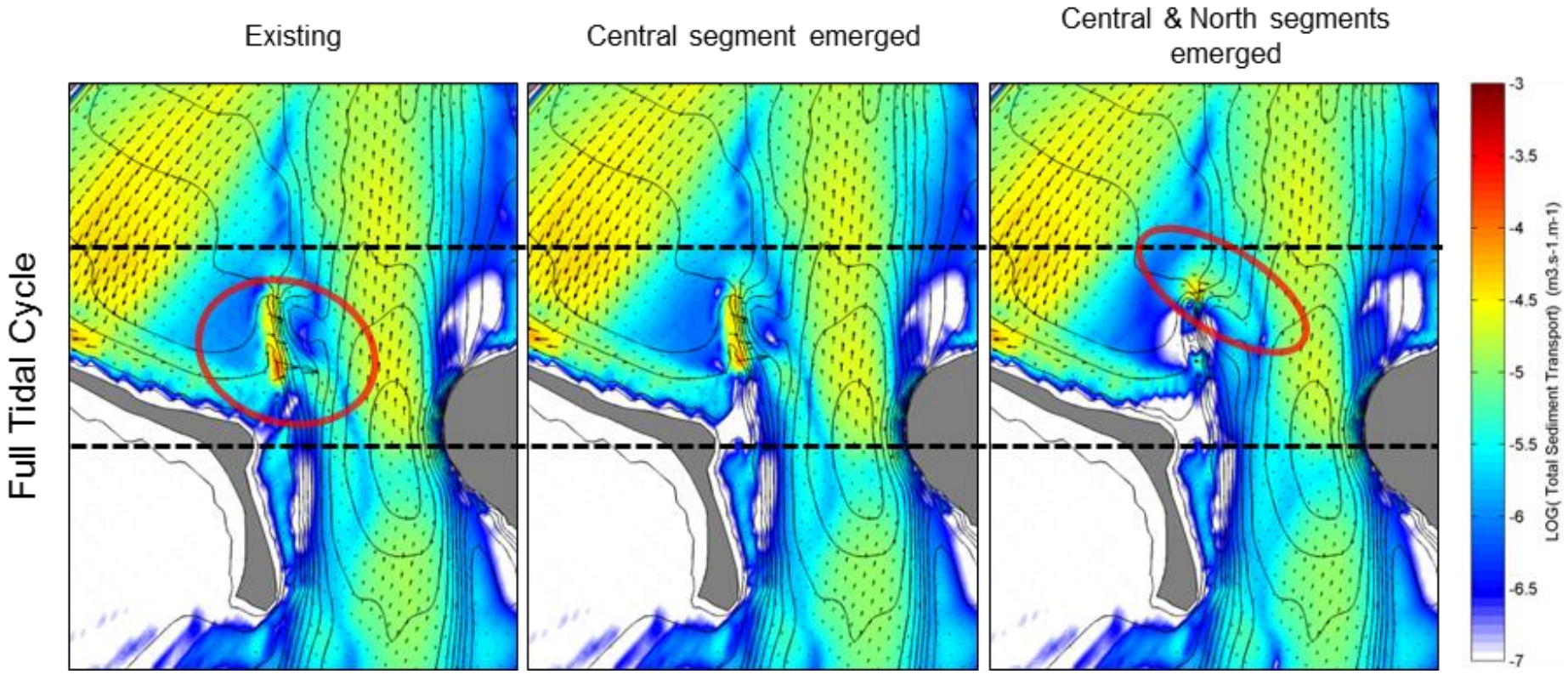

Figure 4.12 Difference in net sediment transport fluxes over the full tidal cycle for the a high energy northeast event (Hs=3m, Dir=45 deg., Tp=10 s.), for the 3 bathymetries considered (left to right, existing, central segment emerged, central and north segments emerged. Note the progressive reduction of the present eastwards transport feature over the Long Mac on the existing bathymetry and associated enhancement of the transport seaward of the emerged tip.

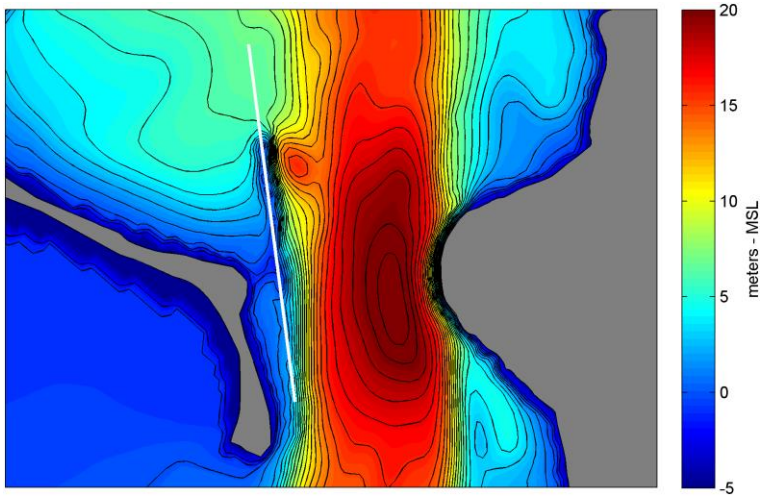

Figure 4.13 Transect position.

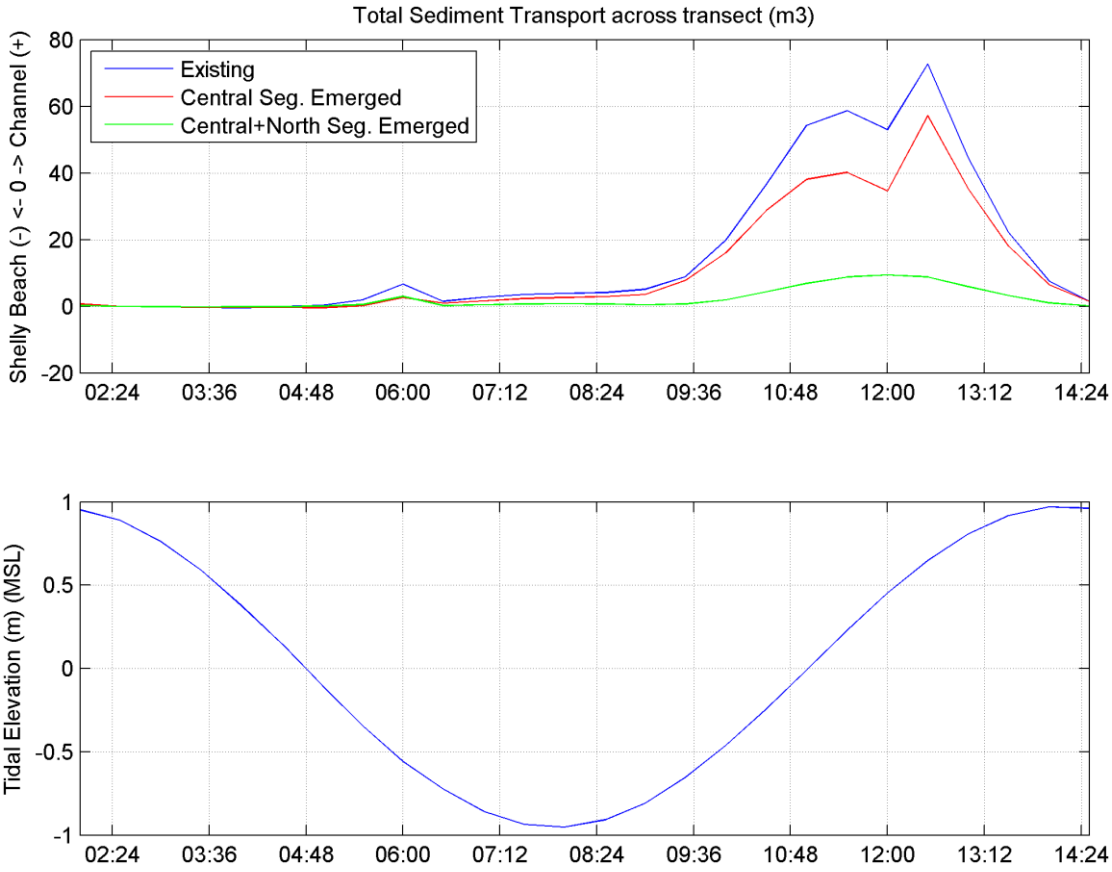

Figure 4.14 Total sediment volumes transported across the transect shown in Figure 4.13 (top) over the tidal cycle considered (bottom). Note the reduction in transport peaks at incoming tide for the cases with emerged segment(s). A positive transport is towards the channel while a negative one is towards Shelly Beach.

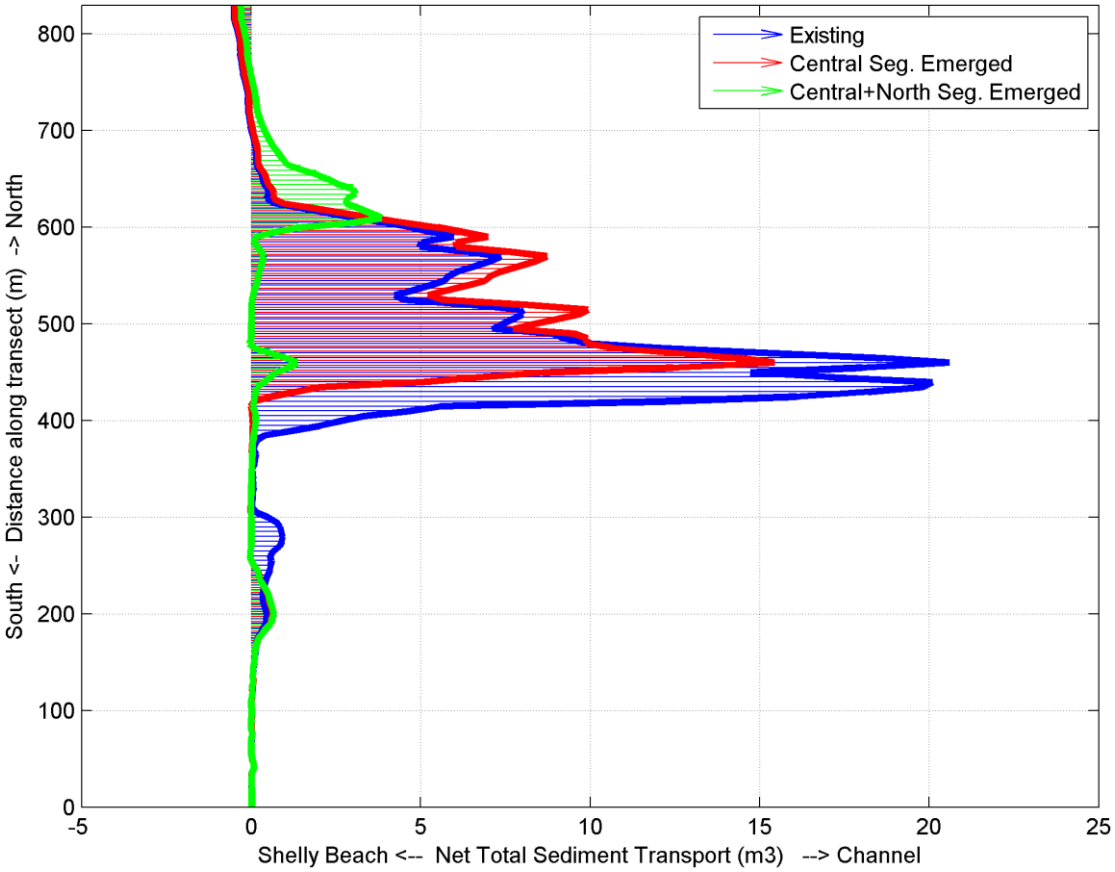

Figure 4.15 Net volumes of sediment transported across each point of the transect shown in Figure 4.13, over the tidal cycle considered. A positive transport is towards the channel while a negative one is towards Shelly Beach. Note the northwards shift in maximum transport position and the magnitude reduction provided by a structure with emergent segment(s).

4.3. Discussion

The physical blocking of the existing incoming flows by a structure with emergent segments appears to be relatively efficient in reducing the main predicted transport feature along Shelly Beach and over the Long Mac that is likely responsible for most of the sediment recirculation into the channel. With respect to the upper entrance region, the flows forced around the emerged structure tip may be the feature with the most potential adverse effects due to possible combination of scour formation and deposition, where Shelly Beach flows merge with the channel. However the “new” predicted transport appears to be at least an order of magnitude less significant than the presently predicted magnitude, especially when both the central and north segments are raised. Since the base mechanism of blocking the water to reduce the water level gradient seems quite efficient, a slightly more inward (i.e. towards Shelly Beach) structure orientation may be interesting to further investigate, as this mechanism will be conserved but any depositional feature would be expected to be similarly shifted inward and thus further away from the channel.

With respect to the lower part of the entrance region, a potential issue that could arise following the compartmenting of Shelly Beach cell is a loss of stability of the lower part of the spit (i.e. south of structure junction to Shelly

Beach) due to relatively reduced sediment supply. There are no obvious signals in the model predictions suggesting that this will be problematic but results should be interpreted with care as that area is not necessarily represented fully realistically given the small scale of structural features, possibly at subgrid resolution, and uncertainties in bathymetry. That being it is expected that alternating ebb and flood flows around the fixed junction would still help to provide a consistent and fairly balanced sediment supply base. Some mitigation of possible adverse effects could include upgrading and/or reconfiguration of the secondary groins already present.

A “softer” measure to allow a better sediment transport balance of the Shelly Beach cell, that can be applied alone or in combination with any structure upgrade, is the use of the return flow along the Mole that seems to generally relax the eastwards transport along the eastern half of the beach. This feature was particularly evident for the high energy north swell event, for which the wave energy reaches the more central part of the beach (Figures 3.14, 3.15, left). The present disposal ground main position seems appropriate, however predominant sediment disposal on the eastern half of the area could help to re-center the wave energy along the beach and drive this return flow along the Mole for a wider range of wave incidence.

5. SUMMARY

A numerical model of the Otago Harbour entrance region has been implemented to investigate the local circulation and sediment transport patterns, with a particular attention to the potential for sediment recirculation into the Harbour. The Delft3D model system coupling wave, circulation and sediment transport models was run for a range of idealized wave events reproducing typical forcing at the site, during a spring tide period.

The main findings of the study are as follows:

- The area is subject to complex tidal hydrodynamics due to the strong water level gradients developing from the coupling of the Harbour with the larger scale regional tidal regime. Outgoing tides are characterized by a strong ebb jet constricted at the Harbour mouth and extending well seaward of the entrance region, all along the large submerged delta bar. The entrance region provides a buffer area to incoming tides. The area fills in faster than what is discharged through the mouth, which results in a distinct eastward flow along Shelly beach accelerating over the Long Mac and meeting constricted flood flows of the channel. This forces eastwards sediment transport fluxes (i.e. channel-directed) in the vicinity of the Long Mac. This process is significant with respect to sediment recirculation in the Harbour.

- Significant amounts of wave energy can reach the entrance region, with magnitude and patterns depending on the incident wave conditions. An onshore sediment transport vector over the disposal ground seaward of Shelly Beach is consistently predicted by the model, coinciding with the overall location of transmitted wave energy bands. This area exposed to wave energy and associated onshore sediment transport coincides with a clear onshore translation of surveyed depth contours thus providing some degree of validation. This indicates the importance of wave-driven sediment transport due to wave asymmetry effects over the disposal ground.

- Wave-driven effects modify the circulation patterns and induce significant sediment transport along Shelly beach. The northeast and southeast cases result in wave energy reaching predominantly the western half of Shelly Beach; at incoming tide phases, wave-driven currents tend to enhance the ambient tidal easterly flows directed towards the channel and associated sediment transport. When the wave energy reaches the central parts of the beach for more northerly wave incidence, an alongshore flow and transport component is forced along the western half of the beach, eventually veering along the Mole in a clockwise motion. This pattern is also reproduced for the northeast event at outgoing tides due to favourable ambient tidal level gradient and slightly shifted wave energy incidence. Net flow fields suggest that the return flow along the Mole can subsequently merge with incoming eastwards currents in the vicinity of the Long Mac. This pattern is not obvious in the net total sediment transport fields but it is present in net

suspended sediment fluxes, with magnitude an order of magnitude less than the total transport. This feature is likely to provide a secondary path for sediment transport back into the Harbour.

- The direct vicinity of the Long Mac is consistently characterized by an eastwards sediment transport vector (i.e. channel-directed) in net sediment transport fields. It is expected that incoming tide phases, when tidal water level gradients work in combination with any superimposed wave-driven easterly longshore flow, will be the most critical times for sediment transport into the Harbour. Based on the wave events considered, it is likely that when wave energy reaches the central part of the beach, rather that its western half, the return flow forced towards and along the Mole may provide a degree of relaxation to the eastwards transport in the Long Mac vicinity.

- Options to reduce sediment recirculation into the Harbour were investigated simulating the effects of a modified Long Mac structure with its central segment emerged, and both its central and north segments emerged. Emergent segments provide a physical barrier to the incoming water mass and modify the water level distribution along the beach. Elevated water levels along the eastern half of the beach tend to balance the longshore level gradient that is presently predicted at incoming tide (i.e. from the beach to the channel), thus relaxing the forcing for the strong longshore flows and transport over the Long Mac.

- For the configurations with emergent structure segments, the merging of the currents originating from and off Shelly Beach with the incoming channel flow is shifted northwards around the structure seaward tip. This results in locally enhanced eastwards transport features (i.e. channel-directed) and modification in transport distribution within the channel north of the existing trough between Harrington point and Shelly Beach eastern end. Channel-directed transport features in the structure tip vicinity are likely to induce some small delta-like features, similar to that presently visible in the latest bathymetric survey where the most intense transport presently occur. However a significant reduction of the net transported sediment volumes can be obtained with the configuration with both the central and north segments emerged, thus reducing the potential for any large depositional feature. Some morphological adjustment of the channel in the present trough vicinity trough is also expected given the different flow dynamics induced by the emerged segments.

6. REFERENCES

Bagnold, R. A., 1966. An approach to the sediment transport problem from general physics. US government Print Office. 344 p.

Battjes, J., and J. Janssen, 1978. Energy loss and set-up due to breaking of random waves, Proceedings of the 16th International Conference Coastal Engineering, ASCE, 569–587.

Brière, C., and Walstra., D. J. R., 2006. Modelling of bar dynamics. Report Z4099, WL Delft Hydraulics, The Netherlands.

Collins, J., 1972. Prediction of shallow water spectra, Journal of Geophysical Research, 77 (15), 2693–2707.

Deltares, 2013a. User Manual Delft3D-WAVE. version: 3.05.27794, Published and printed by: Deltares, 222 p. available online: http://oss.deltares.nl/web/delft3d/manuals

Deltares, 2013b. User Manual Delft3D-FLOW. version: 3.15.2789, May 2013 Published and printed by: Deltares, 706 p. available online: http://oss.deltares.nl/web/delft3d/manuals

Grasmeijer, B. T., 2002. Process-based cross-shore modelling of barred beaches, Phd thesis, University of Utrecht, Utrecht, The Netherlands.

Holthuijsen, L., 2007. Waves in Oceanic and Coastal Waters. Cambridge University Press. ISBN 0521860288, 9780521860284.

Isobe, M., and Horikawa, K. 1982. Study on water particle velocities of shoaling and breaking waves, Coastal Engineering Japan, 25, 109–123.

Kantha, L.H., and. Clayson C.A, 1994: Numerical Models of Oceans and Oceanic Processes. International Geophysics Series, Vol. 66. Academic Press, San Diego. 940 p.

Lesser, G.R., Roelvink, J.A., van Kester, J.A.T.M., Stelling, G.S., 2004. Development and validation of a three dimensional morphological model. Journal of Coastal Engineering, 51, 883-915.

Metocean Solutions Ltd., 2011. Port Otago Dredging - Preliminary wave, current and sediment transport model studies for dredge disposal investigations. Prepared for Port Otago Limited. 62p.

Roelvink, J.A.,and Walstra, D.J.R., 2004. Keeping it simple by using complex models. International Conference on Hydroscience and Engineering, Brisbane, Australia.

Song, Y. and D. B. Haidvogel, 1994: A semi-implicit ocean circulation model using a generalized topography-following coordinate system. Journal of Computational Physics, 115(1), 228-244.

Van Rijn L.C., Walstra D.J.R., and van Ormondt. M., 2004. Description of TRANSPOR2004 and Implementation in Delft3D-ONLINE, WL Delft Hydraulics report Z3748.10. 77p.

Van Rijn, L.C., 2007a. A unified view of sediment transport by current and waves, Part I: Initiation of motion, bed roughness and bed load transport, Journal of Hydraulic Engineering, ASCE.

Van Rijn, L.C., 2007b. A unified view of sediment transport by current and waves, Part II: Suspended transport, Journal of Hydraulic Engineering, ASCE.

Walstra, D.J.R., Van Ormondt, and M., Roelvink, J.A., 2004. Shoreface Nourishment Scenarios, WL Delft Hydraulics report Z3748.21. 85 p.

Walstra, D.J.R., Brière, C.B., Cohen, A.B., Van Dongeren, A.P., Elshoff, I.J.P., Hoyng, C. Van Ormondt, M., Quartel S., De Sonneville, B., Tonnon, P.K., Uunk, L., 2008. Monitoring and modelling of a shoreface nourishment. Report Z4479, Deltares, The Netherlands. 168 p.

Zhang, Y.-L. and Baptista, A.M. (2008). SELFE: A semi-implicit Eulerian-Lagrangian finite-element model for cross-scale ocean circulation. Ocean Modelling, 21 (3-4), 71-96.